DELFT HYDRAULICS LABORATORY

PUBLICATION No. 50

SOME CONSIDERATIONS ABOUT SCALES FOR COASTAL MODELS WITH MOVABLE BED

BY
E.W. BIJKER

NOVEMBER 1967

ABSTRACT

Starting from the increase of the bed shear of a uniform flow due to wave motion, a transport formula for waves and current has been derived.

With this transport formula scale relationships have been derived for models in which material transport, under the combined influence of waves and current has to be reproduced.

ACKNOWLEDGEMENTS

This report is also published as a doctors-thesis at the Delft Technological University. The author likes to express his gratitude to his promotor prof. ir. H.J. Schoemaker for his guidance and encouragement during this study.

He likes also to thank prof. ir. L.J. Mostertman for his support and prof. dr. P. Groen for the constructive criticisme during the preparation of this publication.

The support, interest and constructive criticism of the staff of the Laboratory is highly appreciated.

The availability of the excellent computer facilities of the University of Groningen and of the Laboratory "De Vrije Vlucht" of the Aero- and Astronautical Research Institute, for the numerical computations is also acknowledged.

CONTENTS

CHAPTER I
INTRODUCTION

I.1. Aim of the study

For the study of phenomena along coasts, investigations in hydraulic models are rather often used. In general these models may be devided in two groups, viz.: those with fixed bed, and those with movable bed. In the first group mostly physical phenomena are studied which are rather well known, such as refraction of waves approaching a coast and diffraction of waves when they penetrate into a harbour. In the second group, the development of the bottom configuration is studied. The phenomena governing this problem are not so well known, so that in this case the following statement, made by Birkhoff (8) applies rather well.

> "In practice, theoretical considerations are seldom involved in hydraulic model studies of rivers and harbours. Reliance is based on reproducing various aspects of the observed behaviour under actual conditions. It is hoped that variations in behaviour due to altered conditions will then also be reproduced to scale even though there is no rationed argument to support this hope".

It is clear that Birkhoff meant here models with movable bed. The situation is even more serious since the conditions in the prototype are never completely known. Moreover, they are varying so much that even when they would be known, together with their influences on the development of the bottom configuration, and when it would be possible to reproduce them to scale in the model, it would not be possible to reproduce the complete sequence of events. As a conclusion from this, one could even say that a model is a rather dangerous tool in the hands of a not very cautious and conscientious investigator. On the other hand, however, it is also very true that a model can act as a means to guide the considerations of the engineer in charge of the design of the project. Moreover, the model may give indications about the effect of different well described wave and current conditions on certain obstructions and structures. Particularly when the influences, which different types of structures will have on the development of the bottom configuration will have to be compared, very valuable information may be obtained.

For reproducing of the bed configuration, even qualitative, it is essential that the scale to which the movement of material is reproduced

in the model does not vary too much with the location. When this condition would not be fulfilled shoals would be either too high or too low, and scour holes would be either too deep or not deep enough. It is evident that this may lead to very dangerous conclusions. If, however, the trend of the divergence in behaviour of the model from the prototype is known, reliable results can be obtained, even if a complete invariability of the scale for the sediment transport is not obtained.

In this study an attempt has been made to obtain a better insight in the physical phenomena which govern the reproduction of the bottom configuration in a model with a movable bed, especially if these bottom changes are the result of the combined action of waves and current. In paragraph 2 of this chapter general scale relationships, which are valid for models where waves are reproduced are discussed, whilst in paragraph 3 special attention is drawn to the movement of bed material. In Chapter II an analysis is given of the procedure for the determination of scales. In the Chapters III and IV the physical phenomena, governing bed load movement under influence of waves and current, are discussed and in Chapter V relationships are given between the scales to which the different quantities should be reproduced in the model.

I.2. General scale laws for the reproduction of waves in models

In this study the ratio between the values of a certain quantity in the prototype and in the model will be indicated as the scale of that quantity. This scale will be denoted with the letter "n". A subscript to "n" refers to the quantity concerned. Thus, the length scale, for instance, will be written as "n_l". For completeness' sake the normal scale laws to which waves are reproduced will briefly be discussed.

The orbital velocity for a sinusoidal wave may be written in the first order approximation as:

$$u = \frac{\omega H}{2} \frac{\cosh ky}{\sinh kd} \cos(\omega t - kx) \qquad (I.2\text{-}1)$$

where u = orbital velocity at a distance y above the bed, d = waterdepth, ω = wave frequency = $2\pi/T$, where T = wave period, k = wave number = $2\pi/L$, where L = wave length, H = wave height from crest to trough and t = time. From this follows that the scale for the orbital motion can be written as:

$$n_u = n_\omega \, n_H \, \frac{n_{\cosh ky}}{n_{\sinh kd}} \qquad \text{(I.2-2)}$$

The value of n_u will have a constant value all over the model when the values of $n_{\cosh ky}$ and $n_{\sinh kd}$ are constant. This would only be possible if the values of ky and kd are equal for prototype and model at corresponding locations. This, in turn, would only be possible if the vertical scale would be equal to the scale to which the wave lengths are reproduced, so that:

$$n_d = n_L \qquad \text{(I.2-3)}$$

In that case the values of the scales of the hyperbolic sine and the hyperbolic cosine in equation (I.2-2) are equal to 1 and:

$$n_u = n_\omega \, n_H = \frac{n_H}{n_T} \qquad \text{(I.2-4)}$$

The scale for the wave period can be determined from the relationship between wave length and wave period:

$$L = c_* T \qquad \text{(I.2-5)}$$

where c_* = celerity of wave propagation.
In the first order theory, the celerity of wave propagation is exclusively a function of wave length and waterdepth viz.:

$$c_* = \left(\frac{g}{k} \operatorname{tgh} kd\right)^{1/2} \qquad \text{(I.2-6)}$$

For $n_d = 1/n_k$, the value of the hyperbolic tangent will be equal for prototype and model, so that:

$$n_{c_*} = \frac{1}{n_k^{1/2}} = n_L^{1/2} = n_d^{1/2} \qquad \text{(I.2-7)}$$

From equation (I.2-5) follows that in this case:

$$n_T = n_d^{1/2} \qquad \text{(I.2-8)}$$

and from equation (I.2-4) that:

$$n_u = \frac{n_H}{n_d^{1/2}} \qquad \text{(I.2-9)}$$

The scales for the wave height and for the length dimensions of the model may still arbitrarily be chosen. If, however, the wave steepness in the model were to be equal to that in the prototype, the following relationship would have to be satisfied:

$$n_H = n_L = n_d \qquad \text{(I.2-10)}$$

If this condition is fulfilled, the breaking of the waves in prototype and model is initiated at corresponding depths. The actual breaking phenomenon differs in the model from that in the prototype due to surface tension. From this follows that, if the waves are to be reproduced geometrically to scale at all locations of the model, the following scale laws should be satisfied:

$$n_T = n_d^{1/2} \qquad \text{(I.2-8)}$$

$$n_H = n_d \qquad \text{(I.2-10)}$$

and from this: $$n_u = n_d^{1/2} \qquad \text{(I.2-11)}$$

The length scale of the model can still be freely chosen.

By refraction is understood the phenomenon whereby the propagation of a wave train is governed by the relationships between wave lengths at different locations (19). Due to the fact that the wave height varies only little along the wave crest, the component of the energy flux in the direction of the crest line may be neglected. From this follows that the only requirement for correct reproduction of the refraction is an invariable scale for the wave length over the entire model. Therefore, in the case of refraction due to the bottom configuration, the necessary and sufficient requirement is also:

$$n_T = n_d^{1/2} \qquad \text{(I.2-8)}$$

The scale to which the wave heights are reproduced is free as long as the waves are not too steep.

Apart from changes in wave length due to the bed configuration, changes will also occur due to variations of the current velocity, in magnitude as well as in direction, with varying co-ordinates. In order to calculate this variation, the change in the angle φ between wave crests and current direction with a variation in velocity from v_1 to v_2 will be computed.

If ω is the wave frequency with reference to a fixed co-ordinate system, the wave frequency with respect to a co-ordinate system moving with v in the positive direction of x is:

$$(\omega - k_x v) \qquad \text{(I.2-12)}$$

where $k_x = 2\pi/L_x$, and L_x = wave length in the x direction.
The following relationship exists between k_x and the wave number k_i:

$$k_x = k_i \sin \varphi_i \qquad \text{(I.2-13)}$$

where φ_i = angle between wave crest and x direction.
In the case of a current in the positive x direction, formula (I.2-6) may be written as:

$$(\omega - k_x v_i)^2 = g\, k_i \operatorname{tgh} k_i d \qquad \text{(I.2-14)}$$

If ω, φ_i, v_i and d are known, k_i can be computed.

When a wave travels from an area with velocity v_1 and an angle φ_1 between wave crests and current direction, into an area with velocity v_2, the following relationship exists at the boundary of the two areas:

$$k_1 \sin \varphi_1 = k_x = k_2 \sin \varphi_2 \qquad \text{(I.2-15)}$$

as shown in figure I.2-1.
So equation (I.2-14) can be written as:

$$(\omega - k_x v_2)^2 = (\omega - k_1 v_2 \sin \varphi_1)^2 = \left(\omega - \frac{2\pi\, v_2 \sin \varphi_1}{L_1}\right)^2 = g\, k_2 \operatorname{tgh} k_2 d \qquad \text{(I.2-16)}$$

In this equation ω, k_1, φ_1, v_2 and d are known, whilst k_2 and hence L_2 can be computed. By means of equation (I.2-15) the value of $\sin \varphi_2$ can also be computed. Now the orbital velocity in this area can be computed by means of equation (I.2-1), writing $(\omega - k_i v_i \sin \varphi_i)$ for ω and k_i for k. From this follows that the additional requirement for reproducing of the current refraction to scale is:

$$n_\omega = n_v \cdot n_k$$

or:

$$n_v = \frac{n_\omega}{n_k} = n_d^{1/2} \qquad \text{(I.2-17)}$$

By diffraction is understood the phenomenon whereby a wave train is interrupted by a barrier, which results in an attenuation of the wave height behind this barrier. As a result of this, the wave crests will be strongly curved and big variations in wave height along the wave crests will occur. Therefore, the energy flux has an appreciable component in the direction of the crest line. From the theory (19) follows that the wave height at a given location is determined by the horizontal co-ordinates of that location expressed in wave lengths. In order to reproduce the correct wave heights at corresponding locations in prototype and model, the wave length should, therefore, be reproduced to length scale. Hence, in the case of an area with varying depth, and a wave length which

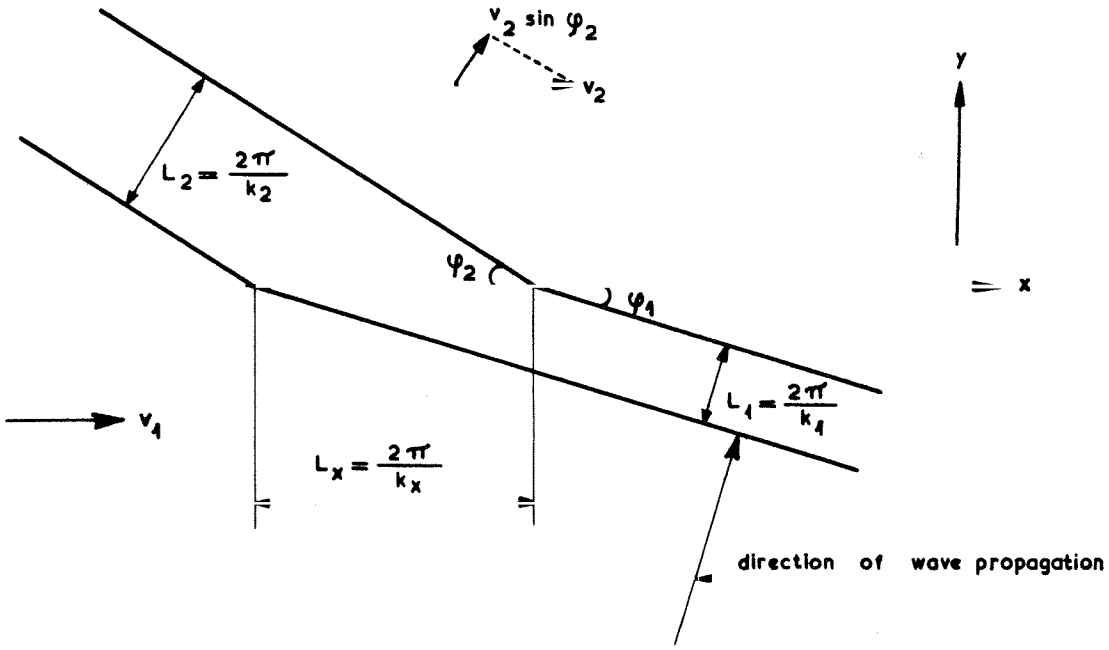

CURRENT REFRACTION

FIGURE I. 2_1

is influenced by the bottom, a model which has to reproduce diffraction phenomena should be undistorted.

If, however, the depth is so large that it has no influence on the wave length, the requirement of an undistorted model is not compulsory, so that the only requirement will then be that: $n_L = n_l$.
In this case d is so large that tgh kd $\approx$ 1 and:

$$n_T = n_L^{1/2} = n_l^{1/2} \qquad \text{(I.2-18)}$$

as follows from equations (I.2-5) and (I.2-6).

If d is so small that tgh kd $\approx$ kd, it follows from the same equations that:

$$n_T = \frac{n_L}{n_d^{1/2}} = \frac{n_l}{n_d^{1/2}} \qquad \text{(I.2-19)}$$

For values of tgh kd between these two extremes, the scale for the wave period should be:

$$n_T = \frac{n_L^{1/2}}{n^{1/2}\ \text{tgh}\ \frac{2\pi d}{L}} = \frac{n_l^{1/2}}{n^{1/2}\ \text{tgh kd}} \qquad \text{(I.2-20)}$$

I.3. Movement of bed material

In the prototype a certain beach profile will develop under influence of the waves approaching the coast. Summarizing very briefly the phenomena which determine the beach slope, it can be said that, due to the changing wave profile under influence of the decrease in depth, a transport of bed material directed towards the coast is generated. For the deeper areas this transport may be also ascribed to the mass-transport of the waves, which generates a current over the bed in the direction of the wave propagation (28). However, as soon as the beach has reached a certain steepness, gravity will prevent a further increase in steepness of the beach slope. This transport of water to the coast will, under certain circumstances, result in a return flow over the bed, directed seawards. This current will sometimes form a longshore bar at some distance from the coast. In case the waves approach the coast obliquely, a longshore current will be generated (9, 10). At certain intervals, this current will break out seawards, in the form of so called "rip currents", or the water will flow back in the form of a more or less evenly spread undertow. Also in the case of waves approaching the coast at right angles,

rip currents may occur at certain intervals, instead of an evenly spread undertow.

It is generally assumed that steep waves (storm waves) will generate one or more longshore bars, with a steep beach at the water level. At this level the coast is eroded and this sand is transported to the longshore bar. The resulting beach profile is called the storm or winter profile. For waves of smaller steepness (swell), the beach is accreting and especially its upper part will attain a more gentle slope. This profile is called the summer profile. The above description is, of course, a simplification which is only true as long as there are no other phenomena playing a role, such as for instance alongshore currents which will influence the configuration of the shoreline. It may very well be possible that, due to a locally increasing littoral current, a beach will be eroded by waves which normally would cause accretion. Another phenomenon may occur during varying wave conditions in the rough-weather season. Due to the variation in wave height and wave period, not only one, but a series of longshore bars develop. This may even lead to a complete absence of a pronounced longshore bar during the rough-weather season.

Most prototype data tend to a critical deep water steepness (H_o/L_o) of the waves of about 0.03 required for the generation of a bar profile. When the waves are steeper than this value one or more longshore bars will be generated. According to Kemp (25) an important factor in the development of longshore bars will be the ratio of the time lag between the break-point and the limit of uprush, and the wave period.

In models the same phenomena occur. However, due to different relationships between the wave characteristics and bed material normally used in models, the model beach slopes are different from those in the prototype. If sand is used as bed material, a storm profile is formed in the model when $H_o/L_o \lesssim 0.03$, where the subscript "o" denotes the values for deep water. When $H_o/L_o \lesssim 0.02$ a summer profile is formed. If, however, a material with lower density is used as bed material, for instance ground bakelite with a density of 1350 kg/m^3, a longshore bar will not be formed with even a wave steepness of $H_o/L_o = 0.04$. These figures are based upon both data from literature (25) and experience of the Delft Hydraulics Laboratory.

Apart from the generation of a profile with or without a longshore bar, the slopes of the beach in model and prototype will differ. A summer profile without a bar in the prototype will generally have a more gentle slope than a corresponding profile in the model. When in a model phenomena have to be investigated which occur in this part of the beach, the

distortion of the model (being the ratio between the length and the depth scales) should be equal to the ratio between the equilibrium slopes in the model and that in the prototype. Another point of concern is, that usually regular waves are applied in model studies. This may cause incorrect test results due to the fact that any irregularity in the beach will be increased as a result of the continuous and unchanging influence of the waves acting on it. Fortunately, however, these irregularities will normally be reduced on account of the fact that usually different water levels will be applied for reproducing the various stages of the tides. This will cause that the wave length will vary as result of the variations in depth. This variation of the wave length will reduce the irregularities in the beach.

The movement of material under the influence of a single current has been treated by several authors. These studies resulted in quite a number of formulae for bed load transport. The most well known formulae are those of Meyer-Peter (30), Einstein (13), Kalinske (22) and Frijlink (14). It appears that most formulae may be written as a relationship between two dimensionless parameters X and Y.
The parameter X may be written as:

$$X = \frac{S}{\sqrt{\Delta g D^3}} \qquad (I.3\text{-}1)$$

where S = transport, that is the volume of bed material moved in the direction of the current per unit of time and unit of width, D = mean grain diameter and $\Delta = \frac{\varrho_s - \varrho}{\varrho}$ = relative apparent density of the material.
If the shear stress at the surface is zero, the parameter Y may be written as:

$$Y = \frac{\Delta D}{\mu dI} = \frac{\Delta DC^2}{\mu v^2} = \frac{\Delta Dg}{\mu v_*^2} = \frac{\Delta D\varrho g}{\mu \tau_c} \qquad (I.3\text{-}2)$$

where d = depth, I = energy slope, μ = ripple coefficient, being an empirical coefficient that seems to indicate which part of the total bed shear is effective in the transport of material, v = mean velocity, C = resistance coefficient, $v_* = (\tau_c/\varrho)^{1/2} = vg^{1/2}/C$ = shear-stress velocity, τ_c = bed shear due to uniform flow. For the relationship $\tau_c = \varrho gdI$ it is assumed that the shear stress at the surface (for instance wind influence) is zero.

Transportation of material in suspension is discussed by Einstein (13) and he comes to a relationship between the transport in suspension and the flow characteristics of the following form:

$$S_s = \int_0^d c(y)\, v(y)\, dy \qquad (I.3\text{-}3)$$

where
$$c(y) = c_a \left(\frac{d-y}{d-a} \cdot \frac{a}{y}\right)^{\frac{w}{\varkappa (gdI)^{1/2}}} \qquad (I.3\text{-}4)$$

where $c(y)$ = concentration at distance y above the bed, c_a = concentration at reference distance a above the bed, w = falling velocity of the material and $v(y)$ = the current velocity at a height y above the bed. The falling velocity w for coarse material is proportional with $(\Delta D)^{1/2}$, and for very fine material, for which the drag coefficient follows the law of Stokes, proportional to ΔD^2. For coarse material the factor determining the concentration and thus the transportation of material in suspension is, apart from the factor μ, equal to that for bedload viz.: $\Delta D/dI$. For finer material this is not exactly valid, since w is proportional to a factor which varies from $(\Delta D)^{1/2}$ to ΔD^2. Also in this case, however, the bed shear which is proportional to dI has an important influence on the transport of material in suspension.

In the foregoing, the transportation of material by a single current has been discussed. The transportation of material by waves is in principle governed by the same phenomena . The velocity shows, however, a periodical fluctuation which necessitates a different approach for the computation of the phenomena occurring in the immediate vicinity of the bed. Another difference is the fact that, in most cases, transportation of material takes place in a direction which makes an angle with the direction of the orbital motion. For these two reasons a different approach is necessary for the study on sediment movement by waves.

This approach can be devided into two groups, viz.: the detailed study of the movement by waves in the direction or even against the direction of wave propagation and the more practically orientated studies about the transport of material by waves along a coast. The detailed studies start from the motion in the boundary layer between the normal orbital motion and the bottom. Very important information about the boundary layer is given by Huon Li (17). Huon Li has performed measurements in the boundary layer above an oscillating plate under a fluid which is at rest. This procedure has been chosen for reasons of experimental technics. Starting from the basic theory for laminar boundary layer as discussed for instance by Lamb (27), Huon Li has measured the transition from laminar to turbulent flow in the boundary layer. Kalkanis (23) has been able even to determine

the velocity profile in the boundary layer both for laminar and turbulent circumstances. His work will be discussed in somewhat more detail in paragraph 1 of Chapter III.

For the movement of bottom material under the influence of waves, the various investigators correlate characteristics for the boundary layer and the grain diameter and density of the material to the measured quantities of transported material. Of the rather numerous publications only those which are of direct importance to this problem will be discussed in more detail in Chapter II.

The more practically orientated studies which discuss the total littoral sand drift, generated by waves hitting the coast obliquely, start from the assumption that the transport is some function of the wave energy supplied to the coast. Practically all available prototype data are incorporated in the formula as published in "Shore Protection Planning and Design" (34) (page 175), of the U.S. Army Coastal Engineering Research Center.

The form of this formula is:

$$S = A\, E_a \,, \tag{I.3-5}$$

where S = littoral drift with the dimension $\left[L^3T^{-1}\right]$ and E_a = alongshore component of the energy flux towards the coast per unit of coast length with the dimension $\left[MLT^{-3}\right]$. From this follows that A has the dimension $\left[L^2T^2M^{-1}\right]$. The energy flux towards the coast is computed with the assumption that energy transport takes place according to the principles which are valid for wave refraction. The place where the alongshore component is computed is chosen at the breaker region. In this case:

$$E_a = E_o \frac{n_o}{n} \sin \varphi_b \cos \varphi_b \,, \tag{I.3-6}$$

where E_o = energy flux of the waves in deep water, φ_b = angle of the breaker crests with the coast line and n_o and n = distances between the wave orthogonals in deep water and in the breaker region.

The energy flux of the waves in deep water may be written as:

$$E_o = \frac{1}{16} \varrho g H_o^2 c_o \tag{I.3-7}$$

where c_o = celerity of wave propagation in deep water.

From this follows for the littoral drift:

$$S = 1.4\ 10^{-2} H_o^2 c_o \frac{n_o}{n} \sin \varphi_b \cos \varphi_b \tag{I.3-8}$$

where S is the transport per unit of time parallel to the coast. The

coefficient $1.4\ 10^{-2}$ is dimensionless and has been deduced from the data published in "Shore Protection Planning and Design" (34).

For reproducing these phenomena in models, scale laws should be derived with as main requirement the invariability of the scale for the material transport over the entire area of the model concerned. For current only, this criterion is extensively discussed by Bijker, Stapel and de Vries (6, 7). In the next chapter the procedures available for models with waves, and particularly with a combination of waves and current, will be discussed.

CHAPTER II
ANALYSIS

II.1. Relationships between scales for main current and wave height

From paragraph I.3, it may be concluded that the transportation of material is governed, among other factors directly or indirectly by the water velocity near the bed. In order to achieve a reproduction to scale of the sediment transport generated by a combination of waves and current, it will be possible to start from the following three different assumptions, which will be discussed more extensively later on in this paragraph.

a. The transportation of material is governed by the resultant velocity near the bed. Hence, the orbital velocity above the bed should be compared with the value of the main current velocity , near the bed, for instance the so called shear-stress velocity $v_* = v g^{1/2}/C$. The same approach could be used in this case for the velocity at any distance from the bed. This approach is, therefore, also rather well suited for transport of material in suspension.

b. The influence of the waves is demonstrated by the mass-transport, which is the resultant water movement due to the wave motion integrated over the period of the wave. The direction of this mass-transport will, as shown by Longuett-Higgins (28), vary with the distance above the bottom. Although this mass-transport velocity is generally rather small, the greatest value occurs usually just above the bottom and is directed in the direction of wave propagation. This velocity should, therefore, be compared with the main current velocity immediate above the bottom. Hence this approach is exclusively valid for bed load movement.

c. The transport of material is regarded as a function of the energy transported by the current and by the waves. For this reason the energy flux of the waves should be compared with that of the current. This approach seems very well suited for the total transport of material, moving as bed load and as suspended load.

The relationship between the scale for the wave heights and the scale for the velocity of the main current will be derived for the above mentioned three assumptions with the following limitations.
The first limitation (i) is the requirement for reproduction of bottom refraction, viz.: $n_T = n_d^{1/2}$, equation (I.2-8).

The second limitation (ii) is the requirement for reproduction of the wave height on depth scale with respect to breaking phenomena, viz.: $n_H = n_d$, equation (I.2-10).
The third limitation (iii) is the requirement for right reproduction of current refraction, viz.: $n_v = n_d^{1/2}$, equation (I.2-17), when also $n_T = n_d^{1/2}$, equation (I.2-8).

Assumption a

According to par. I.2:

$$n_H = n_u \cdot n_T \tag{II.1-1}$$

and since $n_u = n_{v_*} = \frac{n_v}{n_C}$:

$$n_H = \frac{n_v}{n_C} n_T \tag{II.1-2}$$

With limitation (i) this gives:

$$n_H = \frac{n_v}{n_C} n_d^{1/2} \tag{II.1-3}$$

The second limitation (ii) gives:

$$n_v = n_d^{1/2} \cdot n_C \tag{II.1-4}$$

From this follows that the third limitation (iii) can only be met if $n_C = 1$.

Assumption b

According to Longuett-Higgins (28), the mass-transport velocity, immediate above the bottom, can be written as:

$$U = A \frac{k\omega H^2}{4 \pi^2 (\sinh kd)^2} \tag{II.1-5}$$

The requirement of a constant scale for U all over the model, is again an equal value of kd for model and prototype at corresponding locations, so that $n_d = n_L$. This includes already limitation (i) viz.: $n_T = n_d^{1/2}$ according to par. I.2.
In that case:

$$n_H = n_U^{1/2} \cdot n_d^{3/4} \tag{II.1-6}$$

Since $n_U = n_{v_*} = \frac{n_v}{n_C}$:

$$n_H = \frac{n_v^{1/2}}{n_C^{1/2}} \; n_d^{3/4} \qquad \text{(II.1-7)}$$

With the second limitation (ii) concerning the reproduction of the wave height this gives:

$$n_v = n_C n_d^{1/2} \qquad \text{(II.1-8)}$$

Also in this case the third limitation (iii) for the reproduction of current refraction can only be met when $n_C = 1$.

Assumption c

The energy flux per unit of width of the waves can be written as:

$$E_w = \frac{1}{16} \varrho g H^2 \frac{L}{T} \left[1 + \frac{2\,kd}{\sinh 2\,kd}\right] \qquad \text{(II.1-9)}$$

(see Lamb, art. 237 (27).)

The energy transport per unit of width by a current can be written as:

$$E_c = \int_o^d \frac{1}{2} \varrho \, v(y)^3 \, dy \;, \qquad \text{(II.1-10)}$$

where $v(y)$ is the velocity at a distance y above the bed.

In order to achieve that the scale for the energy transport is invariable with the location in the model, $n_d = n_L$, so limitation (i) must be met. From this follows for equal scales for transport of energy by waves and current:

$$n_H = n_d^{1/4} \cdot n_v^{3/2} \qquad \text{(II.1-11)}$$

With the limitation (ii) for reproduction of the wave height:

$$n_v = n_d^{1/2} \qquad \text{(II.1-12)}$$

In this case also the third limitation (iii) about correct reproduction of the current refraction is met.

In order to obtain sufficient bed load movement in the model, especially in areas with little wave motion, it may be necessary to exaggerate the current velocity in the model. This is the so called "ideal velocity scale" (6, 7). When the velocities are exaggerated by a factor $\frac{1}{\zeta}$ as compared with the velocities reproduced on Froude scale and with $\zeta < 1$, the three scales for the wave height then become, according to the three aforecited assumptions:

a. $$n_H = \zeta \frac{n_v}{n_c} n_d^{1/2} \qquad \text{(II.1-13)}$$

b. $$n_H = \zeta^{1/2} \cdot \frac{n_v^{1/2}}{n_c^{1/2}} n_d^{3/4} \qquad \text{(II.1-14)}$$

c. $$n_H = \zeta^{3/2} n_v^{3/2} n_d^{1/4} \qquad \text{(II.1-15)}$$

These results show a great discrepancy between the three different assumptions. Since the mass-transport velocity is normally very low compared to the orbital velocity and the main current velocity, sediment movements as result from this velocity will be small compared with sediment movements resulting from the orbital velocity and the main current velocity. It is, therefore, most likely that assumption b may be omitted.

From this follows that the exaggeration factor of the wave height should be equal to that for the velocity or to the 3/2 power of that value; this with the assumption that the wave length is reproduced to depth scale.

Another approach, which is more or less equal to the above mentioned, is followed by Selim Yalin (33) and based upon dimensional analysis. Yalin starts from characteristic quantities of the fluid outside the boundary layer. By this method his results are not influenced by the state of the boundary layer. In the choice of the parameters on which he applies the dimensional analysis Yalin overlooks, however, the bed conditions, viz. the bed resistance. Furthermore Yalin introduces the physical condition that the distances travelled by the fluid in a certain interval of time should be reproduced to length scale.

The most serious objection which one could have against both approaches mentioned above is, that they do not take into consideration the relationship between bed load movement and flow characteristics. This leads to discrepancies in the results or to impractical values, as obtained in some cases by Yalin where he comes to very great distortions.

Another procedure would be to start from phenomena which are expected to occur in the boundary layer.

Valembois (37) starts from the critical velocity for bed load movement under wave motion as derived by Goddet (15). Goddet derives this critical velocity by studying the movement of the grains in the laminar boundary

layer between the frictionless orbital motion and the bed. His results show a clear difference for laminar and for turbulent regimes of the movement of the grains in this boundary layer. With a general expression for the resistance coefficient of a grain in the transition regime, one expression for the critical velocity as function of grain diameter and thickness of the laminar boundary layer can be obtained. This expression is of the form:

$$u_{cr} = f\ (\Delta,\ D,\ T) \qquad \text{(II.1-16)}$$

where u_{cr} = critical velocity at which movement of material starts, Δ = relative apparent density of bed material and T = wave period.

Using this expression, a scale relationship for the orbital velocity can be obtained. Valembois has written the relationship (II.1-16) as a relationship between critical bed shear, relative density and diameter of the bed material and the Reynolds number of the grains. In this way he obtained scale relationships which may be extrapolated somewhat further. Valembois makes clear, however, that these relationships hold good only in case conditions in the boundary layer, both in model and prototype, are laminar. The fact that the relationships are derived for the critical velocity at which the movement of the bed material starts does not mean a great limitation, according to Valembois. The relationship between this critical velocity and bed characteristics can be written in the same form as the normal bed load formulae so that extrapolation seems to be allowed.

Goddet and Jaffry (16) discuss the transportation of material by a combination of waves and current. For the scale relationships for material transport they also start from Goddet for the beginning of motion. For the established motion they use the general empirical formula which is written in this case as:

$$S = A\ H^2 T\ f(\varphi) \qquad \text{(II.1-17)}$$

For the relationships for sediment transport by current they use, both for the beginning of motion and established transport, the transport formulae of Meyer-Peter (27) and Eguiazaroff (11). For different grain diameters compared with the boundary layer thickness, for distorted and undistorted models, and for exaggerated and non exaggerated wave heights, they give scale relationships based on the above mentioned assumptions. For the combination of waves and current they only compare the various scale relationships and state whether there is a possibility for agreement or not. Thus they just compare the scale relationships derived for only current and only wave motion. No attempt is made to derive a scale relationship for the combined influence of waves and current.

II.2. Procedure in use at the Delft Hydraulics Laboratory

In paragraph I.2 the general scale laws for wave motion have been derived, whereas in paragraph I.3 the general principles for material movements are mentioned. In paragraph II.1 the relationships between the scales to which waves and current have to be reproduced in coastal models have been discussed. For the ultimate choice of the scales the following considerations are of importance.

As stated already in paragraph I.3, the distortion of the model is determined by the ratio between equilibrium beach slopes in model and prototype. This requirement is particularly of importance when phenomena close to the beach line have to be investigated. For phenomena further offshore, where the sea bed is more close to horizontal, this criterion is of less importance since in that region it is better possible to prescribe a certain slope for the sea bed in the model.

Under the assumption that bottom refraction has to be reproduced to scale, the wave period is normally reproduced on the square root of the depth scale. When also stream refraction plays an important role, the velocity scale should be equal to the scale for the wave celerity. This is, when the first requirement is met, equal to the square root of the depth scale.

Studies on the sediment transport by waves, hitting a coast obliquely, have demonstrated that the material is in principle moved by a current which is generated by the waves (2, 9, 10, 26). Of course this transport is activated by the waves by stirring up the bottom material. In the model it will be necessary to reproduce this current seperately, since this current is not only a function of the beach slope and wave characteristics, but also of the length over which the littoral current may develop, so of the distance between the successive rip currents (2). Normally this length will not be reproduced to scale in the model, since this current is the result of beach form and roughness on one hand and the wave form on the other hand. Since all these phenomena cannot be reproduced truly to scale, the distances between two successive rip currents will not be reproduced to scale and for this reason the relationship between these currents in model and prototype will be arbitrary. Moreover, the scale for these currents has to be determined with the single aim of correct reproduction of the material transport. This aspect will even be more important in the case of a tidal or sea current, running along the coast. When in the prototype this current would be able to transport also material in a region with little wave motion, for instance behind a cliff, the scale

law for this current will be determined by the scale laws for a mere current (6, 7). This will also be the case when a river outflow or tidal inlet is studied. In the latter case, moreover, strongly curved streamlines may be expected. Since the curvature of the flow lines is influenced by the bottom roughness, corrections to the reproduction of this bottom roughness may be necessary by adding artificial roughness in the model (6, 7, 31). Although the effect of artificial roughness on the material transport has been studied (18), not very much is as yet known about this phenomenon. Up to the present moment, the only way is to compare the development of the bottom in those regions in the model with that in the prototype and to determine the scales by trial and error.

As a result of the above mentioned considerations, and those listed in chapter I, the following procedure is used in the Delft Hydraulics Laboratory up to the present.

a. The distortion of the model, hence the relationship between length and depth scale, is determined from the ratio between the equilibrium slope of the beach in the prototype and in the model.
b. The actual values of the scales are determined with respect to the required accuracy. It goes without saying that a model of a narrow entrance to a fishing harbour with a required depth of 5 m needs a smaller scale (scale defined as prototype value over model value) than a model of an oil harbour with a required depth of 16 m.
c. The wave period is reproduced on the square root of the depth scale in order to achieve correct reproduction of refraction pattern.
d. The wave height is reproduced to depth scale or is made as much higher as would be possible without reproducing the breaking at an entirely wrong location.
e. The current velocity is reproduced a little bit stronger than would be in accordance with the square root of the depth scale in order to be as close to the ideal velocity scale as possible. Since this exaggeration may cause discrepancies in the reproduction of the stream refraction, it is kept as small as possible.
f. When in front of the harbour entrance strongly curved streamlines occur, artificial roughness is sometimes applied in order to meet the requirement of $n_l/n_d = n_c^2$ (see paragraph V.1 and V.3).

Apart from the considerations given above, also the choice of the waves and currents to be reproduced in the model is very important as stated already in paragraph I.1. In principle, the dominant circumstances

should be reproduced; that is a wave and a current which would have the same effect on the shore and the beach development, when applied during the whole year, as the actually occurring circumstances, which are continuously varying in magnitude, It is rather difficult to determine the characteristic wave height, and even more difficult to determine the combined influence of waves and currents, which has the same effect, when applied continuously, as the actual varying phenomena. In cases where clearly different conditions occur during calm and during rough seasons, it may be necessary to reproduce also two different combinations of circumstances in the model.

From the points discussed in the foregoing, it will be clear that, even if the scales to which the different phenomena have to be reproduced were known, it is very difficult, if not impossible, to determine the values of wave height and wave period and of the current velocity which have to be applied in the model to attain correct reproduction. However, the considerations given in this paragraph and to be discussed below, are necessary to avoid the obtaining of entirely wrong conclusions.

II.3. Outline for future procedure

In the preceding two paragraphs of this chapter basic considerations and some procedures have been discussed which may be of assistance in reaching acceptable scale values in a coastal model with movable bed. An empirical approach is still very important. This empirical approach may cause serious difficulties, namely in the case that no prototype data for comparison are available or in the case that the influence of the structure is so great that the existing conditions will change considerably.

An example of the above is a coast of which no other data are known than beach slope, grain-size distribution, wave motion and currents. It must be said at once that it is normally very seldom that sufficient data are available for determining the dominant wave or waves, and the dominant currents. This makes it practically even impossible to determine the littoral transport from these data without having available prototype data on the sediment transport. Assuming, however, that sufficient data would be available to determine the littoral drift, it will always be possible to find a combination of waves and currents in the model which produces the known littoral drift to a certain scale. One could state at that moment that the ratios between corresponding values in prototype and model constitute the required scales. There is however no guarantee that

a satisfactory good reproduction would also be obtained in case a substantial change would occur in the current and wave conditions.

The same situation might arise when an existing structure, protruding from a coast, would be extended in such a way that the current velocities in front of the structure increase. Although in this case there exists always a combination of waves and currents that can be reproduced and checked in the model, the increase in current velocity, resulting from the extension of the structure, with respect to the waves might cause serious discrepancies in the reproduction of the sediment transport.

From the foregoing considerations the conclusion may be drawn that the only requirement for a coastal model with a movable bed is that the transport scale is invariable all over the model, hence invariable for depth, bottom roughness, wave motion and current velocity. In principle this is nothing else than the concept of the ideal velocity scale as described by Bijker, Stapel and de Vries (6, 7).

The principle of the method developed by the author in this study is that the transport, resulting in the prototype from the combined action of waves and current, is compared with the transport in the model, resulting from analogous effects. No attention will be paid to detailed phenomena in the boundary layer beyond that which is necessary to establish these general relationships. As early as 1948 Einstein (12) suggested that the approach to the computation of sand transport by waves could be similar to that for uniform flow. Since for uniform flow the bed shear is one of the determining factors for the bed load and suspended load transport (see paragraph I.3), firstly the bed shear under the combined influence of waves and currents will be studied. Although a general theory had been developed, measurements were carried out for angles between wave crests and current of 0° and 15° only, since these angles are the most common ones in normal cases. The next step has been to relate the transport to the bed shear. The measurements, on which the derived relationships are based, are again only performed for values of the angle between wave crests and current between 0° and 30°. Moreover, all tests were executed with a horizontal bed. By means of these relationships it will be possible to determine scales for the various quantities to be reproduced in the model based upon the requirement that the value of the transport scale should be constant, or almost constant, over the entire model.

In this method the following limitations are still present.

First: the theory is developed and checked only for a horizontal bed and for relatively low, at any rate non-breaking, waves. The next step

should be to study whether and, if so, how this relationship has to be adapted for use on strongly sloping beaches and in breaker regions.

Secondly: the bottom roughness has to be estimated since from this, together with the wave and current characteristics, the bed shear has to be derived. The determination of the bottom roughness is, especially for the prototype, rather difficult but it should be stated emphatically that this difficulty is inherent to the problem and cannot be avoided by any other procedure.

CHAPTER III

INCREASE IN BED SHEAR OF A CURRENT DUE TO WAVE MOTION

III.1. Introduction

The problem of the bed shear of a combination of waves and current is mentioned by Jonsson and Lundgren in 1961 (21). They suggest a superposition of the uniform current velocity and the orbital velocity immediately above the boundary layer. In this respect under boundary layer is understood the transition zone between the frictionless orbital motion and the bed. Jonsson elaborated this theory for a single wave motion (20). He applied a logarithmic velocity distribution in the above defined boundary layer between the frictionless orbital motion of the waves and the bed. This logarithmic velocity profile holds good under certain circumstances for uniform flow. Jonsson arrived in this way at a thickness of this boundary layer equal to a few times the bottom roughness.

The thickness of the boundary layer has been discussed extensively for the case of a laminar boundary layer. The value of the thickness at which the different investigators arrived varies with the assumption about the value of the amplitude of the orbital velocity at which the limit of the boundary layer is assumed, from $\delta = 6.5\ (\nu/\omega)^{1/2}$ to $\delta = 3.2\ (\nu/\omega)^{1/2}$, where ν is the kinematic viscosity coefficient. The characteristic of the transition of the boundary layer from the laminar to the turbulent state is based upon the thickness of the originally laminar boundary layer, δ, the amplitude of the velocity immediately above this layer, u_o, and the viscosity, ν. Huon Li (17) indicates that for $u_o\delta/\nu > 800$ the boundary layer will be turbulent. For the tests described in this paragraph, this value will range from 200 to 2000. Vincent (38) indicates that, due to bed roughness, r, turbulence will occur in the boundary layer when $2\ u_o r/\nu > 60$. Since, in the tests described hereafter, the bed roughness was appreciable greater than the calculated value for the thickness of the laminar boundary layer, the requirement for a turbulent boundary layer was certainly met.

Kalkanis (23) has assumed a form of the equation of the turbulent boundary layer almost similar to that of a laminar boundary layer as given by Lamb (27), viz.:

$$u_b - u = u_o f_1(y) \sin(\omega t - f_2(y)) \qquad \text{(III.1-1)}$$

in which u = velocity in the boundary layer at a distance y above the bed u_b = orbital velocity at the limit of the boundary layer and u_o = amplitude

of the frictionless orbital velocity at this level. From experimental results Kalkanis arrives at values of $f_1(y)$ and $f_2(y)$. Using this velocity distribution, Kamphuis (24) arrived, after an approximative calculation, at a value for the thickness of the turbulent boundary layer which is in order of magnitude equal to the bottom roughness.

Manohar (29) suggested for the turbulent boundary layer a form equal to that for the laminar layer in which, however, the kinematic viscosity was replaced by the eddy viscosity. In the nomenclature of this study he comes to an equation of the form:

$$u_b - u = u_o e^{-\beta' y} \sin(\omega t - \beta' y) \qquad \text{(III.1-2)}$$

where $\beta' = (\omega/2\varepsilon)^{1/2}$, ε = eddy viscosity, which has been taken constant in this boundary layer and e = base of natural logarithme.

A similar approach is used by the author. However, for $\beta'y$ an arbitrary function Y of y is chosen, as demonstrated in paragraph 5 of this chapter. The author started from the assumption that for the calculation of the resultant bed shear the orbital velocity at a certain level could be superimposed on the velocity of the main current at this level. For this level a distance of er/33, in which r is the bed roughness, is chosen. Since the boundary layer for the orbital motion, which is assumed to be turbulent, will extend above this level, a value of p times the orbital velocity at the bottom, as calculated with the first order theory, will be introduced (see figure III.3-1). The resultant bed shear, in the direction of the main current, has been measured and from these measurements and the values of wave height, wave period and current velocity, the value of p has been computed. The measurements are described in paragraph 2 of this chapter and the computation of the resultant bed shear is executed in paragraph 3. From the results of the tests, as presented in paragraph 4, it becomes clear that p has a constant value. This is discussed in paragraph 4. Finally, the physical meaning of the fact that p is constant is discussed in paragraph 5.

Since for average beach conditions, the angle between current and wave crests is smaller than 20°, tests have been carried out by the author for angles of 0° and 15° respectively. The first results of this study are published in the seminars of the IAHR Congress at Leningrad in 1965 (3), at the Conference on Coastal Engineering at Tokyo in 1966 (4) and in a revised and corrected form as a publication of the Delft Hydraulics Laboratory (5).

III.2. Description and accuracy of the measurements

The tests were performed in a basin which was 27 m long and 17 m wide (figure III.2-1). On one of the longer sides a wave generator was installed, and on the opposite side a bank with a slope of 1:7 was constructed in order to avoid reflection and to dissipate the energy of the waves. In figure III.2-2 the wave height distribution over a cross section at right angles to the talus is given for some tests. Although the wave height is certainly not constant the variation seems acceptable. The wave heights were measured by means of a resistance wave height meter. A maximum flow of 0.7 m^3/sec could be adjusted with a degree of accuracy of 3% by an automatically governed inlet sluice. This discharge was distributed by means of an overflow weir and a grid over that part of the model which had a constant depth. In figure III.2-3 the velocity distribution over a cross section is given for three different tests. In figure III.2-4 the velocity profile in a number of points of this cross section for one test is given.

As the flow was practically uniform, the energy gradient could be determined by measuring the slope of the water surface. This was done by measuring the differences in waterlevel at two points at a mutual distance of 10 m along the centre line of the model. The waterlevels were recorded by means of floats, placed in drums next to the model. The drums were connected by means of a pipe to measuring points at the bed of the model. Special precautions were taken in order to ensure that the waterlevel was recorded without any velocity effect. By means of potentiometers, attached to the floats, the difference in waterlevel at the two points was recorded with an accuracy of 0.05 mm. Because it is not feasible to measure the bed shear directly, an indirect method had to be chosen. Determination of the bed shear by means of the velocity profile in the vicinity of the bed is not feasible in this case as the combined velocity profile is of a rather complicated nature . The bed shear was, therefore, determined by means of the energy gradient. This was possible because the shear stress at the surface of the water was zero. The tests were executed with a bed consisting of small rock stones with a mean diameter of 3 to 4 cm, and with a sand bottom covered with ripples of some cm's height (see figures IV.1-2 through 9).

The accuracy of the determination of the shear from the slope of the waterlevel is limited, due to the fact that this slope is computed from a very small difference of two piezometric heights which can be measured

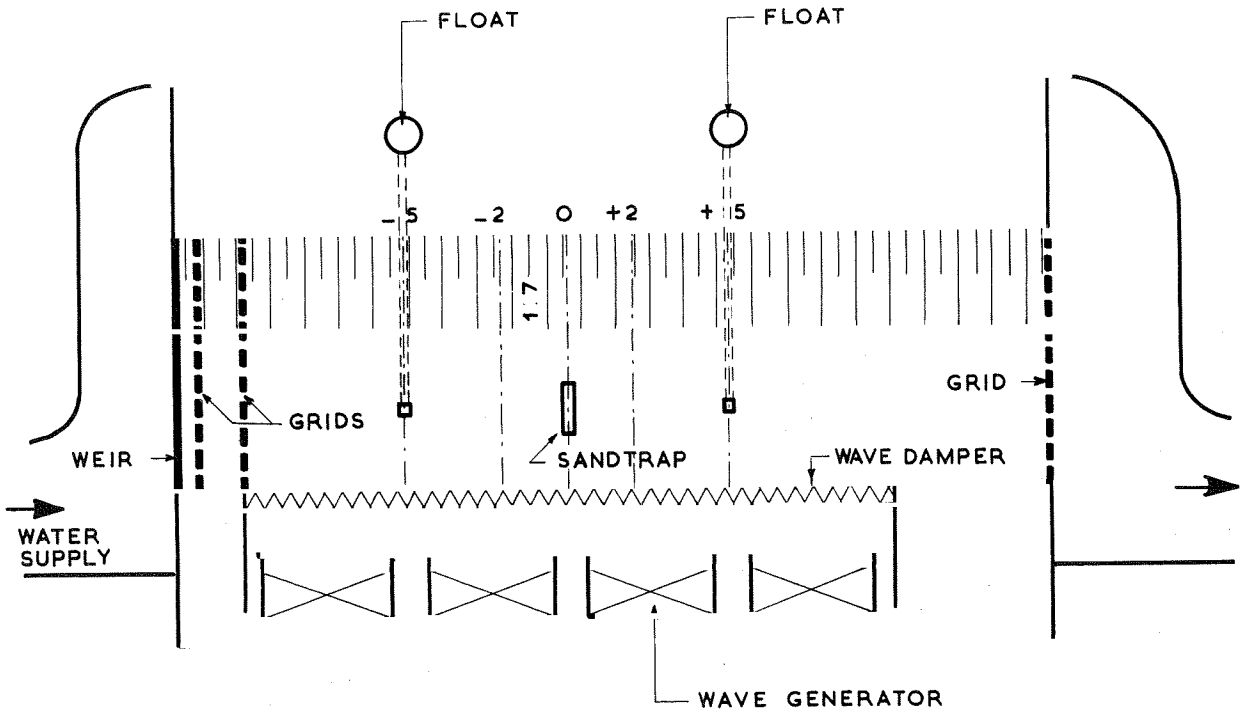

LAYOUT OF MODEL BASIN

FIGURE III. 2_1

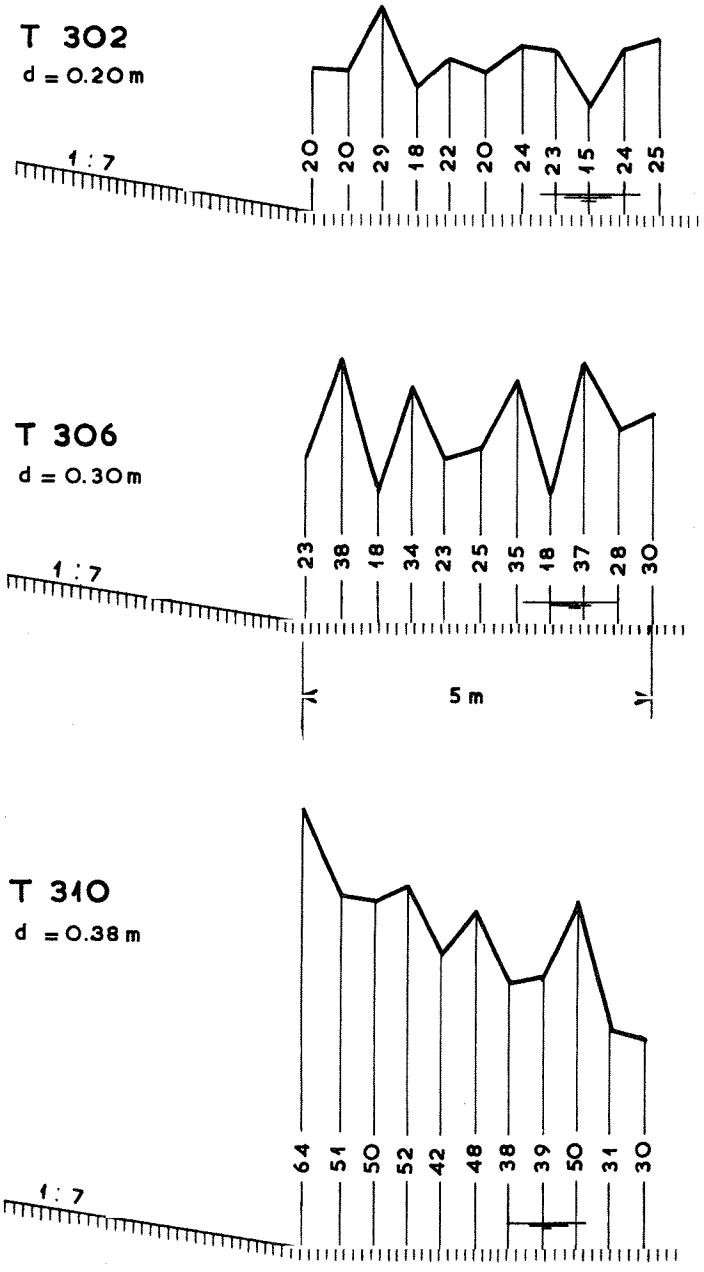

WAVE - HEIGHT IN mm

WAVE HEIGHT DISTRIBUTION IN CROSS SECTION O

FIGURE III. 2-2

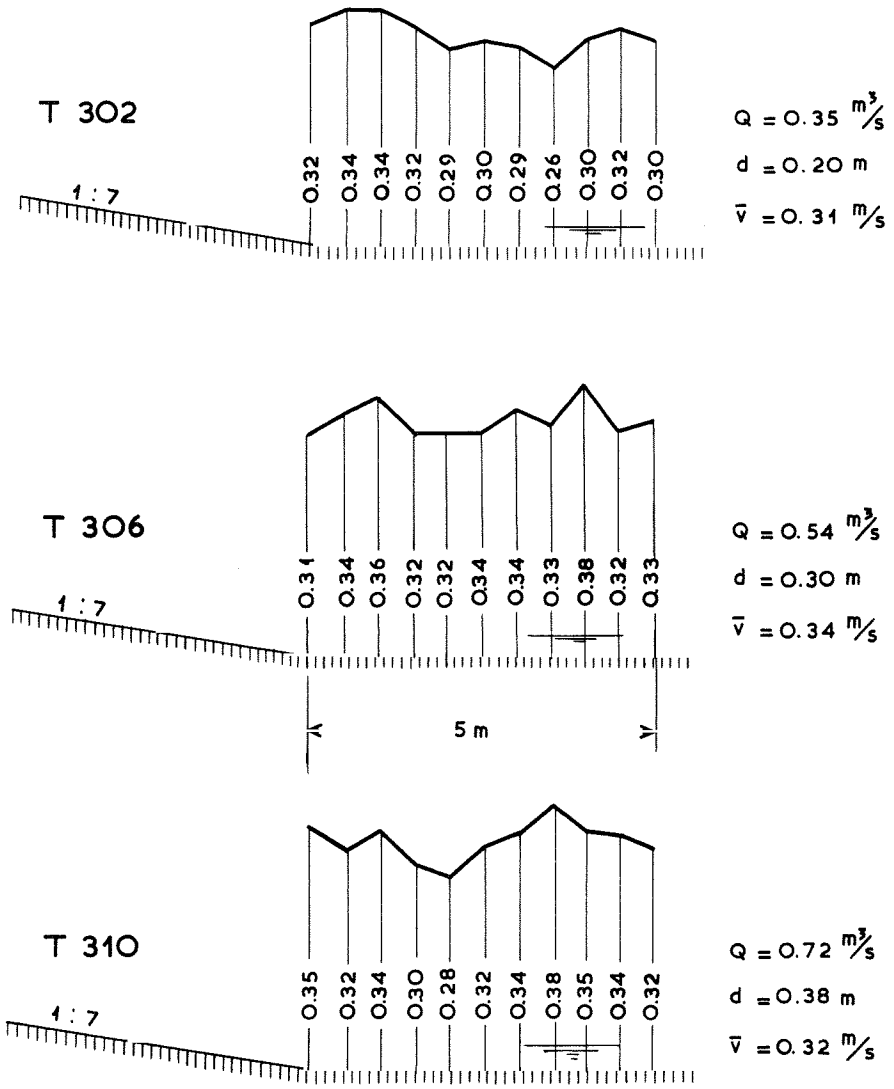

MEAN VELOCITY DISTRIBUTION IN CROSS_SECTION O

FIGURE III.2_3

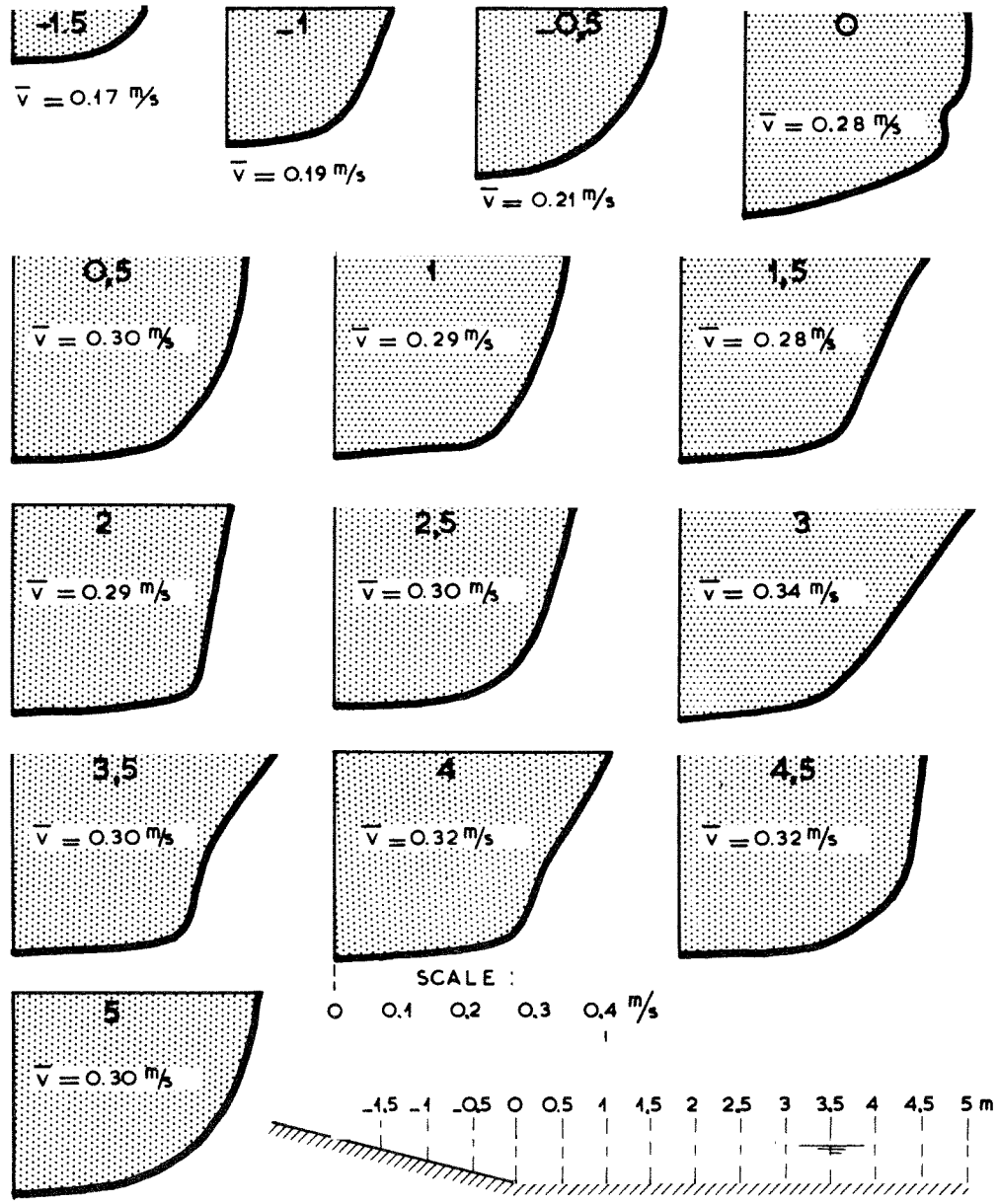

MEASURED VELOCITY_PROFILES T 306 II

CROSS_SECTION O

FIGURE III.2_4

only with limited accuracy. In order to see what results may be obtained, the roughness values will be analysed. Variations in the roughness of the sand bed may be contributed, not only to inaccuracy of the measuring method, but also to changes in the ripple height and form. Therefore, only the roughness-values r for the bed covered with stones will be considered in this respect. The different values for r, as calculated from the tests, range from 2 to 6.7 10^{-2} m. The mean value is 3.7 10^{-2} m, whereas the standard deviation is 1.8 10^{-2} m, which is about 50% of the actual value.

From the inaccuracy of the single records of the piezometric heights, it can be judged whether this inaccuracy is acceptable. The inaccuracy of a single reading of the piezometric height is 0.05 10^{-3} m. Therefore the inaccuracy in the difference from which the slope is calculated is $2^{1/2}$. 0.05 mm = 0.07 mm. The difference in waterlevel between the two measuring points is in the order of magnitude of 1.4 mm. Consequently the inaccuracy of this difference is about 5%. From this follows for the inaccuracy of C, about 6%, when the inaccuracy of the velocity is estimated at 3%. For the calculation of the bed roughness by means of the resistance coefficient C, the logarithmic formula:

$$C = 18 \log 12 \left(\frac{d}{r}\right) \qquad \text{(III.2-1)}$$

has been used (36). The value of C, as well as of the coefficient 18 are expressed in $m^{1/2}/s$. For the estimation of the inaccuracy of r the Manning-Strickler formula can also be used. This formula may be written as:

$$C = A \left(\frac{d}{r}\right)^{1/6} \qquad \text{(III.2-2)}$$

where C and A are expressed in $m^{1/2}/s$.
Strickler (35) has originally determined the value of A as 21.1 but after changing the value of the bed roughness r from D_{50} to D_{90}, that is from the grain diameter of the bed material which is exceeded in size by 50% respectively by 10% in weight, the value of A has become 25. From this formula follows that the inaccuracy of r will be 6 times that of C, that is about 40%. This is of the same order of magnitude as the standard deviation which is found from the tests, so that there are at any rate no hidden sources of errors in the tests.

It is regrettable that the accuracy of the test results is so low. Compilation of the test results, however, revealed a clear tendency which has been accepted as a base for the scale laws.

III.3. Computation of the resultant bed shear

According to Prandtl, the intensity of the bed shear in a turbulent current may be written as:

$$\tau = \varrho l^2 \left(\frac{\partial v(y)}{\partial y}\right)^2_{bottom} \qquad \text{(III.3-1)}$$

where l = mixing length, $v(y)$ = velocity at height y above the bed, ϱ = density, τ = bed shear and y = distance from the bed.
According to the theory of Prandtl for a rough bed, l is determined by the roughness of this bed and the distance to the bed so that:

$$l = \varkappa y, \text{ for small values of } y \qquad \text{(III.3-2)}$$

in which $\varkappa$ is a universal constant with the value 0.4, the constant of von Kármán.

For a normal fully turbulent current the differential quotient of the velocity distribution (the velocity gradient) outside the laminar sublayer to the bottom can be written as:

$$\frac{\partial v(y)}{\partial y} = \frac{v_*}{\varkappa y} \qquad \text{(III.3-3)}$$

where

$$v_* = \left(\frac{\tau}{\varrho}\right)^{1/2} = (gdI)^{1/2} = \frac{v\, g^{1/2}}{C}, \qquad \text{(III.3-4)}$$

where v_* = shear-stress velocity, d = waterdepth, I = slope of energy gradient, v = mean velocity, C = resistance coefficient of Chezy and g = acceleration due to gravity.
Integration of equation (III.3-3) gives the vertical distribution of the velocity (32), viz.:

$$v(y) = \frac{v_*}{\varkappa} \ln \frac{y}{y_o} \qquad \text{(III.3-5)}$$

where y_o = distance above the bed where the velocity according to this distribution is equal to zero. According to experiments $y_o = r/33$, in which r is a value for the bed roughness.
For the computation of the bed shear $(\partial v(y)/\partial y)_{bottom}$ must be known. According to figure III.3-1 it will be assumed that (32)

$$\left(\frac{\partial v(y)}{\partial y}\right)_{bottom} = \frac{v_{y'}}{y'} = \frac{v_*}{\varkappa y'} \qquad \text{(III.3-6)}$$

So that in this case:

$$v_{y'} = \frac{v_*}{\varkappa} \qquad \text{(III.3-7)}$$

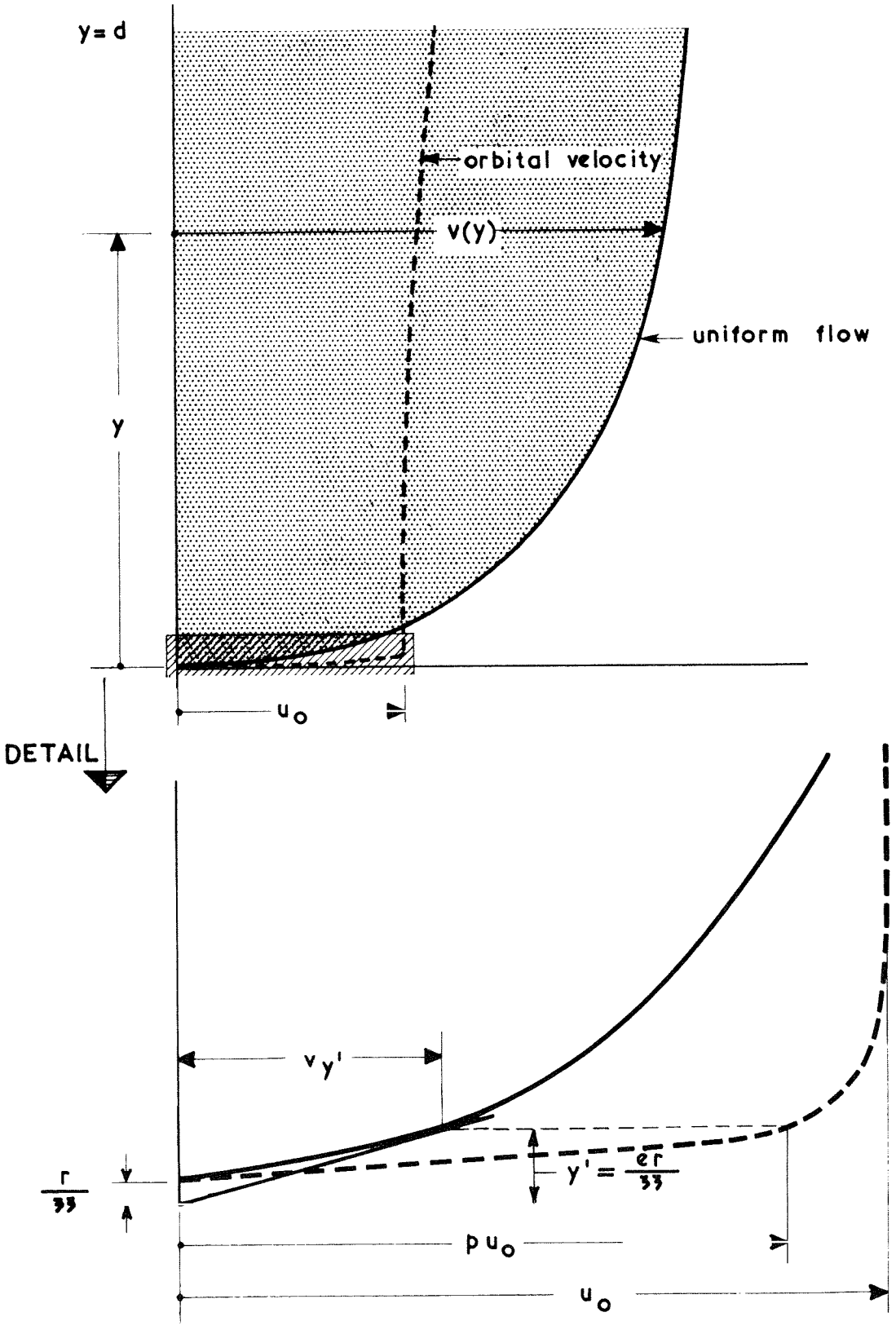

COMPARISON BETWEEN LOGARITHMIC VELOCITY DISTRIBUTION OF UNIFORM FLOW AND ORBITAL VELOCITY DISTRIBUTION OF WAVES

FIGURE III.3_1

After substituting this value in equation (III.3-5) for the vertical distribution of the velocity one finds:

$$y' = \frac{er}{33} \qquad \text{(III.3-8)}$$

The meaning of a layer with a thickness of y' is mainly hypothetical, although sometimes it is regarded as a viscous sublayer .

The calculation of the bed shear of the combination of waves and current starts from the principle of superposition of orbital motion and uniform current in the boundary layer. According to this principle and the procedure described above, the vertical gradient of the resultant vector should be determined. Due to the different form of the velocity profile for wave motion and uniform current (see figure III.3-1) the end point of the resultant vector will at any arbitrarily chosen moment describe a space curve. Hence, also the direction of the shear stress will vary with the height above the bed. It is assumed in this respect that $\partial v/\partial y$ at any height will determine the shear stress at that height. The same procedure for calculation of the bed shear as applied for uniform flow and described above is also applied for the combination of waves and current. Hence, in this case the gradient of the combined vector at a distance er/33 from the bed will be determined. Therefore the value of this vector at this distance of the bed will be used and a value $p\ u_b$ for the orbital velocity at this height will be introduced as illustrated in figure III.3-1. In this expression p is a coefficient which has to be determined by experiments. Abou Seida (1) assumes under the turbulent boundary layer a viscous sublayer. This layer could be compared to the layer with a thickness er/33. In paragraph III.5 the physical meaning of this value p will be discussed.

The frictionless orbital velocity at the bottom u_b is a function of the time according to the equation:

$$u_b = u_o \sin \omega t \qquad \text{(III.3-9)}$$

with:

$$u_o = \frac{\omega H}{2 \sinh kd} \qquad \text{(III.3-10)}$$

In the case where the orbital velocity makes an angle of φ with the normal to the main current, the resultant velocity, $V_{y'}$, at a distance er/33 from the bed can be written as:

$$V_{y'} \cong \sqrt{v_{y'}^2 + p^2 u_b^2 + 2\, v_{y'}\, p\, u_b \sin \varphi} \qquad \text{(III.3-11)}$$

(see figure III.3-2)

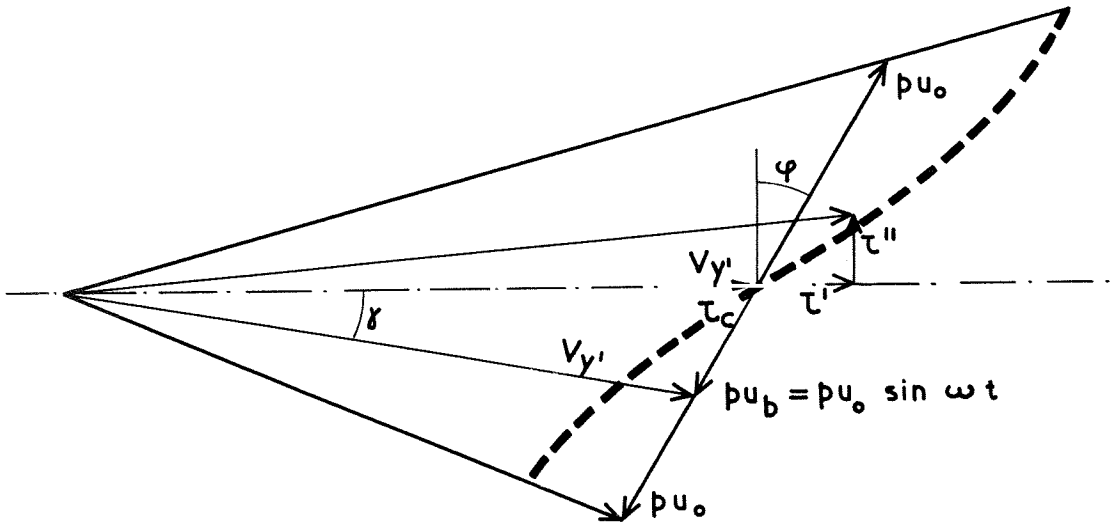

COMBINATION OF ORBITAL VELOCITY AND MAIN CURRENT

FIGURE III.3_2

The angle γ between the resultant instantaneous bed shear and the main current is in this case defined by:

$$\cos\gamma(t) = \frac{v_{y'} + pu_b \sin\varphi}{\sqrt{v_{y'}^2 + p^2u_b^2 + 2\, v_{y'}\, pu_b \sin\varphi}} \qquad \text{(III.3-12)}$$

Bed shear in the direction of the current

The component of the resultant bed shear in the direction of the main current is in this case, using equations (III.3-1) and (III.3-6), given by:

$$\tau'(t) = \frac{v_{y'} + pu_b \sin\varphi}{\sqrt{v_{y'}^2 + p^2u_b^2 + 2\, v_{y'}\, pu_b \sin\varphi}} \varrho l^2 . \frac{v_{y'}^2 + p^2u_b^2 + 2\, v_{y'}\, pu_b \sin\varphi}{y'^2} \qquad \text{(III.3-13)}$$

With $l = \kappa y'$ this can be written as:

$$\tau'(t) = \varrho\, v_*^2 (1 + \xi \frac{u_o}{v} \sin\omega t \sin\varphi) . \sqrt{1 + \xi^2 \frac{u_o^2}{v^2} \sin^2\omega t + 2\,\xi \frac{u_o}{v} \sin\omega t \sin\varphi} \qquad \text{(III.3-14)}$$

So that:

$$\frac{\tau'(t)}{\tau_c} = (1 + \xi \frac{u_o}{v} \sin\omega t . \sin\varphi) . \sqrt{1 + \xi^2 \frac{u_o^2}{v^2} \sin^2\omega t + 2\,\xi \frac{u_o}{v} \sin\omega t \sin\varphi} \qquad \text{(III.3-15)}$$

in which $\xi = p\kappa C/g^{1/2}$.

The mean value can be obtained by means of integration over the wave period.

$$\frac{\tau'}{\tau_c} = \frac{2}{T} \int_{-\frac{T}{4}}^{+\frac{T}{4}} \left[(1 + \xi \frac{u_o}{v} \sin\omega t \sin\varphi) . \sqrt{1 + \xi^2 \frac{u_o^2}{v^2} \sin^2\omega t + 2\xi \frac{u_o}{v} \sin\omega t . \sin\varphi} \right] dt \qquad \text{(III.3-16)}$$

This integral is of the elliptic type and has been computed numerically. The results of this computation are given in figure III.3-3 for different values of φ. With the technique of the least squares the results of this calculation for the different values of φ can be given in the form:

$$\frac{\tau'}{\tau_c} = a + b\, (\xi \frac{u_o}{v})^c \qquad \text{(III.3-17)}$$

Although, for small values of $\xi\, u_o/v$, the value of τ'/τ_c should tend to "1", the closest approximation of the exact curve (III.3-16), by the

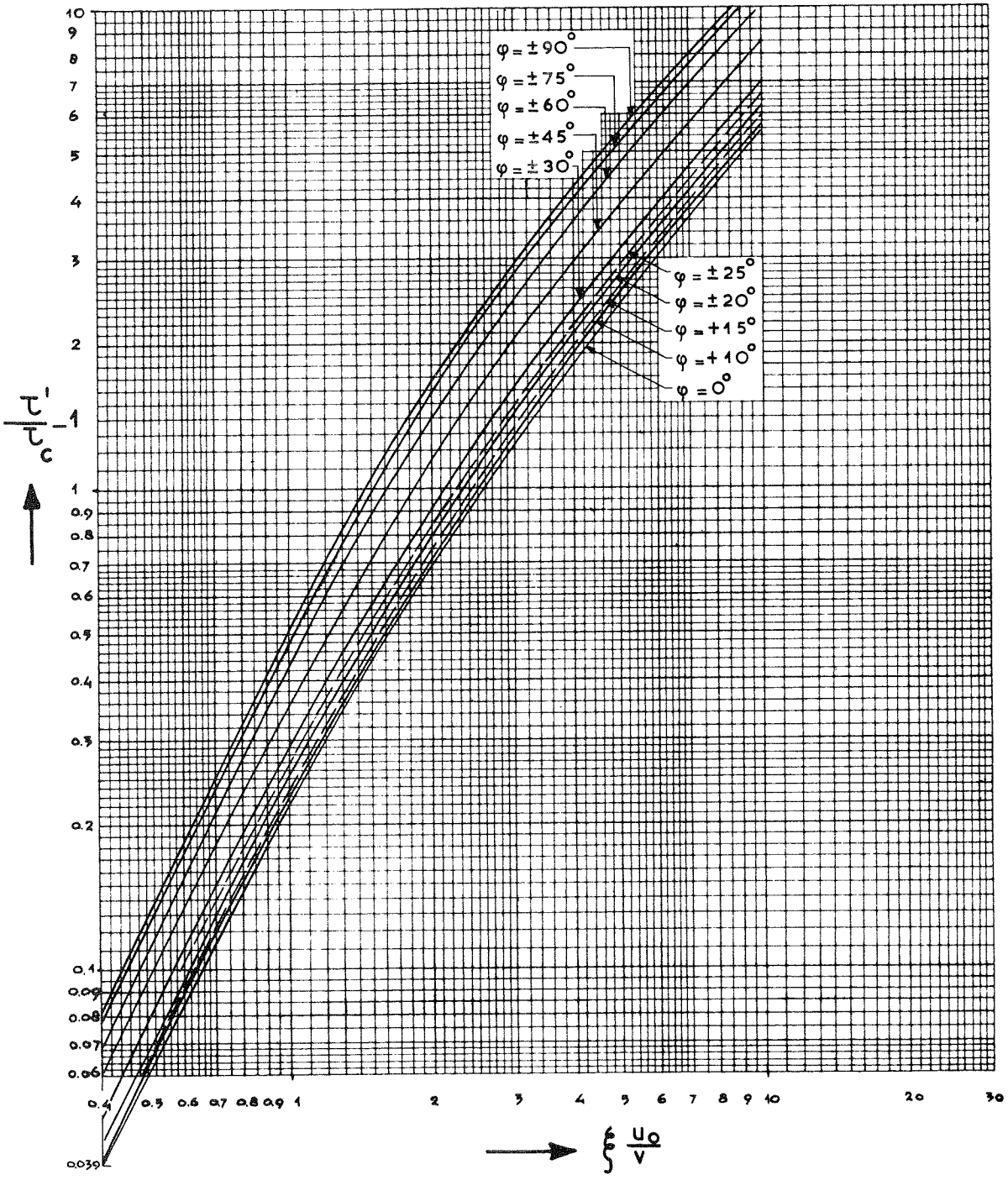

COMPUTED VALUES OF $\frac{\tau'}{\tau_c} = f(\xi \frac{u_o}{v})$

FIGURE III.3-3

approximated curve (III.3-17) will, for values of $\xi\, u_o/v > 1$, not necessarily lead to a value "a" which is equal to "1".
With a computer program the differences between the values of $\xi\, u_o/v$ according to equation (III.3-16) and according to equation (III.3-17) were minimized. The following results were obtained.

Table 1.

$$\frac{\tau'}{\tau_c} = 0.78 + 0.42 \left(\xi \frac{u_o}{v}\right)^{1.13} \qquad \varphi = 0^o$$

$$\frac{\tau'}{\tau_c} = 0.77 + 0.43 \left(\xi \frac{u_o}{v}\right)^{1.13} \qquad \varphi = 5^o$$

$$\frac{\tau'}{\tau_c} = 0.77 + 0.44 \left(\xi \frac{u_o}{v}\right)^{1.13} \qquad \varphi = 10^o$$

$$\frac{\tau'}{\tau_c} = 0.75 + 0.46 \left(\xi \frac{u_o}{v}\right)^{1.12} \qquad \varphi = 15^o$$

$$\frac{\tau'}{\tau_c} = 0.73 + 0.50 \left(\xi \frac{u_o}{v}\right)^{1.12} \qquad \varphi = 20^o$$

$$\frac{\tau'}{\tau_c} = 0.71 + 0.54 \left(\xi \frac{u_o}{v}\right)^{1.11} \qquad \varphi = 25^o$$

$$\frac{\tau'}{\tau_c} = 0.69 + 0.58 \left(\xi \frac{u_o}{v}\right)^{1.10} \qquad \varphi = 30^o$$

$$\frac{\tau'}{\tau_c} = 0.58 + 0.75 \left(\xi \frac{u_o}{v}\right)^{1.08} \qquad \varphi = 45^o$$

$$\frac{\tau'}{\tau_c} = 0.48 + 0.92 \left(\xi \frac{u_o}{v}\right)^{1.06} \qquad \varphi = 60^o$$

$$\frac{\tau'}{\tau_c} = 0.41 + 1.06 \left(\xi \frac{u_o}{v}\right)^{1.05} \qquad \varphi = 75^o$$

$$\frac{\tau'}{\tau_c} = 0.38 + 1.11 \left(\xi \frac{u_o}{v}\right)^{1.04} \qquad \varphi = 90^o$$

In figure III.3-4, 5 and 6 the actually calculated and the approximated values are given for $\varphi = 0^o$, 15^o and 45^o. Normally the angle between wave crests and current along the coast will not exceed 20^o. The relationship between τ'/τ_c and $\xi\, u_o/v$ can be written for values of $0 < \varphi < 20^o$, with good approximation as:

$$\frac{\tau'}{\tau_c} = 0.75 + 0.45 \left(\xi \frac{u_o}{v}\right)^{1.13} \qquad \text{(III.3-18)}$$

In figure III.3-7 this line is given together with the actual results of $\varphi = 0^o$, 10^o and 20^o.

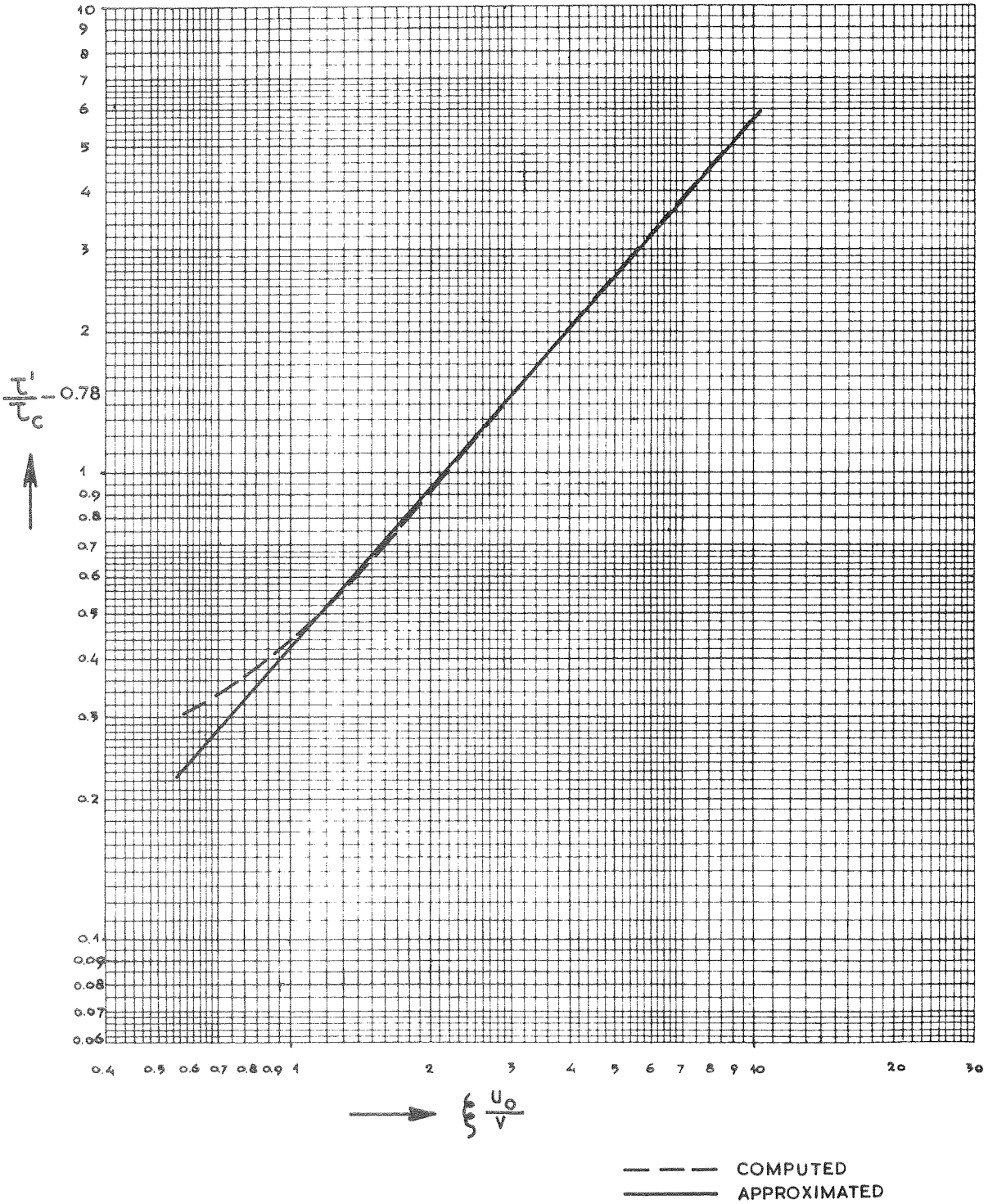

COMPUTED AND APPROXIMATED VALUES OF

$\frac{\tau'}{\tau_c} = f\left(\xi \frac{u_o}{v}\right)$ FOR $\varphi = 0°$

FIGURE III . 3_4

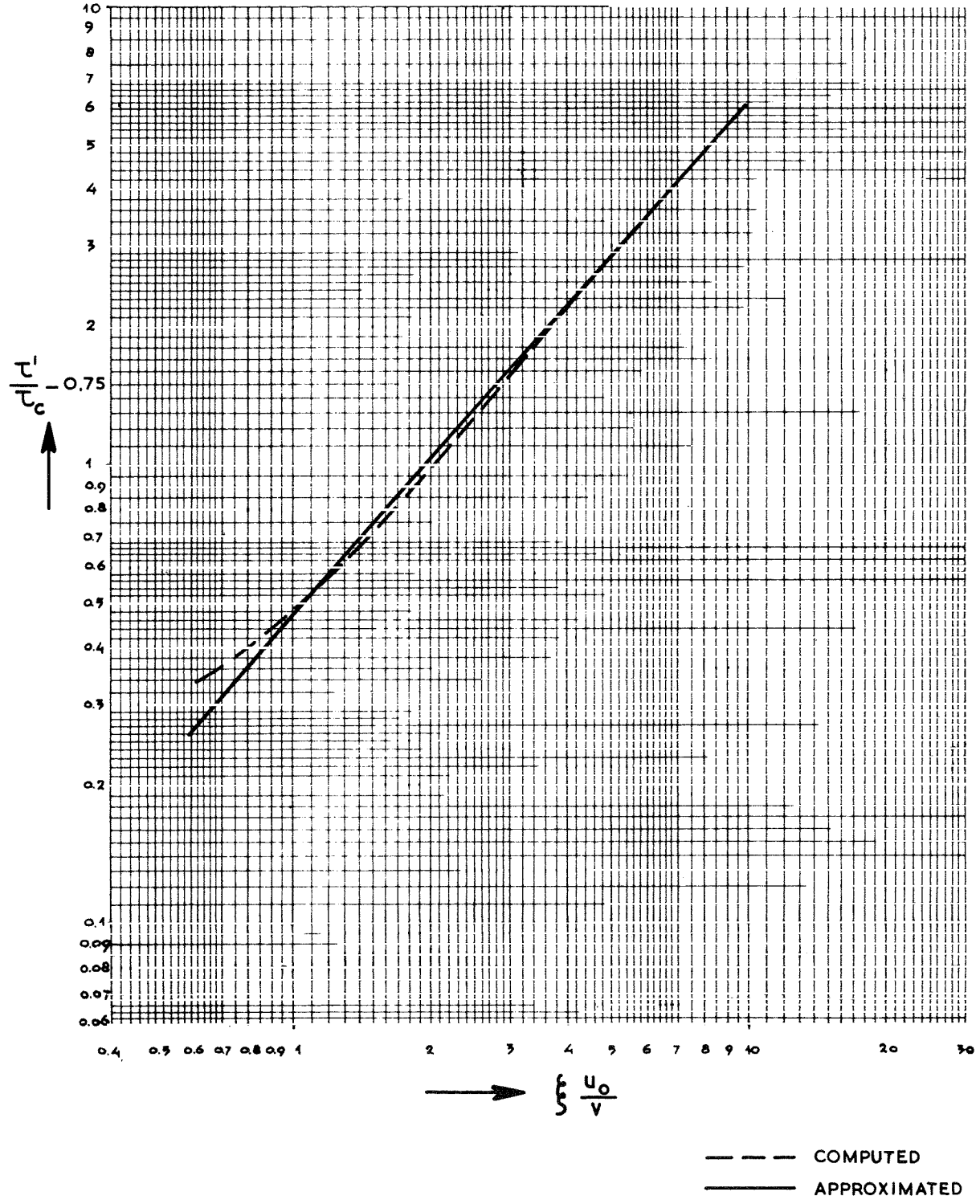

COMPUTED AND APPROXIMATED VALUES OF $\frac{\tau'}{\tau_c} = f\left(\xi \frac{u_o}{v}\right)$ FOR $\varphi = 15°$

FIGURE III.3_5

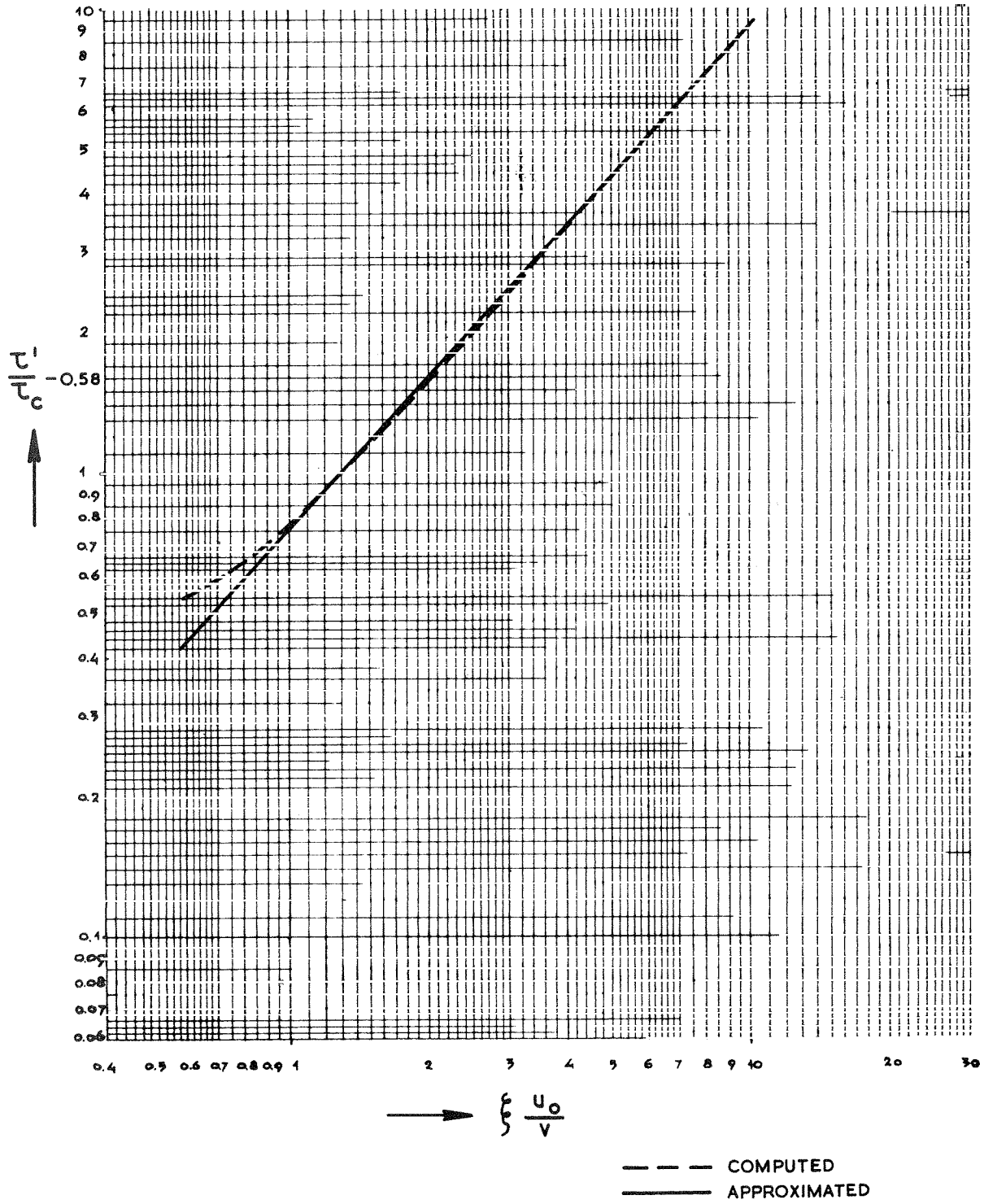

COMPUTED AND APPROXIMATED VALUES OF

$\frac{\tau'}{\tau_c} = f\left(\xi \frac{u_o}{v}\right)$ FOR $\varphi = 45°$

FIGURE III .3_6

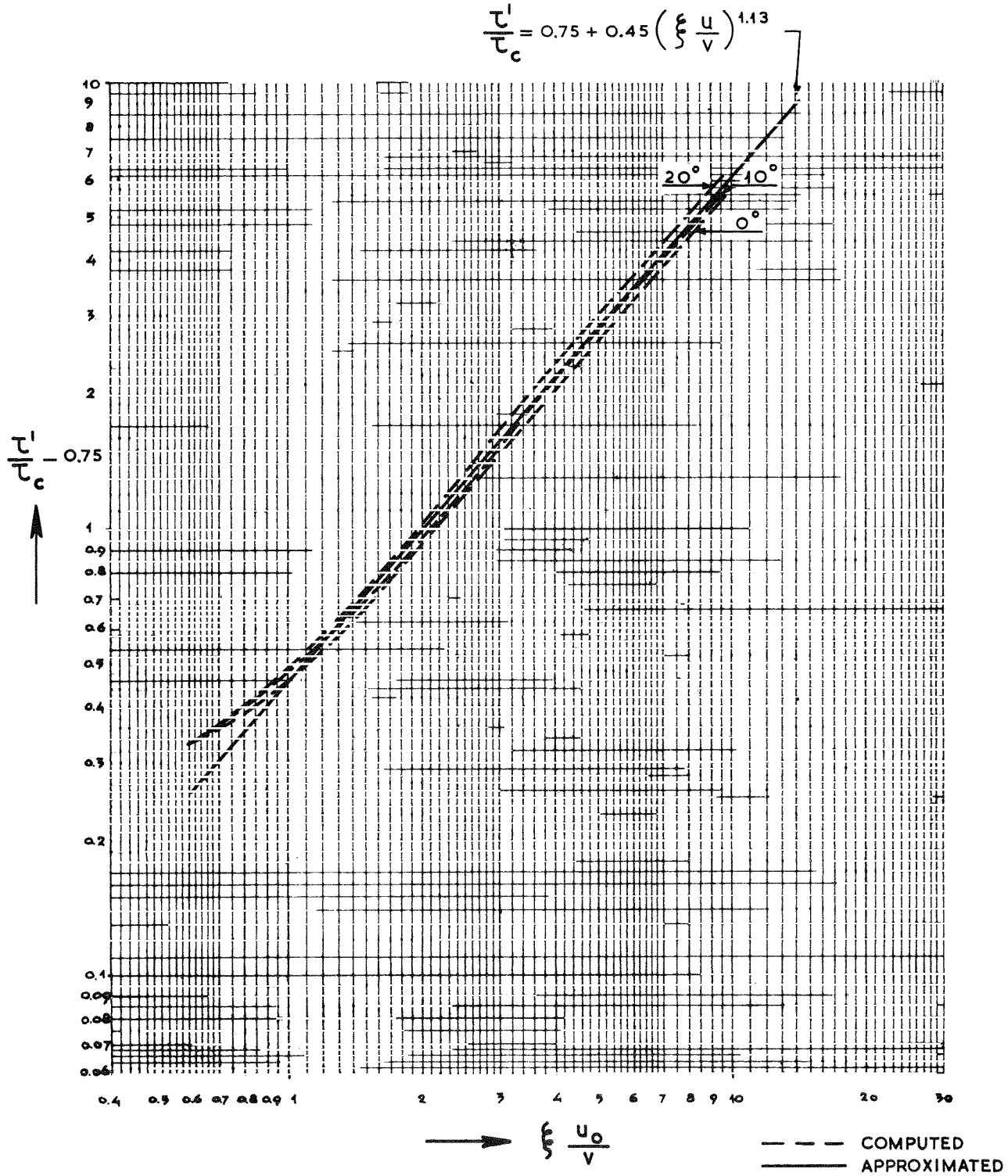

$\frac{\tau'}{\tau_c} = 0.75 + 0.45\left(\xi \frac{u_o}{v}\right)^{1.13}$ COMPARED WITH COMPUTED VALUES

FIGURE III . 3_7

In order to be able to predict the value of τ'/τ_c for greater variations of φ, the results will also be represented in the form of:

$$\left(\frac{\tau'}{\tau_c} - 1\right) = N \left(\xi \frac{u_o}{v}\right)^{1.5} \qquad \text{(III.3-19)}$$

where N is a function of φ.
The values of N are determined by tracing straight lines with a slope of 1.5 on double logarithmic paper as close as possible to the "exact" curves representing the computed results. The slope of 1.5 has been chosen because straight lines with this slope come closest to the "exact" curves. The value of 1.5 is, therefore, purely empirical. This is shown in figures III.3-8 and 9 for $\varphi^o = 0$ and 15^o. By this procedure the values of N for all values of φ are determined.

The value of N can be written as:

$$N = 0.36 - 0.14 \cos 2\varphi \qquad \text{(III.3-20)}$$

and is shown on figure III.3-10.

Bed shear at right angles to the current

As is demonstrated by figure III.3-2, a resultant bed shear component will occur at right angles to the direction of the current when the wave crests make an angle with the current direction, hence for values of $\varphi \neq o$. When the component of wave propagation parallel to the current direction is opposing the current, the additional shear component τ'' will be against the direction of wave propagation. When the component of wave propagation parallel to the current direction is pointed in the same direction as the current, the extra shear component will point in the direction of wave propagation.

The component of the bed shear at right angles to the main current can be written as:

$$\tau''(t) = \varrho v_*^2 \, \xi \frac{u_o}{v} \sin \omega t \cos \varphi . \sqrt{1 + \xi^2 \frac{u_o^2}{v^2} \sin^2 \omega t + 2 \xi \frac{u_o}{v} \sin \omega t \sin \varphi} \, , \qquad \text{(III.3-21)}$$

so that the mean value over the wave period may be written as:

$$\frac{\tau''}{\tau_c} = \frac{2}{T} \int_{-\frac{T}{4}}^{+\frac{T}{4}} \left[\xi \frac{u_o}{v} \sin \omega t \cos \varphi . \sqrt{1 + \xi^2 \frac{u_o^2 \sin^2 \omega t}{v^2} + 2 \xi \frac{u_o}{v} \sin \omega t \sin \varphi} \right] dt \qquad \text{(III.3-22)}$$

$$\frac{\tau'}{\tau_c} = \frac{2}{T}\int_{-T/4}^{T/4} \sqrt{1 + \xi^2 \frac{u_o^2}{v^2}\ \sin^2 \omega t}\ dt$$

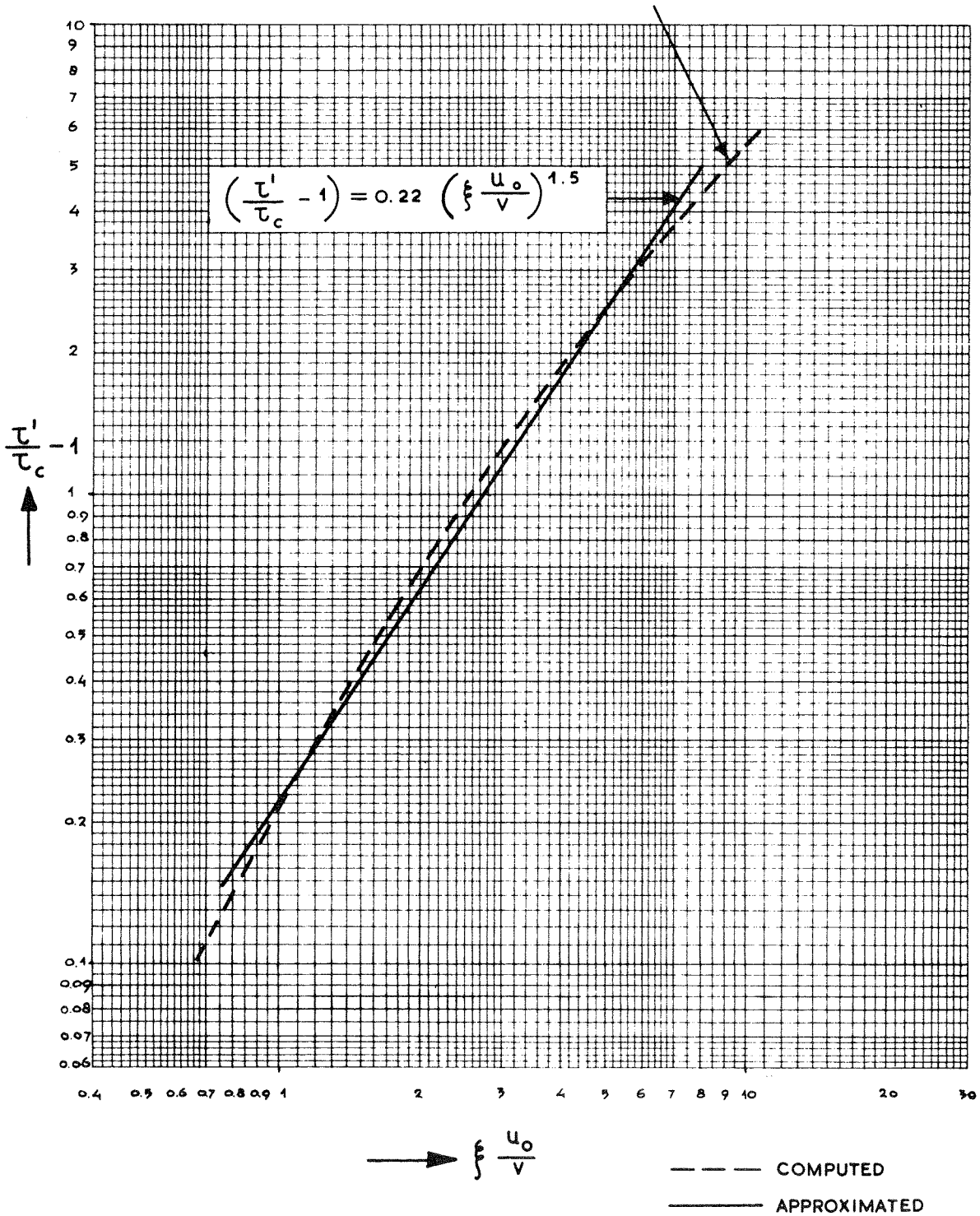

$\left(\frac{\tau'}{\tau_c} - 1\right)$ VERSUS $\left(\xi \frac{u_o}{v}\right)$ FOR $\varphi = 0°$

FIGURE III. 3-8

$$\frac{\tau'}{\tau_c} = \frac{2}{T}\int_{-T/4}^{+T/4}\left[\left(1+\xi\frac{u_o}{V}\sin\omega t\sin\varphi\right)\sqrt{1+\xi^2\frac{u_o^2}{V^2}\sin^2\omega t+2\xi\frac{u_o}{V}\sin\omega t\sin\varphi}\right]dt$$

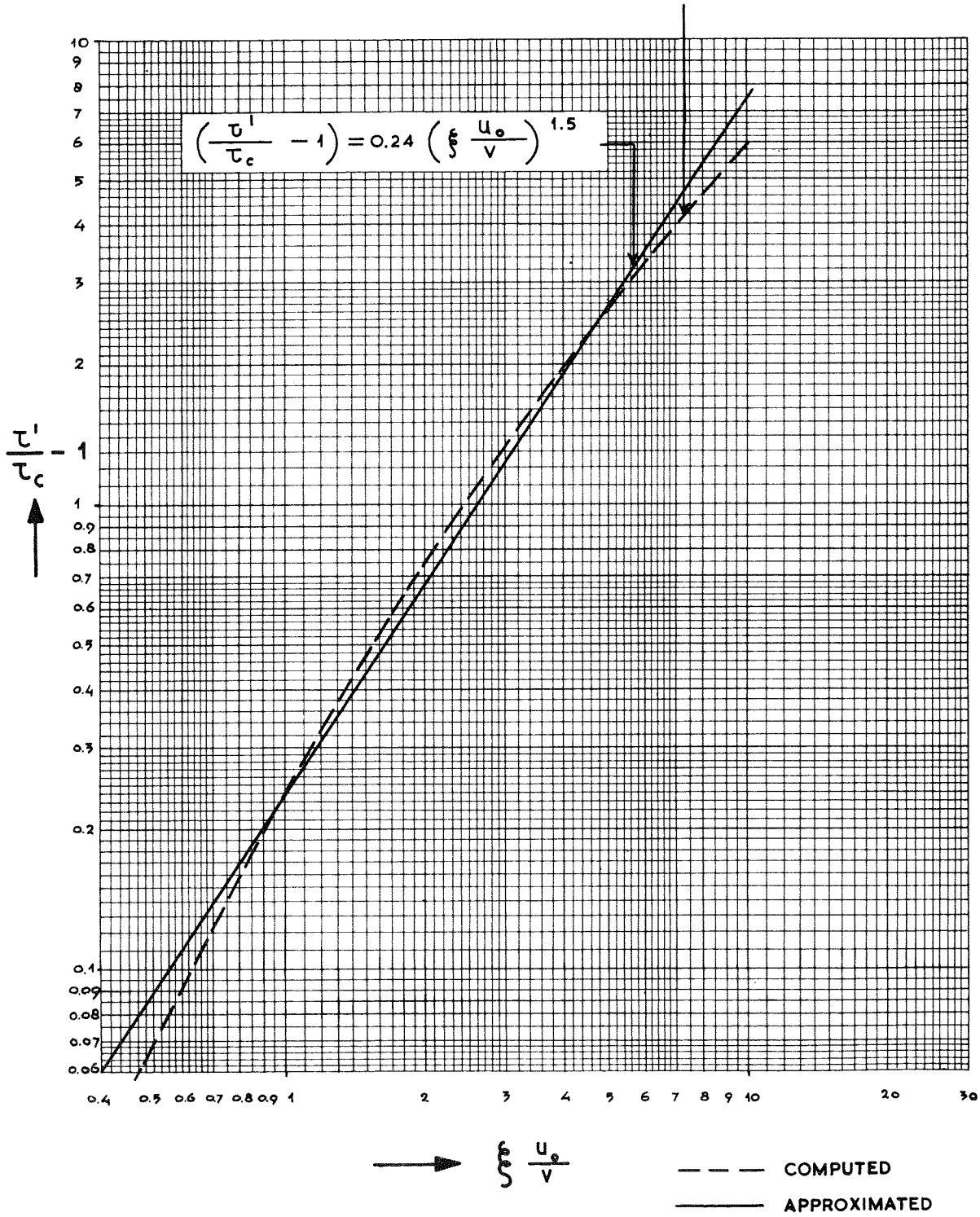

$\left(\frac{\tau'}{\tau_c}-1\right)$ VERSUS $\left(\xi\frac{u_o}{V}\right)$ FOR $\varphi = 15°$

FIGURE III . 3_9

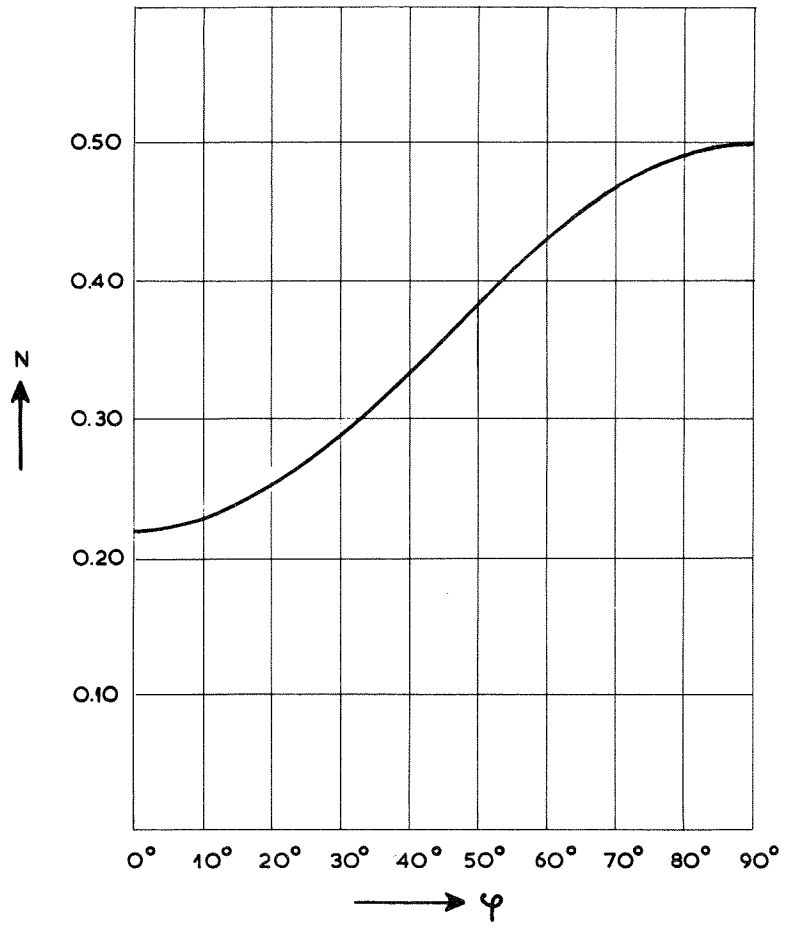

N VERSUS φ FOR τ'

FIGURE III. 3-10

This elliptical integral has been computed also numerically, and the results are given in figure III.3-11. The results have been given also in the form:

$$\frac{\tau''}{\tau_c} = a + b\,(\xi \frac{u_o}{v})^c \qquad \text{(III.3-23)}$$

with the technique of the least squares. Although, for small values of $\xi\, u_o/v$, the value of τ''/τ_c should tend to "0", the closest approximation of the exact curve (III.3-22), by the approximated curve (III.3-23) will, for values of $\xi\, u_o/v > 1$, not necessarily lead to a value of "a" which is equal to "0".
Again the differences between the values of $\xi\, u_o/v$ according to equation (III.3-22) and according to equation (III.2-23) were minimized. The results are given in table 2.

Table 2

$$\frac{\tau''}{\tau_c} = -0.01 + 0.01\,(\xi \frac{u_o}{v})^{0.99} \qquad \varphi = 1^o$$

$$\frac{\tau''}{\tau_c} = -0.03 + 0.06\,(\xi \frac{u_o}{v})^{0.99} \qquad \varphi = 5^o$$

$$\frac{\tau''}{\tau_c} = -0.05 + 0.12\,(\xi \frac{u_o}{v})^{0.98} \qquad \varphi = 10^o$$

$$\frac{\tau''}{\tau_c} = -0.07 + 0.17\,(\xi \frac{u_o}{v})^{0.98} \qquad \varphi = 15^o$$

$$\frac{\tau''}{\tau_c} = -0.09 + 0.22\,(\xi \frac{u_o}{v})^{0.98} \qquad \varphi = 20^o$$

$$\frac{\tau''}{\tau_c} = -0.11 + 0.26\,(\xi \frac{u_o}{v})^{0.98} \qquad \varphi = 25^o$$

$$\frac{\tau''}{\tau_c} = -0.13 + 0.30\,(\xi \frac{u_o}{v})^{0.98} \qquad \varphi = 30^o$$

$$\frac{\tau''}{\tau_c} = -0.15 + 0.36\,(\xi \frac{u_o}{v})^{0.97} \qquad \varphi = 45^o$$

$$\frac{\tau''}{\tau_c} = -0.12 + 0.32\,(\xi \frac{u_o}{v})^{0.96} \qquad \varphi = 60^o$$

$$\frac{\tau''}{\tau_c} = -0.06 + 0.18\,(\xi \frac{u_o}{v})^{0.95} \qquad \varphi = 75^o$$

$$\frac{\tau''}{\tau_c} = -0.004 + 0.013\,(\xi \frac{u_o}{v})^{0.95} \qquad \varphi = 89^o$$

In figure III.3-12 the actual values of the integral and the minimized

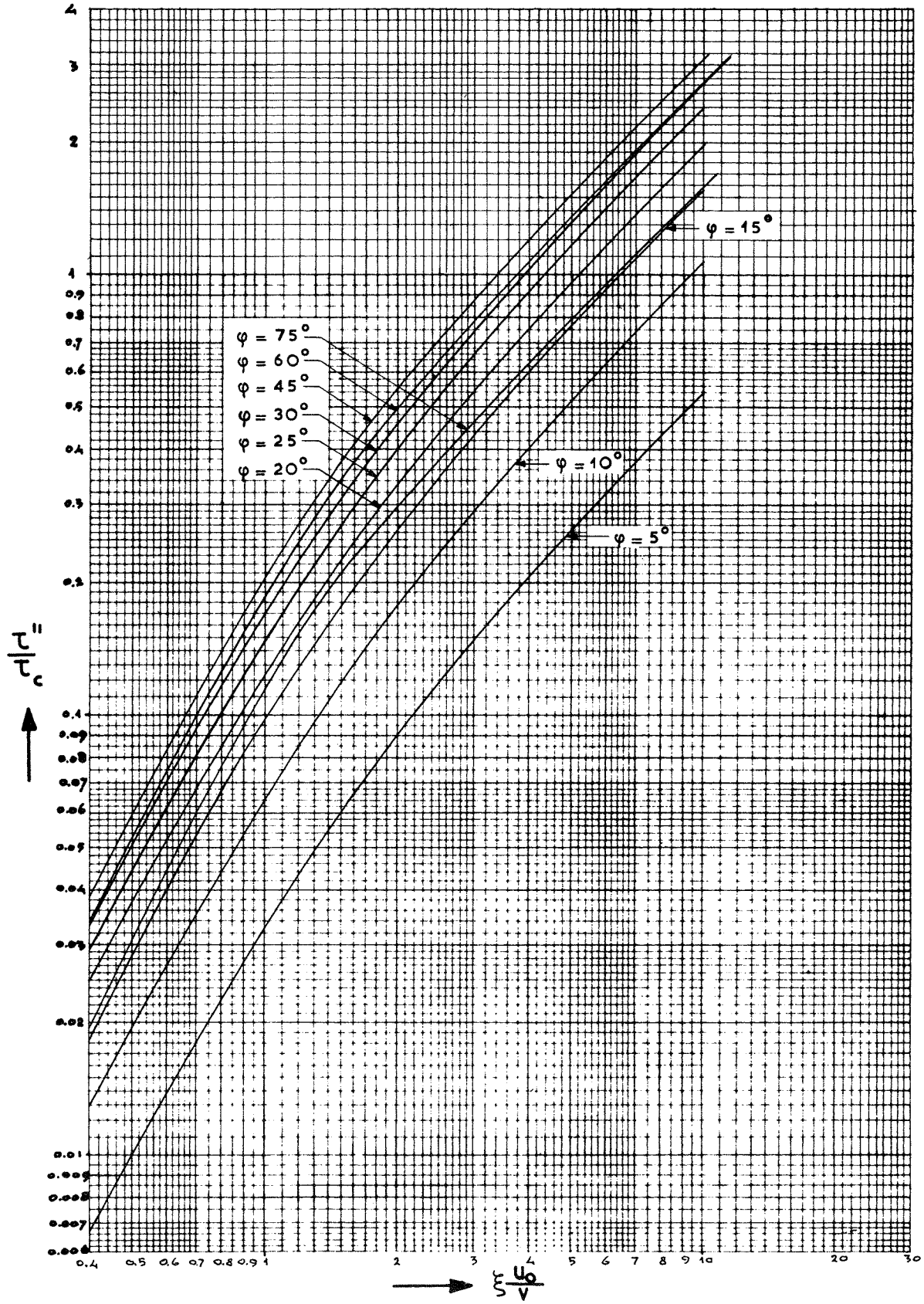

COMPUTED VALUES OF $\frac{\tau''}{\tau_c} = f\left(\xi \frac{u_0}{v}\right)$

FIGURE III. 3_11

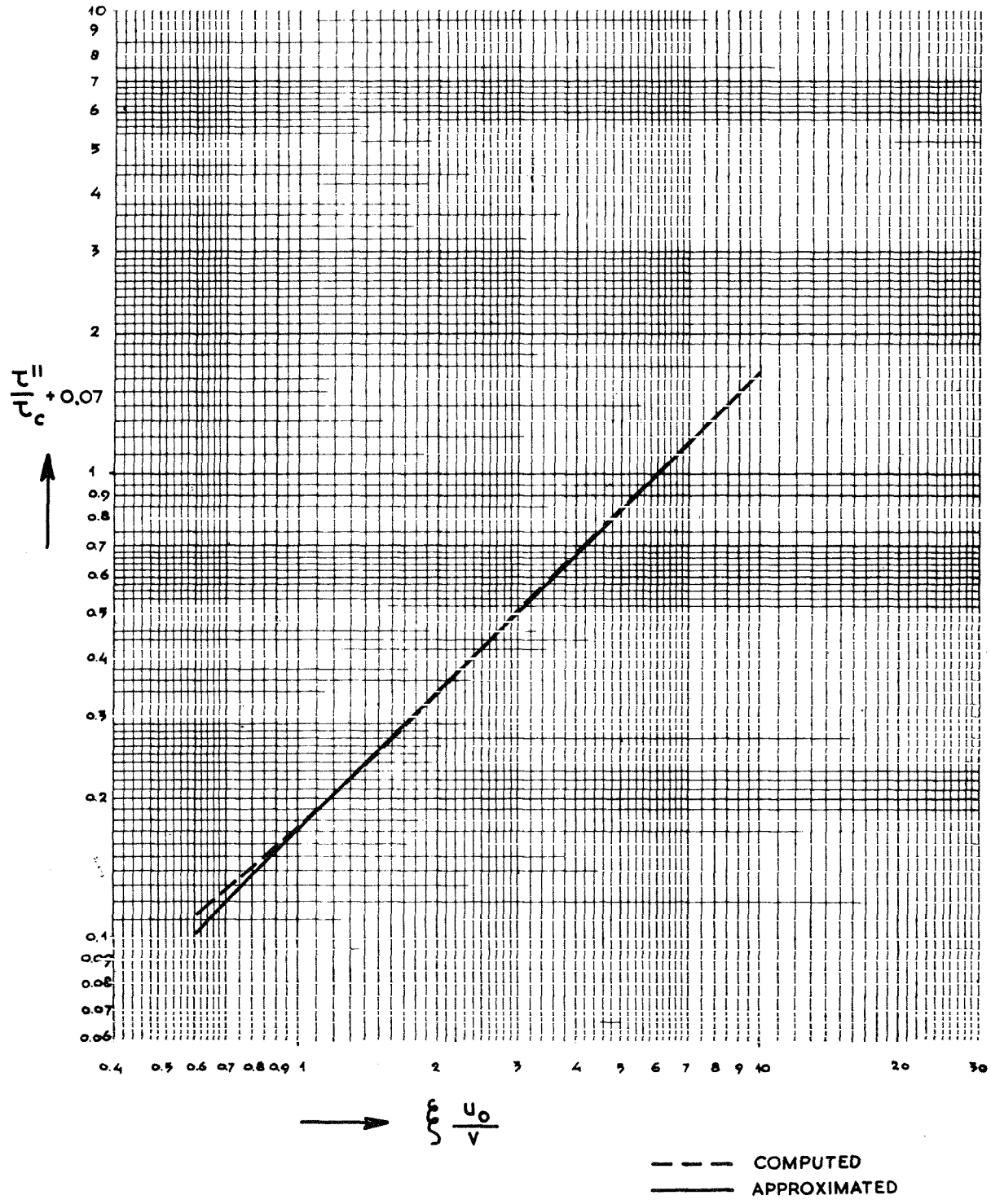

COMPUTED AND APPROXIMATED VALUES OF

$\frac{\tau''}{\tau_c} = f\left(\xi \frac{u_o}{v}\right)$ FOR $\varphi = 15°$

FIGURE III.3_12

values are given for $\varphi = 15^{o}$. For values of $0^{o} < \varphi < 15^{o}$, the results can be written as:

$$\frac{\tau''}{\tau_c} = \varphi \left(- 0.3 + 0.7 \left(\xi \frac{u_o}{v}\right)^{0.98}\right) \qquad \text{(III.3-24)}$$

with φ in radians.

Also in this case one formula which gives all results for varying values of φ has been derived. This formula will be of the form:

$$\frac{\tau''}{\tau_c} = M \left(\xi \frac{u_o}{v}\right)^{1.25} \qquad \text{(III.3-25)}$$

where M is a function of φ.
M is determined in the same way as N. Also in this case the coefficient 1.25 is purely empirical. The straight lines do not follow the curves as well as for the curves of τ'/τ_c. An example is given in figure III.3-13.

The value of M can be written as

$$M = 0.205 \sin 2\varphi \qquad \text{(III.3-26)}$$

and is shown in figure III.3-14.

The total bed shear

The mean value of the ratio between the total bed shear and the bed shear due to current only can be written according to the same derivation as:

$$\frac{\tau_r}{\tau_c} = \frac{2}{T} \int_{-\frac{T}{4}}^{+\frac{T}{4}} \left(1 + \xi^2 \frac{u_o^2}{v^2} \sin^2\omega t + 2\xi \frac{u_o}{v} \sin \omega t \sin \varphi\right) dt = \left(1 + \frac{1}{2} \xi^2 \frac{u_o^2}{v^2}\right) \qquad \text{(III.3-27)}$$

Equation (III.3-16) which gives τ'/τ_c as $f(\varphi, \xi\, u_o/v)$ gives for $\varphi = 90^{o}$, in which case τ' coincides with τ_r, a different value from equation (III.3-27). The reason is that for τ_r the integration is executed for the absolute value of τ_r, where for the calculation of τ' the direction of τ is taken into consideration. This is elucidated in figure III.3-15 where the variation of τ' and τ_r is indicated during the wave period. From this it is evident that this discrepancy occurs only when $p u_o > v_{y'}$. The formulae which give τ'/τ_c as $f(\xi\, u_o/v)$ are obtained for values of $\xi\, u_o/v$ ranging from 0.6 to 10. From the line $\tau'/\tau_c = f(\xi\, u_o/v)$ for $\varphi = 90^{o}$ on figure III.3-3, it is evident that for values of $\xi\, u_o/v < 1$ the function is $(\tau'/\tau_c) - 1 = \frac{1}{2} (\xi\, u_o/v)^2$ which is the same as for the resultant bed

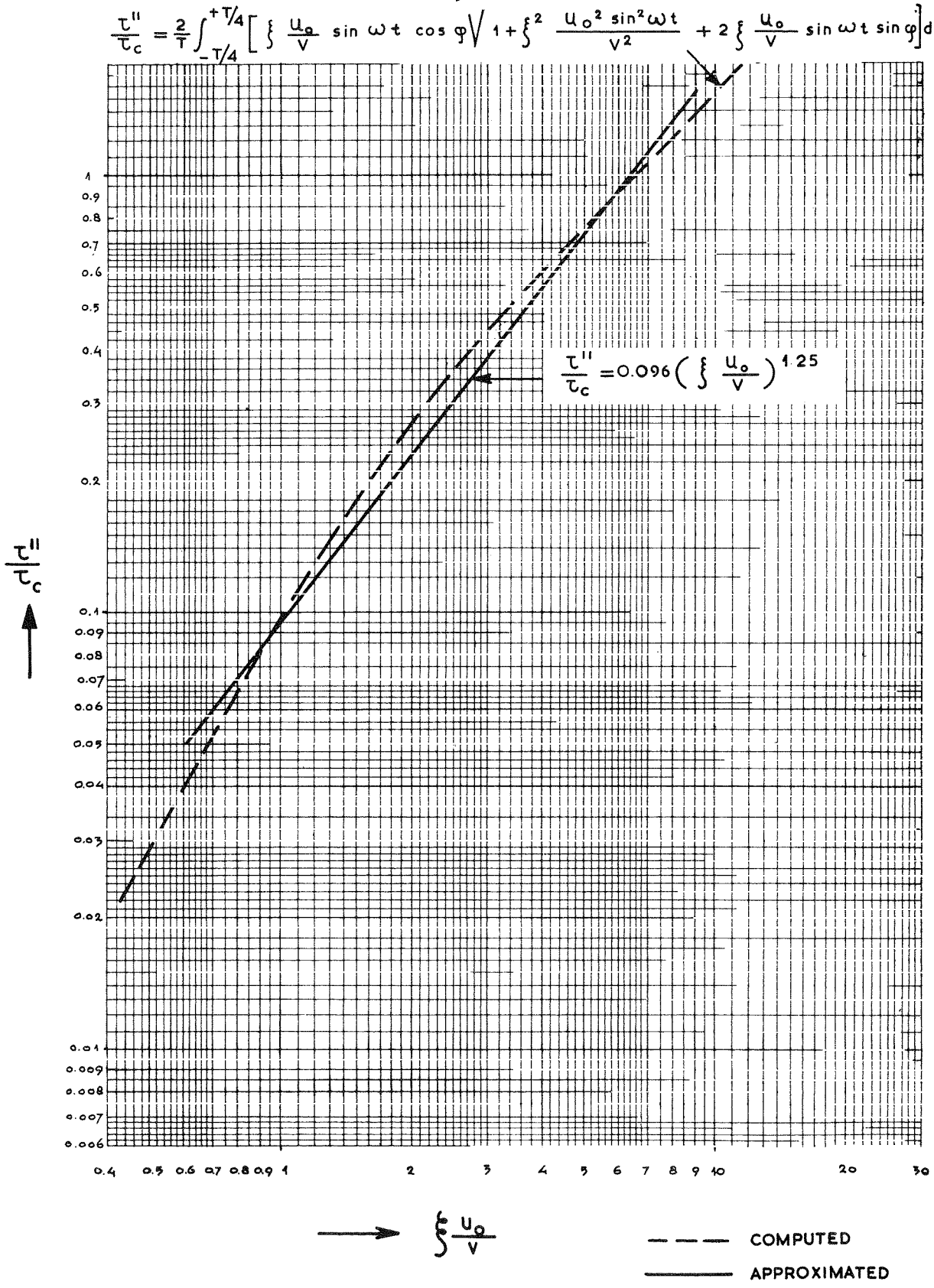

$\frac{\tau''}{\tau_c}$ = VERSUS $\left(\xi\frac{u_o}{v}\right)$ FOR $\varphi = 15°$

FIGURE III.3_13

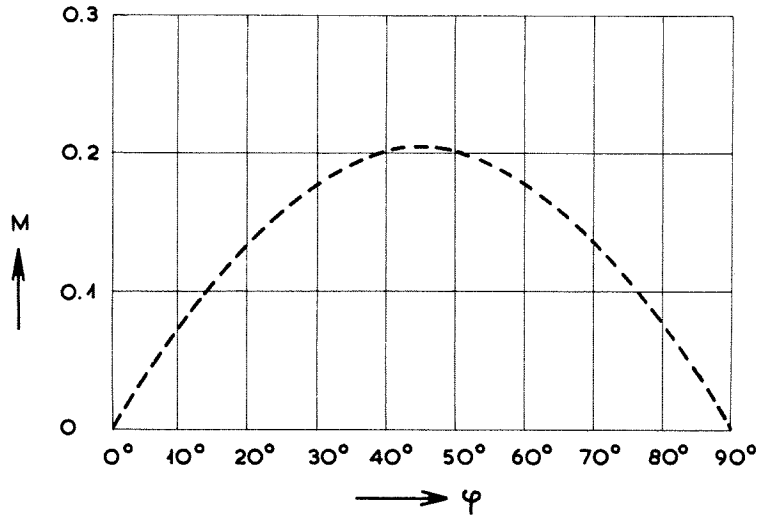

M VERSUS φ FOR τ^{II}

FIGURE III. 3-14

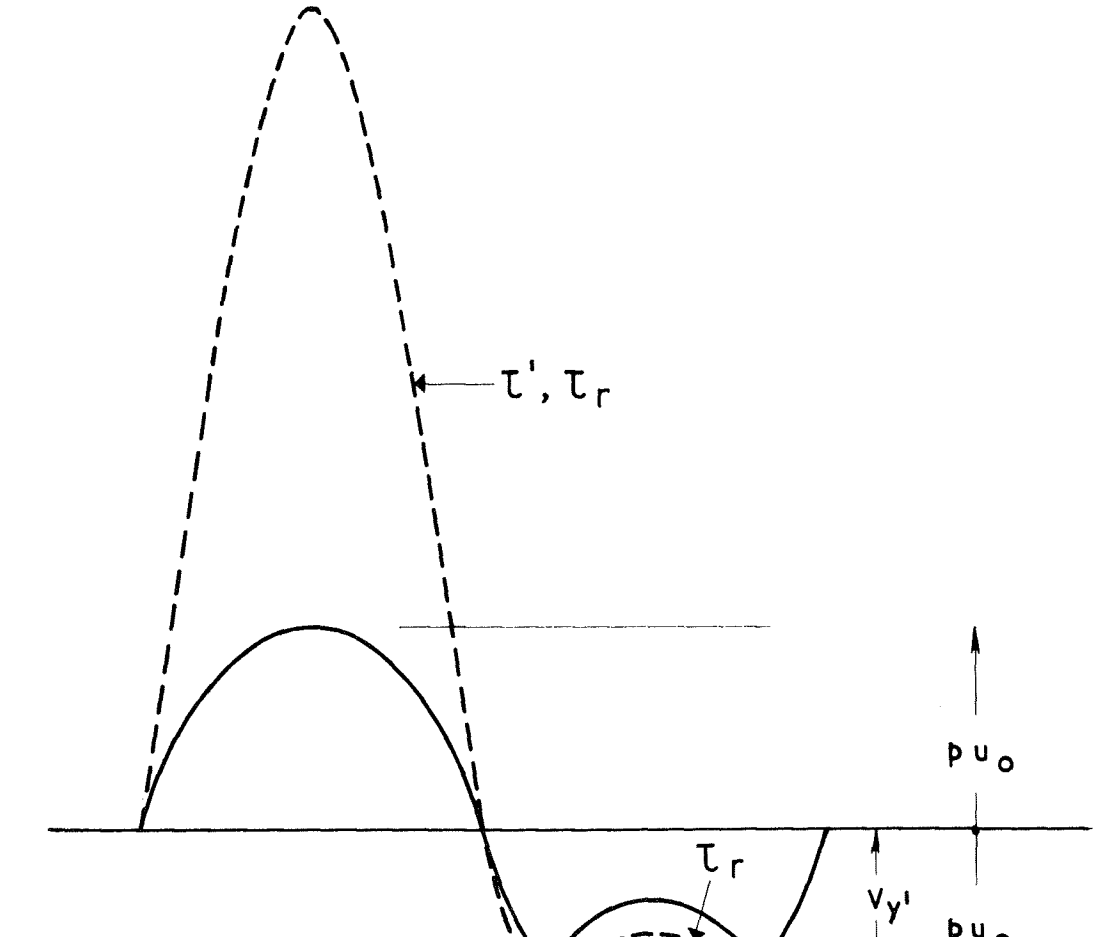

VALUES OF τ_r AND τ' AS $f(t)$ FOR $\varphi = 90^\circ$

FIGURE III . 3_15

shear τ_r.

No attempt is made to derive two separate formulae for the regions $\xi\, u_o/v > 1$ and $\xi\, u_o/v < 1$ because for the derivation of the scale laws the exact values of the coefficients a, b and c are not very important, and in most cases, studied here, the value of $\xi\, u_o/v$ will just be around "1".

III.4. Elaboration of the measurements

The measurements were executed for $\varphi = 0^o$ and $\varphi = 15^o$. In the case where $\varphi = 0^o$, viz. direction of current and wave propagation normal to each other, firstly tests were carried out with waves of 1.57 s period. Two different bed conditions were used, namely a bed covered with stones with a mean diameter of 3 to 4 cm and a sand bed covered by ripples of some cm's height. Afterwards some tests were conducted with $\varphi = 0^o$ and a wave period of 0.68 sec. In this case the bed consisted of a sand layer covered by ripples. The tests with $\varphi = 15^o$ were performed with two wave periods, viz. 0.68 and 2 sec. In this case the sand bed was covered also by ripples.

For the computation of the bed shear with $\varphi = 15^o$, the influence of the stream refraction has to be taken into account. Due to this stream refraction, the angle φ was increased to about 16^o and the orbital velocity at the bottom was increased by about 10 to 25%. All data have been corrected for this effect. The results of the measurements and these corrections are given in tables 3 through 7. With the results of these measurements the value of p in $\xi = p\,\kappa C/g^{1/2}$ has been determined. For the calculation of p the formula $\tau'/\tau_c = a + b\,(\xi\, u_o/v)^c$, as derived in paragraph III.3, was used. The values of a, b and c were chosen for the relevant values of φ, as given in table 1. As these values change only slowly with varying φ, no corrections on a, b and c due to stream refraction are necessary. The values of τ'/τ_c and $\kappa C\, u_o/vg^{1/2} = p^{-1}\, \xi\, u_o/v$ which result from the measurements are given in the tables 3 through 7.

With the technique of the least squares p has been determined with minimization over the least accurate value, τ'/τ_c. The results are given in table 8.

Finally all results as given in tables 3 through 7 are plotted in figure III.4-1. Equation (III.3-17) is written for this purpose as:

$$\frac{\frac{\tau'}{\tau_c} - a}{b} = \left(\xi\, \frac{u_o}{v}\right)^c \qquad \text{(III.4-1)}$$

TABLE 3

Series I Bottom with stones $\varphi = 0^{o}$ T = 1.57 s

Test	d m	v m/s	H m	u_o m/s	I 10^{-4}	C $m^{1/2}/s$	r 10^{-2} m	τ'/τ_c	$\frac{C\kappa}{\sqrt{g}} \frac{u_o}{v}$
121	0.20	0.10			0.39	36	2.4		
121g	0.20	0.10	0.036	0.11	0.64			1.62	5.2
122	0.21	0.19			1.45	34	3.3		
122g	0.21	0.19	0.036	0.11	1.90			1.31	2.5
124*	0.35	0.21			1.00	36	4.2		
124*g	0.35	0.21	0.068	0.15	1.58			1.57	3.2
124	0.33	0.30			2.04	36	4.0		
124g	0.33	0.30	0.066	0.15	2.73			1.34	2.3
126	0.19	0.21			2.24	32	3.8		
126g	0.19	0.21	0.022	0.07	2.66			1.18	1.44
101	0.19	0.22			2.56	31	4.4		
101g	0.19	0.22	0.026	0.08	2.96			1.15	1.56
101*	0.20	0.21			2.91	28	6.7		
101*g	0.20	0.21	0.026	0.08	3.24			1.11	1.40
102	0.21	0.24			2.57	33	3.7		
102g	0.21	0.24	0.028	0.09	3.02			1.17	1.46
103	0.32	0.21			0.89	39	2.8		
103g	0.32	0.21	0.034	0.08	1.06			1.19	1.90
104	0.32	0.25			1.34	38	2.8		
104g	0.32	0.25	0.038	0.09	1.56			1.16	1.72
105	0.36	0.24			0.84	44	1.8		
105g	0.36	0.24	0.047	0.10	1.06			1.29	2.3
106	0.36	0.27			1.17	42	2.0		
106g	0.36	0.27	0.044	0.09	1.40			1.19	1.84
114	0.31	0.25			1.95	32	6.2		
114g	0.31	0.25	0.060	0.14	2.41			1.24	2.3
115	0.35	0.14			0.36	39	2.9		
115g	0.35	0.14	0.066	0.14	0.64			1.78	5.2
116	0.35	0.27			1.60	36	4.2		
116g	0.35	0.27	0.066	0.14	2.18			1.36	2.4

TABLE 4

Series II Sandbottom with ripples $\varphi = 0^{o}$ T = 1.57 s

Test	d	v	H	u_o	I	C	r	τ'/τ_c	$\frac{C\kappa}{\sqrt{g}}\frac{u_o}{v}$
	m	m/s	m	m/s	10^{-4}	$m^{1/2}/s$	10^{-3} m		
312*	0.20	0.13			0.22	62	0.9		
312*g	0.20	0.13	0.037	0.12	0.69			3.14	7.0
314	0.21	0.28			1.28	54	2.5		
314g	0.21	0.28	0.043	0.13	2.17			1.69	3.2
315	0.21	0.40			4.24	45	7.9		
315g	0.21	0.40	0.043	0.13	5.29			1.25	1.82
316	0.30	0.12			0.12	63	0.8		
316g	0.30	0.12	0.058	0.14	0.39			3.25	9.2
316*	0.30	0.12			0.12	63	0.8		
316*g	0.30	0.12	0.058	0.14	0.34			2.83	9.2
317	0.30	0.21			0.43	59	1.9		
317g	0.30	0.21	0.056	0.13	0.82			1.91	4.8
318	0.30	0.30			1.03	54	3.6		
318g	0.30	0.30	0.055	0.13	1.66			1.61	3.0
319	0.30	0.40			2.66	50	6.0		
319g	0.30	0.40	0.064	0.15	3.65			1.37	2.4
320	0.38	0.15			0.12	70	0.6		
320g	0.38	0.15	0.073	0.15	0.37			3.08	8.6
322	0.38	0.31			0.91	53	5.2		
322g	0.38	0.31	0.075	0.15	1.48			1.62	3.3
300	0.20	0.13			0.27	56	1.8		
300g	0.20	0.13	0.025	0.08	0.43			1.59	4.3
302*	0.20	0.30			1.50	55	2.1		
302*g	0.20	0.30	0.022	0.07	1.75			1.17	1.61
302	0.20	0.31			1.64	54	2.4		
302g	0.20	0.31	0.023	0.07	2.02			1.23	1.65
303	0.20	0.37			4.27	40	14.5		
303g	0.20	0.37	0.023	0.07	4.58			1.07	1.02
304	0.30	0.13			0.14	64	1.0		
304g	0.30	0.13	0.026	0.06	0.20			1.43	3.8
306	0.30	0.33			0.79	68	0.6		
306g	0.30	0.33	0.028	0.07	0.92			1.16	1.74
306*	0.30	0.33			0.89	64	1.0		
306*g	0.30	0.33	0.028	0.07	1.21			1.36	1.64
307	0.30	0.39			2.33	47	8.8		
307g	0.30	0.39	0.034	0.08	2.70			1.16	1.26
310	0.38	0.32			0.52	72	0.5		
310g	0.38	0.32	0.045	0.09	0.87			1.67	2.6

TABLE 5

Series III Sandbottom with ripples $\varphi = 0^{o}$ T = 0.68

Test	d	v	H	u_o	I	C	r	τ'/τ_c	$\frac{C\,\varkappa}{\sqrt{g}}\frac{u_o}{v}$
	m	m/s	m	m/s	10^{-4}	$m^{1/2}/s$	10^{-3} m		
357	0.12	0.29			6.04	34	18.6		
357g	0.12	0.29	0.030	0.09	6.99			1.16	1.29
358	0.14	0.32			9.35	28	43		
358g	0.14	0.32	0.034	0.09	9.76			1.04	0.99
362	0.20	0.39			6.64	34	33.8		
362g	0.20	0.39	0.047	0.07	7.38			1.12	0.76
365*	0.30	0.30			1.37	47	9.0		
365*g	0.30	0.30	0.065	0.04	1.52			1.10	0.81
356	0.12	0.21			0.988	62	0.55		
356g	0.12	0.21	0.040	0.12	1.54			1.56	4.4
355	0.12	0.10			0.168	71	0.16		
355g	0.12	0.10	0.038	0.11	0.431			2.56	9.8
360	0.20	0.22			0.519	70	0.31		
360g	0.20	0.22	0.052	0.08	0.865			1.67	3.1
359	0.20	0.12			0.124	76	0.13		
359g	0.20	0.12	0.054	0.08	0.324			2.63	6.8

TABLE 6

Series IV Sandbottom with ripples $\varphi = 15^{\circ}$ T = 0.68 s

Test	d m	v m/s	H m	u_o m/s	u_o corr. m/s	φ corr.	I 10^{-4}	C $m^{1/2}/s$	r 10^{-3} m	$\frac{\tau'}{\tau_c}$	$\frac{\kappa C}{\sqrt{g}} \frac{u_o}{v}$ corr.
340*	0.20	0.14					0.36	52	3		
340*g	0.20	0.14	0.058	0.09	0.10	16°	0.70			1.96	4.7
341*	0.20	0.25					2.04	39	16		
341*g	0.20	0.25	0.056	0.08	0.12	16°47'	2.56			1.26	2.6
343*	0.27	0.16					0.26	61	1.3		
343*g	0.27	0.16	0.065	0.06	0.06	16°14'	0.44			1.72	3.2
342*	0.20	0.35					5.08	35	28		
342*g	0.20	0.35	0.052	0.08	0.10	17°33'	5.69			1.12	1.3
349	0.13	0.10					0.35	47	3.9		
349g	0.13	0.10	0.038	0.10	0.11	15°33'	0.60			1.71	6.6
350	0.20	0.11					0.18	59	1.3		
350g	0.20	0.11	0.062	0.09	0.10	15°46'	0.25			1.46	7.1
351	0.27	0.11					0.13	58	2.0		
351g	0.27	0.11	0.063	0.05	0.06	15°49'	0.23			1.72	4.1
343	0.27	0.16					0.36	51	5.4		
343g	0.27	0.16	0.065	0.06	0.06	16°14'	0.44			1.20	2.7
344	0.27	0.25					1.03	47	8.0		
344g	0.27	0.25	0.063	0.05	0.07	16°53'	1.28			1.25	1.68
340	0.20	0.14					0.54	42	11.1		
340g	0.20	0.14	0.058	0.09	0.10	16°	0.77			1.42	3.8
341	0.20	0.25					1.38	48	5.3		
341g	0.20	0.25	0.055	0.08	0.10	16°47'	1.82			1.32	2.5
342	0.20	0.33					2.86	44	9.1		
342g	0.20	0.33	0.052	0.08	0.09	17°22'	3.61			1.26	1.74
342'	0.20	0.33					3.08	42	11.2		
342'g	0.20	0.33	0.052	0.08	0.09	17°22'	3.76			1.23	1.66

TABLE 7

Series V Sandbottom with ripples $\varphi = 15^{\circ}$ T = 2 s

Test	d m	v m/s	H m	u_o m/s	u_o corr. m/s	φ corr.	I 10^{-4}	C $m^{1/2}/s$	r 10^{-3} m	$\frac{\tau'}{\tau_c}$	$\frac{\kappa C}{\sqrt{g}}$	$\frac{u_o}{v}$ corr.
323	0.28	0.22					0.62	53	3.8			
323g	0.28	0.22	0.088	0.24	0.24	$15^{\circ}33'$	1.27			2.04	7.5	
324	0.29	0.35					1.05	63	1.1			
324g	0.29	0.35	0.087	0.23	0.23	16°	1.79			1.70	5.7	
325	0.20	0.22					1.11	47	5.9			
325g	0.20	0.22	0.080	0.26	0.27	$15^{\circ}45'$	2.31			2.08	7.5	
326	0.20	0.30					3.63	35	24.6			
326g	0.20	0.30	0.094	0.30	0.31	$15^{\circ}45'$	4.55			1.26	4.8	
327	0.30	0.12					0.22	47	8.8			
327g	0.30	0.12	0.071	0.18	0.18	$15^{\circ}21'$	0.76			3.46	9.4	
329	0.30	0.25					0.67	55	3.1			
329g	0.30	0.25	0.064	0.16	0.17	$15^{\circ}45'$	1.48			2.19	4.9	
331	0.20	0.10					0.12	65	0.6			
331g	0.20	0.10	0.047	0.15	0.15	$15^{\circ}12'$	0.32			2.66	13.0	
333	0.34	0.11					0.21	41	21.5			
333g	0.34	0.11	0.067	0.16	0.16	$15^{\circ}10'$	0.72			3.44	7.7	
334	0.34	0.22					0.56	51	6.0			
334g	0.34	0.22	0.071	0.17	0.17	$15^{\circ}28'$	2.00			3.58	5.2	
335	0.34	0.34					1.76	44	14.7			
335g	0.34	0.34	0.073	0.17	0.18	$15^{\circ}49'$	2.53			1.44	3.0	
332	0.21	0.37					4.78	37	21.9			
332g	0.21	0.37	0.055	0.18	0.18	$16^{\circ}21'$	5.22			1.09	2.4	
334*	0.34	0.22					0.49	54	4.1			
334*g	0.34	0.22	0.067	0.16	0.16	$15^{\circ}28'$	1.08			2.21	5.2	

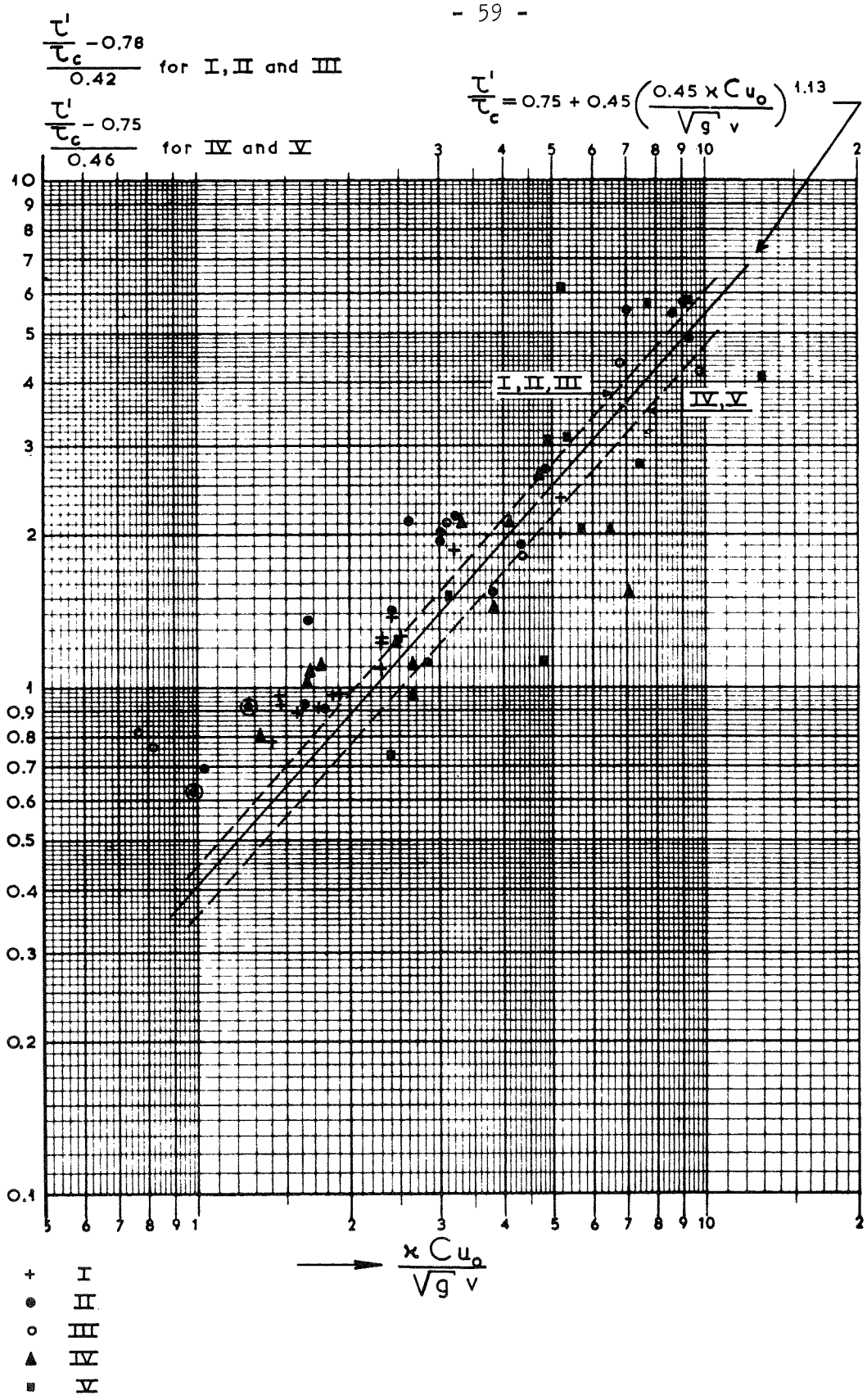

$\frac{\tau'}{\tau_c}$ VERSUS $\frac{\varkappa C u_o}{\sqrt{g}\,\nu}$

FIGURE III.4_1

Table 8

Series	number of data	p	
I. Stones $\varphi = 0^o$. T = 1.57 s	15	0.45	mean value 0.49
II. Sand with ripples $\varphi = 0^o$. T = 1.57 s	19	0.52	
III. Sand with ripples $\varphi = 0^o$. T = 0.68 s	8	0.43	
IV. Sand with ripples $\varphi = 15^o$. T = 0.68 s	13	0.36	mean value 0.40
V. Sand with ripples $\varphi = 15^o$. T = 2.0 s	12	0.42	
All data	67	0.45	

Equation (III.4-1) may also be written as:

$$\log\left(\frac{\frac{\tau'}{\tau_c} - a}{b}\right) = c \log\left(p \frac{\kappa C}{g^{1/2}} \frac{u_o}{v}\right) = c \log p + c \log \frac{\kappa C}{g^{1/2}} \frac{u_o}{v} \qquad \text{(III.4-2)}$$

In figure III-4-1 the dotted lines represent equation (III.3-17) with the values a, b and c for $\varphi = 0^o$ and 15^o as given in table 1 and the corresponding values of p as given in table 8. The full line represents equation (III.3-18):

$$\frac{\tau'}{\tau_c} = 0.75 + 0.45 \left(\xi \frac{u_o}{v}\right)^{1.13}$$

with the mean value of p = 0.45.

Since a considerable scatter exists in the points of the graph in figure III.4-1, an attempt has been made to study whether it would be allowed to reproduce all data by means of a formula of the form of equation (III.3-19). As the equation (III.3-19) is not linear it is not possible to use the normal procedure for the determination of the regression and the standard deviation of p. Therefore, equation (III.3-19) will now be written as:

$$\frac{\frac{\tau'}{\tau_c} - 1}{N} = p^{3/2} \left[\frac{\kappa C u_o}{g^{1/2} v}\right]^{3/2}, \qquad \text{(III.4-3)}$$

with the assumption that both:

$$\frac{\frac{\tau'}{\tau_c} - 1}{N} \quad \text{and} \quad \left[\frac{\kappa C\, u_o}{g^{1/2} v}\right]^{3/2}$$

are stochastic variables with a normal distribution.
The values of τ'/τ_c and $\kappa C\, u_o/vg^{1/2}$, as given in tables 3 through 7 are used, and for N the values as determined from equation (III.3-20) and the actual values of φ are introduced. The regression of:

$$\frac{\frac{\tau'}{\tau_c} - 1}{N} \quad \text{on} \quad \left[\frac{\kappa C\, u_o}{g^{1/2} v}\right]^{3/2}$$

which gives p_1 and the regression of

$$\left[\frac{\kappa C\, u_o}{g^{1/2} v}\right]^{3/2} \quad \text{on} \quad \frac{\frac{\tau'}{\tau_c} - 1}{N}$$

which gives p_2 will be calculated. Since $(\tau'/\tau_c - 1)/N$ has probably a lesser accuracy than $(\kappa C\, u_o/vg^{1/2})^{3/2}$ the value of p_1 will be the most likely one. Moreover the correlation coefficient for linear regression and the standard deviation of $(p_1)^{3/2}$, $s'_{(p_1)^{3/2}}$ has been calculated. For the correlation coefficient the value of $(p_1/p_2)^{1/2}$ has been introduced.

The results are summarized in table 9.

Table 9

Tests	Number of data	Correlation coefficient for linear regression	Required correlation for 95% confidence	$p_1^{3/2}$	$s'_{(p_1)^{3/2}}$	p_1	$p_2^{3/2}$	p_2
I Stones $\varphi = 0^o$. T = 1.57 s	15	0.97	0.53	0.31	0.12	0.46	0.33	0.48
II Sand with ripples $\varphi = 0^o$. T = 1.57 s	19	0.97	0.47	0.38	0.10	0.53	0.40	0.54
III Sand with ripples $\varphi = 0^o$. T = 0.68 s	8	0.95	0.72	0.28	0.11	0.43	0.31	0.46
IV Sand with ripples $\varphi = 15^o$. T = 0.68 s	13	0.84	0.57	0.24	0.13	0.38	0.34	0.49
V Sand with ripples $\varphi = 15^o$. T = 2.0 s	12	0.85	0.59	0.26	0.15	0.40	0.36	0.50
All data	67	0.90	0.25	0.3	0.04	0.45	0.37	0.51

From these results it is evident that there is a marked linear regression for all series. It is also evident that no significant difference appears between the regression coefficients $(p_1)^{3/2}$ for tests with waves normal to the current and with waves which make an angle of $\varphi = 15^{o}$ with the current. The asymmetry of the waves apparently does not have sufficient influence on the increase of the bed shear of the current due to the waves, that it could be determined by these measurements. It has, therefore, been decided not to try a second order theory for the description of the wave motion.

III.5. Discussion of factor p

From the tests of Kalkanis (23) follows a velocity distribution of the motion, immediately above the bed, of the following form:

$$u_b - u = u_o \, 0.5 \, e^{-133 \frac{Y}{\alpha \beta D}} \sin(\omega t - 0.5 \, (\beta y)^{2/3}) \qquad \text{(III.5-1)}$$

where $\beta = (\omega/2\nu)^{1/2}$ and α = the amplitude of the orbital excursion at the bottom. D is the grain diameter and in this way a measure for the bottom roughness. Abou-Seida (1) concludes from this equation (III.5-1) that the velocity at the outside of the viscous sublayer, which is assumed by him to be present under the turbulent boundary layer, must be $0.5\ u_b$. This value could be compared with the value of $p\ u_b$ which is assumed by the author to exist at the hypothetical distance er/33 from the bed. From the experiments follows a constant value of "p" irrespective of the bottom roughness, the wave height and the wave period. Since this result is not so very obvious, this point will be discussed in this paragraph in somewhat greater detail.

According to Lamb (27) (art. 328), the motion near the bed can be described by:

$$\frac{\partial u}{\partial t} = X + \frac{1}{\varrho} \frac{\partial \tau}{\partial y} \, , \qquad \text{(III.5-2)}$$

where τ = shear stress at a distance y from the bottom as acting from the upper layer on the lower layer, u = velocity at a distance y from the bed. Furthermore:

$$X = f \cos \omega t = \omega \, u_o \cos \omega t = \frac{\partial u_b}{\partial t} \qquad \text{(III.5-3)}$$

where

$$u_b = u_o \sin \omega t \qquad \text{(III.5-4)}$$

So that equation (III.5-2) can be written in the form:

$$\frac{\partial}{\partial t}(u_b - u) = -\frac{1}{\varrho}\frac{\partial \tau}{\partial y} \qquad \text{(III.5-5)}$$

In order to make it possible to solve this equation, an additional relationship between τ and u should be known. The following relationship is valid for the entire viscous case:

$$\tau = \varrho\nu \frac{\partial u}{\partial y} \qquad \text{(III.5-6)}$$

Equation (III.5-5) can in this case be written in the form:

$$\frac{\partial}{\partial t}(u_b - u) = -\nu \frac{\partial^2 u}{\partial y^2} \qquad \text{(III.5-7)}$$

From this follows for the velocity distribution near the bed:

$$u_b - u = u_o\, e^{-\beta y} \sin(\omega t - \beta y) \qquad \text{(III.5-8)}$$

where $\mu = (\omega/2\nu)^{1/2}$. (Lamb art. 347) (27)

The order of magnitude of ω for the tests was 6 s^{-1} and the order of magnitude of ν was 10^{-6} m^2/s. Therefore β is in order of magnitude $2.10^3 m^{-1}$. For $\beta y = 3$, u will be almost (95%) equal to u_b and from this it follows that the thickness of the viscous sublayer will be of the order of magnitude of millimeters. For almost all tests this is much smaller than the bed roughness. It is, therefore, reasonable to assume a turbulent boundary layer between the bed to the frictionless orbital velocity.

In analogy with the fully developed turbulent boundary layer, the normal formula will be applied for the bed shear, viz.:

$$\tau = \varrho l^2 \frac{\partial u}{\partial y}\left|\frac{\partial u}{\partial y}\right| \qquad \text{(III.5-9)}$$

where for the lower part of the fluid $l = \kappa y$.
In analogy with the viscous case the following velocity distribution in the boundary layer between the frictionless orbital motion and the bed will be assumed:

$$u_b - u = u_o\, e^{-Y} \sin(\omega t - Y) = u_o\, e^{-Y} \sin\left(\psi - \frac{\pi}{4}\right) \qquad \text{(III.5.10)}$$

where: $$\omega t - Y + \frac{\pi}{4} = \psi \qquad \text{(III.5-11)}$$

From this follows:

$$\frac{\partial u}{\partial y} = u_o\, e^{-Y} \frac{\partial Y}{\partial y}\, 2^{1/2} \sin\psi \qquad \text{(III.5-12)}$$

$\frac{\partial u}{\partial y}$ and consequently, τ must have the sign of $\sin\psi$ which is indicated by sign (ψ) which is positive for $0 < \psi < \pi$ and negative for $\pi < \psi < 2\pi$. The expression of the shear stress is now:

$$\tau = \varrho \kappa^2 y^2 \left(\frac{\partial u}{\partial y}\right)^2 \text{sign } (\psi) \qquad \text{(III.5-13)}$$

Hence, equation (III.5-5) may now be written as:

$$\frac{\partial}{\partial t}(u_b - u) = -\kappa^2 \frac{\partial}{\partial y}\left[y^2 \left(\frac{\partial u}{\partial y}\right)^2 . \text{sign } (\psi)\right] \qquad \text{(III.5-14)}$$

This proves to be:

$$\frac{\partial}{\partial t}(u_b - u) = -2\kappa^2 \text{ sign } (\psi)\left[y \left(\frac{\partial u}{\partial y}\right)^2 + y^2 \frac{\partial u}{\partial y}\frac{\partial^2 u}{\partial y^2}\right] \qquad \text{(III.5-15)}$$

It will now be possible to determine the unknown function Y of y from equation (III.5-15).

The following expressions can be written:

$$\frac{\partial}{\partial t}(u_b - u) = \omega u_o e^{-Y} \cos(\omega t - Y) = \omega u_o e^{-Y} \cos\left(\psi - \frac{\pi}{4}\right) =$$

$$\omega u_o e^{-Y} (1/2)^{1/2} (\sin\psi + \cos\psi) \qquad \text{(III.5-16)}$$

$$\frac{\partial u}{\partial y} = u_o e^{-Y} \frac{\partial Y}{\partial y} 2^{1/2} \sin\psi \qquad \text{(III.5-17)}$$

$$\frac{\partial^2 u}{\partial y^2} = u_o e^{-Y}\left[-\left(\frac{\partial Y}{\partial y}\right)^2 2 \sin\psi + \frac{\partial^2 Y}{\partial y^2} 2^{1/2} \sin\psi - \left(\frac{\partial Y}{\partial y}\right)^2 2^{1/2} \cos\psi\right] \qquad \text{(III.5-18)}$$

$$\frac{\partial u}{\partial y}\frac{\partial^2 u}{\partial y^2} = 2 u_o^2 e^{-2Y}\left[-\left(\frac{\partial Y}{\partial y}\right)^3 \sin^2\psi + \frac{\partial Y}{\partial y} . \frac{\partial^2 Y}{\partial y^2} \sin^2\psi - \left(\frac{\partial Y}{\partial y}\right)^3 \sin\psi \cos\psi\right] \qquad \text{(III.5-19)}$$

Equation (III.5-15) can now be written as:

$$\omega u_o e^{-Y} (1/2)^{1/2} (\sin\psi + \cos\psi) =$$
$$-2\kappa^2 u_o^2 e^{-2Y} \text{sign } (\psi)\left[2y \frac{\partial Y}{\partial y} \sin^2\psi - 2y^2 \left(\frac{\partial Y}{\partial y}\right)^3 \sin^2\psi\right.$$
$$\left. + y^2 \frac{\partial Y}{\partial y} . \frac{\partial^2 Y}{\partial y^2} \sin^2 2\psi - y^2 \left(\frac{\partial Y}{\partial y}\right)^3 \sin\psi \cos\psi\right] =$$
$$-2\kappa^2 u_o^2 e^{-2Y} \text{sign } (\psi)\left[y \frac{\partial Y}{\partial y} - y \frac{\partial Y}{\partial y} \cos 2\psi - y^2 \left(\frac{\partial Y}{\partial y}\right)^3\right.$$
$$\left. + y^2 \left(\frac{\partial Y}{\partial y}\right)^3 \cos 2\psi + y^2 \frac{\partial Y}{\partial y} . \frac{\partial^2 Y}{\partial y^2} - y^2 \frac{\partial Y}{\partial y} \frac{\partial^2 Y}{\partial y^2} \cos 2\psi - y^2 \left(\frac{\partial Y}{\partial y}\right)^3 \sin 2\psi\right] =$$
$$-2\kappa^2 u_o^2 y \frac{\partial Y}{\partial y} e^{-2Y} \text{sign } (\psi)\left[F - F \cos 2\psi - G \sin 2\psi\right] . \qquad \text{(III.5-20)}$$

in which:

$$F = \frac{\partial Y}{\partial y} - y \left(\frac{\partial Y}{\partial y}\right)^2 + y \frac{\partial^2 Y}{\partial y^2} \quad \text{and} \tag{III.5-21}$$

$$G = y \left(\frac{\partial Y}{\partial y}\right)^2 \tag{III.5-22}$$

When the right hand side of (III.5-20) is developed in a Fourier series and only the terms with $\sin\psi$ and $\cos\psi$ are taken into account:

$$\omega u_o e^{-Y} (1/2)^{1/2}(\sin\psi + \cos\psi) = - 2\kappa^2 u_o^2 y \frac{\partial Y}{\partial y} e^{-2Y} \left[\left(\frac{4F}{\pi} + \frac{4F}{3\pi}\right) \sin\psi - \frac{8G}{3\pi} \cos\psi\right] \tag{III.5-23}$$

Taking the coefficients of the sine and cosine terms at both sides equal the following equations are obtained:

$$- 2\kappa^2 u_o^2 y \frac{\partial Y}{\partial y} e^{-2Y} \frac{16}{3\pi} F = \omega u_o e^{-Y} (1/2)^{1/2} \tag{III.5-24}$$

$$+ 2\kappa^2 u_o^2 y \frac{\partial Y}{\partial y} e^{-2Y} \frac{8}{3\pi} G = \omega u_o e^{-Y} (1/2)^{1/2} \tag{III.5-25}$$

From this follows that:

$$- 2 \frac{F}{G} = 1 \qquad \text{or}$$

$$2 \left(\frac{\partial Y}{\partial y} - y \left(\frac{\partial Y}{\partial y}\right)^2 + y \frac{\partial^2 Y}{\partial y^2}\right) + y \left(\frac{\partial Y}{\partial y}\right)^2 = 0 \tag{III.5-26}$$

So that: $$\frac{\partial^2 Y}{\partial y^2} - \frac{1}{2} \left(\frac{\partial Y}{\partial y}\right)^2 + \frac{1}{y} \frac{\partial Y}{\partial y} = 0 \tag{III.5-27}$$

The solution of this equation is:

$$Y = - 2 \ln \ln \left(\frac{A}{y}\right) + B \tag{III.5-28}$$

From equation (III.5-28) follows:

$$\frac{\partial Y}{\partial y} = 2 \left(\ln \frac{A}{y}\right)^{-1} . y^{-1} \tag{III.5-29}$$

When this value is introduced in equation (III.5-25) the following relationship between A and B is obtained:

$$\ln \frac{A}{y} = \frac{128\ 2^{1/2}\ \kappa^2\ u_o}{3\pi\ \omega\ y} e^{-B} \tag{III.5-30}$$

With the expression of Y in y and the constants A and B as given by equation (III.5-28), the equation (III.5-10) of the velocity in the

boundary layer now becomes:

$$u = u_o\left[\sin \omega t - e^{-B} \left(\ln \frac{A}{y}\right)^2 \sin \left(\omega t - 2 \ln \ln \frac{A}{y} - B\right)\right] \qquad \text{(III.5-31)}$$

When the relationship between A and B according to equation (III.5-30) is introduced in equation (III.5-31), the following expression for the velocity distribution is obtained:

$$u = u_o\left[\sin \omega t - \left\{\frac{128\ 2^{1/2} \kappa^2 u_o e^{-3B/2}}{3\pi\ \omega}\right\}^2 y^{-2} . \sin\left(\omega t + 2 \ln \frac{128 . 2^{1/2} \kappa^2 u_o}{3\pi\ \omega\ y} - 3B\right)\right] \qquad \text{(III.5-32)}$$

If, in accordance with the procedure for a uniform flow, as applied in this study, the velocity will be assumed zero at a distance r/33 from the bed (see figure III.3-1), the following expression for B is obtained:

$$B = \frac{2}{3} \ln\left[\frac{33}{r} . \frac{128\ 2^{1/2} \kappa^2 u_o}{3\pi\ \omega}\right] \qquad \text{(III.5-33)}$$

With this expression for B equation (III.5-32) now becomes:

$$u = u_o\left[\sin \omega t - \left(\frac{r}{33y}\right)^2 \sin \left(\omega t + \ln \left(\frac{r}{33y}\right)^2\right)\right] \qquad \text{(III.5-34)}$$

This expression represents a hyperbolic velocity distribution in the boundary layer which approaches the frictionless orbital motion in a asymtotical way. If the upper limit of the boundary layer is assumed at the height where $u = 0.95\ u_o$, the thickness of the boundary layer becomes:

$$\frac{r}{33\ (0.05)^{1/2}} = 0.14\ r \qquad \text{(III.5-35)}$$

This value is in reasonable accordance with visual observations in the wave canals of the Delft Hydraulics Laboratory.
The following expression is found from equation (III.5-34) for the vertical velocity gradient:

$$\frac{\partial y}{\partial y} = 2^{3/2} \left(\frac{r}{33}\right)^2 y^{-3} u_o \sin \left(\omega t + \ln \left(\frac{r}{33y}\right)^2 + \frac{\pi}{4}\right) \qquad \text{(III.5-36)}$$

When, according to the procedure described in paragraph III.3, the bed shear is computed from the velocity gradient at a distance er/33 above the bed, the following expression for this bed shear is obtained:

$$\tau = \varrho l^2 \left[2^{3/2} \left(\frac{r}{33}\right)^2 \left(\frac{33}{er}\right)^3 \sin \left(\omega t - \ln e + \frac{\pi}{4}\right)\right]^2 u_o^2 \qquad \text{(III.5-37)}$$

The procedure for computing the bed shear according to equations (III.3-1)

and (III.3-6) gives:

$$\tau = \varrho l^2 \frac{p^2 u_o^2 \sin^2 \omega t}{(er/33)^2} \qquad \text{(III.5-38)}$$

By comparing the moduli of the expressions for the bed shear according to equations (III.5-37) and (III.5-38) the following value of p is obtained:

$$p = 2^{3/2} \left(\frac{r}{33}\right)^2 . \left(\frac{33}{er}\right)^2 = 2^{3/2} e^{-2} = 0.39 \qquad \text{(III.5-39)}$$

This expression demonstrates that p is indeed independent of bed and wave conditions. The theoretically computed value is, moreover, rather close to the value of 0.45 as obtained from the experiments.

CHAPTER IV
TRANSPORTATION OF BED MATERIAL DUE TO THE COMBINATION OF WAVES AND CURRENT

IV.1. Description of tests with narrow sand trap

In the same model as described in the preceding chapter also transport of bed material was measured by a sand trap as indicated in figure III.2-1. The dimensions of the sand trap where 1.5 m normal to the current direction and 0.15 m in the current direction. The small dimension in the current direction was chosen in order to decrease that part of the transport which enters the sand trap in the direction of the waves, to an acceptable degree. However, as a result of the application of this sand trap, with short dimension in the direction of the current, not all the transport is trapped. The sediment transport measurements will, therefore, only be used to establish the form of the relationship and not to determine the coefficients. By comparing the results for only current with those for the combination of waves and current , the coefficients for the latter can, moreover, be derived from the well-known coefficients for a mere current. Also some tests with a larger sand trap will be described. Although these test results prove that not all transport is caught by the narrow trap used in the above described tests, they also prove the necessity of this narrow trap since a considerable amount of sand is brought by the waves into the trap sideways (see figures IV.3-1 and 2). Moreover, these tests showed also a lower transport than that calculated by the normal bedload formulae.

The bed material consisted of fine sand with a mean diameter of 0.25 mm. The grain size distribution is given in figure IV.1-1. As may be seen from the figures IV.1-2 through 9, different ripple patterns may occur. In general, three different patterns can be distinguished viz.:

(i) ripples normal to the direction of the main current (figures IV.1-2 through 4).

(ii) ripples normal to the direction of wave propagation (figures IV.1-5 and 6).

(iii) ripples forming a cross pattern or alternating normal to the directions of main current and to that of wave propagation (figures IV.1-7 through 9).

From the test results may be concluded that for values of u_o/v_* less than 6 the ripple pattern is of type (i). For values of u_o/v_* greater than 6 and less than 20 the pattern is of type (iii), whilst for values greater

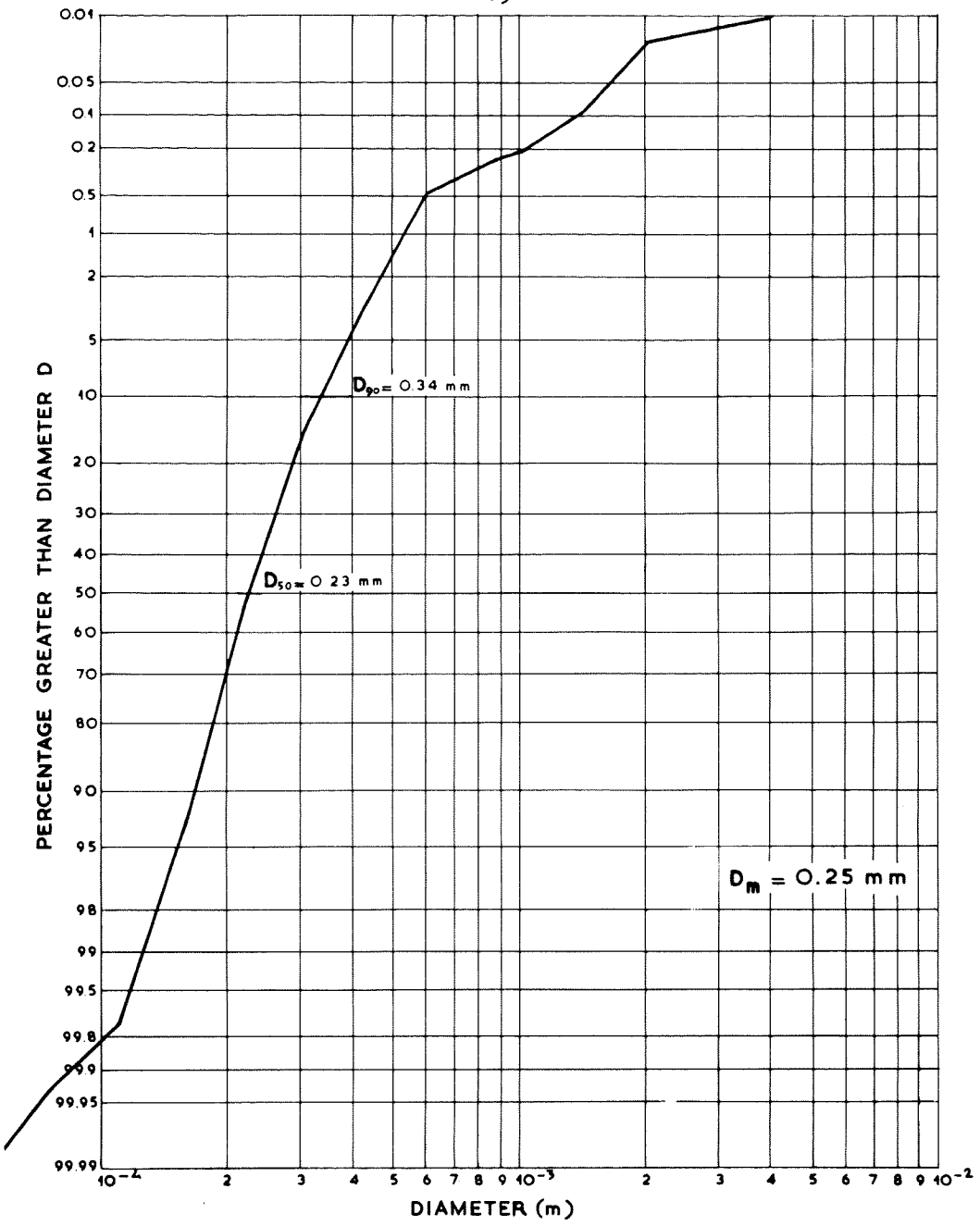

GRAIN SIZE DISTRIBUTION MODEL SAND

FIGURE IV.1_1

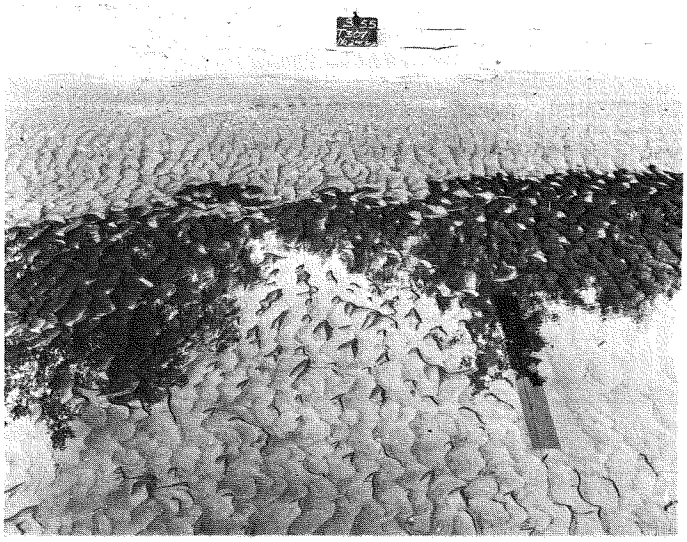

Figure IV.1-2
T 307
type i
r = 3 mm

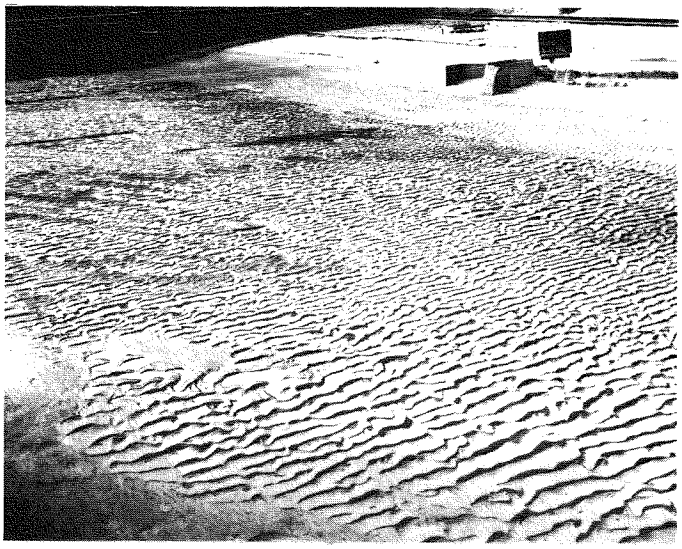

Figure IV.1-3
T 341
type i
r = 9 mm

Figure IV.1-4
T 365
type i
r = 29 mm

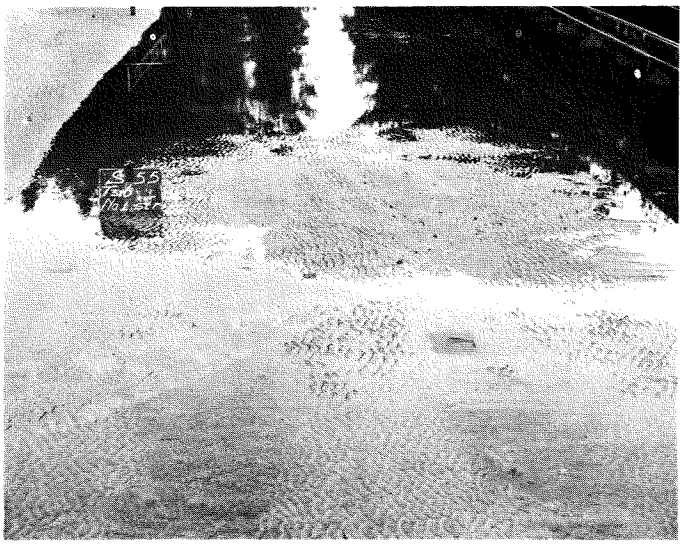

Figure IV.1-5
T 316
type ii
r = 3 mm

Figure IV.1-6
T 316
type ii
r = 3 mm

Figure IV.1-7
T 314
type iii
r = 3 mm

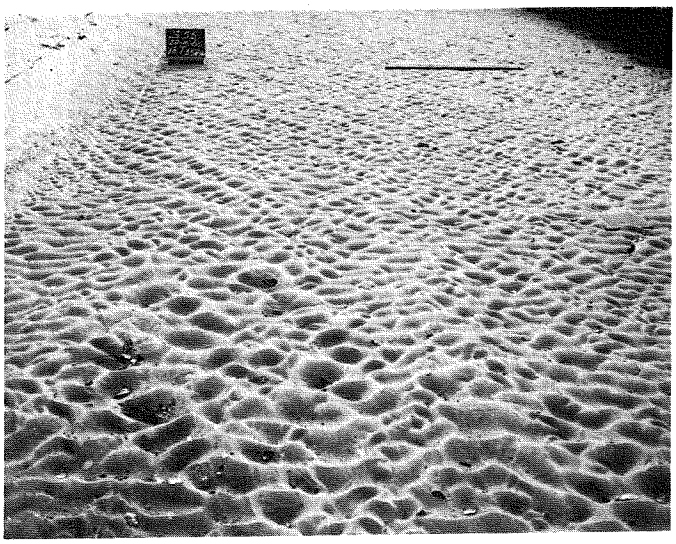

Figure IV.1-8
T 358
type iii
r = 29 mm

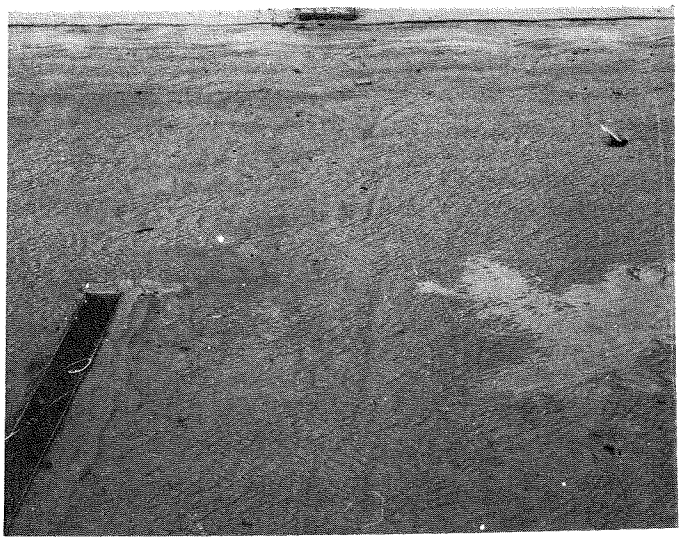

Figure IV.1-9
T 356
type iii
r = 3 mm

than 20, type (ii) will occur. In chapter III it is stated that, for the determination of the resultant bed shear of a combination of waves and current, the velocities of both current and wave motion, at the limit of the hypothetical viscous sublayer with thickness $y' = er/33$, have been taken into account. For the main current this velocity has a value of v_*/κ and for the orbital motion $0.45\ u_o$. It might be assumed that for the ripple pattern the ratio of the two velocities at this distance above the bottom will be decisive. If it be assumed that the transition from pattern (i) to pattern (iii) will start when $u_{y'}/v_{y'} \gg 1$, this leads to a value of $u_o/v_* \gg 3.5$. This is rather well in agreement with the test results.

In order to predict the bottom roughness, it might also be necessary to take into account the orientation of the ripples with respect to the current direction. This would lead to complications, not only in the case of patterns of type (iii), but also for patterns of types (i) and (ii), since the velocity vector will change in direction during the wave period. The roughness of the bottom will, therefore, be determined from the ripple height irrespective of the pattern. This is even more logical since also in the case of patterns of types (i) and (ii) the ripple crests are never long and regular.

Although for every test, in which the transportation of bed material was measured also the bed shear was determined, this value has not been used for the computation. From the foregoing chapter, it is evident that the scatter in the results of the determination of the bed shear is rather great. In order to obtain better results, mean values have been used, which were based upon more tests than only those which were carried out during the bed load measurements. For the tests, carried out with waves approaching the coast at right angles, a value of the bottom roughness of 3 mm was chosen for the tests 302 through 360 and of 29 mm for the tests 357 through 365*. For oblique waves, a roughness value of 9 mm was determined. It has been assumed that the test conditions of these three groups were so similar, that no further differentiation in bed roughness was allowed for. With these values of r the resistance factors C were calculated, and with the formula:

$$\mu = \left(\frac{C}{C_{d_{90}}}\right)^{3/2} \qquad (IV.1-1)$$

the ripple factor μ was determined (14).

From the mean velocity, the value of $v^2/C^2 = dI = \tau/\varrho g$ was determined, using these values of C. With the value of $\xi\ u_o/v = 0.45\kappa C\ u_o/g^{1/2}v$ and

the theory developed in the preceding chapter, the magnitude of the resultant bed shear in the direction of the main current was computed. The magnitude of the orbital velocity was corrected for the influence of the stream refraction.

In tables 10 and 11 all data and results of the computation for respectively, wave approach at right angles and for oblique wave approach are presented. For the calculation of τ'/τ_o from the value of $\xi\, u_o/v$ the formula

$$\frac{\tau'}{\tau_o} = 1 + (0.36 - 0.14 \cos 2\varphi)(\xi \frac{u_o}{v})^{1.5} , \qquad (IV.1-2)$$

which is a combination of equations(III.3-19) and (III.3-20) has been used. The difference with the actual values is not so great that an important influence has to be expected.

In order to make it possible to compare the bed load of the mere current with that of the combination of current and waves, it is most practical to compute, by means of the available data, the coefficients in some bed load transportation formula. Since especially in this case the low transports are rather important, a formula has been chosen without a critical bed shear. The most appropriate formula seems to be the formula of Kalinske-Frijlink, (14) viz.:

$$\frac{S}{(g\Delta D^3)^{1/2}} = 5\,(\frac{\mu dI}{\Delta D})^{1/2}\, e^{-0.27\,\frac{\Delta D}{\mu dI}} = 5\,(\frac{\mu\tau}{\Delta D\varrho g})^{1/2}\, e^{-0.27\,\frac{\Delta D\varrho g}{\mu\tau}} \qquad (IV.1-3)$$

or:

$$\frac{S}{D(\mu\tau/\varrho)^{1/2}} = b\, e^{a\,\frac{\Delta D\varrho g}{\mu\tau}} \qquad (IV.1-4)$$

The values of a and b can not be determined in the normal way by means of the method of the least squares, because the magnitude of the parameter $S/D(\mu\tau/\varrho)^{1/2}$ ranges from 1 to 10^{-4}. Due to this large range, the influence on the results of points with high values is predominant. Although this is quite right in principle, it gives in this case erroneous results because the low transports are also important. Hence, a weight has to be given to the different values of $S/D(\mu\tau/\varrho)^{1/2}$, so that the influence of the low transports on the magnitude of a and b is about equal to that of the high values. This can be obtained by not using the value $S/D(\mu\tau/\varrho)^{1/2}$, but its logarithme.

Equation (IV.1-4) will be written for this purpose as:

$$\log \frac{S}{D(\mu\tau/\varrho)^{1/2}} = \log b + a\,\frac{\Delta D\varrho g}{\mu\tau} \log e \qquad (IV.1-5)$$

Table 10 Wave-approach at right angles

Test	$\frac{S}{D(\Delta Dg)^{1/2}}$ 10^{-4}	r 10^{-3} m	C $m^{1/2}/s$	$C_{d_{90}}$ $m^{1/2}/s$	μ	$(\mu hI)_c = \mu \frac{\tau_c}{\varrho g}$ 10^{-5} m	$\xi \frac{u_o}{v}$	$\frac{\tau'}{\tau_c}$	$\frac{\tau_r}{\tau_c}$
302	3.3	3	52	70	0.64	2.27			
302g	8.7	3	52	70	0.64	2.27	0.70	1.13	1.25
302*	4.3	3	52	70	0.64	2.13			
302*g	10.6	3	52	70	0.64	2.13	0.69	1.13	1.24
303	178	3	52	70	0.64	3.24			
303g	243	3	52	70	0.64	3.24	0.59	1.10	1.17
306'	0.95	3	54	73	0.64	2.39			
306"	4.4	3	54	73	0.64	2.39			
306'g	2.2	3	54	73	0.64	2.39	0.63	1.11	1.20
306"g	12.9	3	54	73	0.64	2.39	0.63	1.11	1.20
307	62	3	54	73	0.64	3.34			
307g	51	3	54	73	0.64	3.34	0.64	1.11	1.20
310	8.8	3	57	74	0.67	2.11			
310g	12.9	3	57	74	0.67	2.11	0.92	1.19	1.42
314	4.7	3	53	70	0.66	1.84			
314g	44	3	53	70	0.66	1.84	1.42	1.37	2.00
314'	4.4	3	53	70	0.66	1.84			
314'g	40	3	53	70	0.66	1.84	1.42	1.37	2.00
315'	188	3	53	70	0.66	3.76			
315'g	304	3	53	70	0.66	3.76	0.99	1.22	1.49
315	198	3	53	70	0.66	3.76			
316g	18.1	3	54	73	0.64	0.32	3.56	2.54	7.35
316'g	18.2	3	54	73	0.64	0.32	3.56	2.47	7.35
316"g	44	3	54	73	0.64	0.32	3.56	2.47	7.35
318	3.5	3	54	73	0.64	1.98			
318g	76	3	54	73	0.64	1.98	1.35	1.34	1.91
318'	2.6	3	54	73	0.64	1.98			
318'g	56	3	54	73	0.64	1.98	1.35	1.34	1.91
319	123	3	54	73	0.64	3.51			
319g	250	3	54	73	0.64	3.51	1.18	1.28	1.70
319'g	255	3	54	73	0.64	3.51	1.18	1.28	1.70
320g	25	3	57	75	0.66	0.46	3.18	2.19	6.05
322	9.3	3	57	75	0.66	1.95			
322g	143	3	57	75	0.66	1.95	1.59	1.44	2.26
322'	16.1	3	57	75	0.66	1.95			

Table 10 continued Wave-approach at right angles

Test	$\frac{S}{D(\Delta Dg)^{1/2}}$ 10^{-4}	r 10^{-3} m	C $m^{1/2}/s$	$C_{d_{90}}$ $m^{1/2}/s$	μ	$(\mu hI)_c = \mu \frac{\tau_c}{\varrho g}$ 10^{-5} m	$\xi \frac{u_o}{v}$	$\frac{\tau'}{\tau_c}$	$\frac{\tau_r}{\tau_c}$
322'g	68	3	57	75	0.66	1.95	1.59	1.44	2.26
356g	2.3	3	49	66	0.64	1.18	1.52	1.41	2.15
360g	1.2	3	52	70	0.64	1.14	1.06	1.24	1.56
357g	133	29	31	66	0.32	2.80	0.53	1.10	1.14
358	342	29	32	67	0.33	3.30			
358g	613	29	32	67	0.33	3.30	0.51	1.09	1.13
362	926	29	35	70	0.35	4.34			
362g	2446	29	35	70	0.35	4.34	0.36	1.05	1.06
365*	58	29	38	73	0.38	2.37			
365*g	16	29	38	73	0.38	2.37	0.30	1.04	1.04

Table 11 Oblique wave-approach

Test	$\frac{S}{D(\Delta Dg)^{1/2}}$ 10^{-4}	r 10^{-3} m	C $m^{1/2}/s$	$C_{d_{90}}$ $m^{1/2}/s$	μ	$(\mu hI)_c = \mu \frac{\tau_c}{\varrho g}$ 10^{-5} m	$\xi \frac{u_o}{v}$	$\frac{\tau'}{\tau_c}$	$\frac{\tau_r}{\tau_c}$
340g	2.3	9	44	70	0.50	0.50	1.78	1.56	2.58
341	3.3	9	44	70	0.50	1.6			
341g	21	9	44	70	0.50	1.6	1.02	1.25	1.52
342	49	9	44	70	0.50	2.8			
342'	56	9	44	70	0.50	2.8			
342g	173	9	44	70	0.50	2.8	2.30	1.84	3.65
342'g	191	9	44	70	0.50	2.8	2.30	1.84	3.65
344	0.2	9	46	72	0.51	1.5			
344g	11.4	9	46	72	0.51	1.5	0.74	1.15	1.27
340*g	2.3	9	44	70	0.50	0.50	1.80	1.57	2.62
341*	3.2	9	44	70	0.50	1.6			
341*g	21	9	44	70	0.50	1.6	1.02	1.25	1.52
323g	340	9	46	72	0.51	1.16	2.94	2.19	5.23
324	7	9	47	73	0.52	2.9			
324g	1260	9	47	73	0.52	2.9	1.90	1.62	2.80
325g	606	9	44	70	0.50	1.25	3.17	2.28	6.00
326	7	9	44	70	0.50	2.3			
326g	630	9	44	70	0.50	2.3	2.74	2.08	4.75
327g	93	9	47	73	0.52	0.34	4.21	3.03	9.90
329g	180	9	47	73	0.51	1.4	1.91	1.63	2.82
329	14	9	47	73	0.51	1.4			
331g	108	9	44	70	0.50	0.25	3.96	2.86	8.85
333g	36	9	48	74	0.52	0.27	4.06	2.93	9.25
332	245	9	44	70	0.50	3.5			
332g	495	9	44	70	0.50	3.5	1.29	1.35	9.30
334	0.6	9	48	74	0.52	1.05			
334g	75	9	48	74	0.52	1.05	2.21	1.78	3.45
335	15	9	48	74	0.52	2.6			
335g	217	9	48	74	0.52	2.6	1.50	1.44	2.12
335g	147	9	48	74	0.52	2.6	1.50	1.44	2.12
334*g	75	9	48	74	0.52	1.05	2.08	1.71	3.16

IV.2. Elaboration of data of tests with the narrow sand trap

In figure IV.2-1, the test results for only current and in figures IV.2-2 and 3, the test results for the combination of waves and current are reproduced. In figures IV.2-2 and 3, some points are entirely outside the range of the other results. Apparently, the correction of the bed shear for wave influence is not sufficient to cover all results. The tests which show this discrepancy, viz.: 316, 316", 316" and 320 for series B and 340, 340', 327, 331 and 333 for series F, have all very low values of the bed shear. So low, in fact, that even the corrected increased value is not sufficient to cause transport of any importance. The physical explanation of the fact, that there is nevertheless an appreciable transport, is that the bed material is stirred up by the wave motion, and that a very low velocity, or bed shear, is sufficient to move the material in the direction of the current.

This physical phenomenon may be described by a formula in which one part is responsible for the concentration of the material stirred up by the turbulence and a second part for the transport of this material, moving more or less in suspension in a thin layer above the bottom. In the formula of Kalinske-Frijlink (14):

$$\frac{S}{D\,\frac{v}{C}\,(\mu g)^{1/2}} = b\, e^{a\,\frac{\Delta D \varrho g}{\mu \tau}} \qquad \text{(IV.2-1)}$$

the value $D(\mu\tau/\varrho)^{1/2} = Dv(\mu g)^{1/2}/C$, can be seen as the factor which governs the transport of material, which has been stirred up from the bed, in the direction of the current. The parameter $S/D(\mu\tau/\varrho)^{1/2}$ will therefore be called the "transport" parameter and the bed shear in this parameter will be the component of this bed shear in the direction of the current. In this parameter the transport S is the resultant transport, since the actual transport at any moment and height above the bed is directed in the direction of the actually occurring current. The value $\exp.(a\Delta D\,\varrho g/\mu\tau)$ may be regarded as the parameter determining the quantity of material which is stirred up. This parameter will, therefore, be called the "stirring" parameter. The bed shear in this parameter will be the resultant total bed shear, since this value governs the quantity of material which is stirred up from the bed.

The fact that two different current systems are considered for the transportation of the bed material, viz.: (1) the resultant velocity, which is held responsible for stirring up the material and (2) the main current, which transports the material in the direction of this main

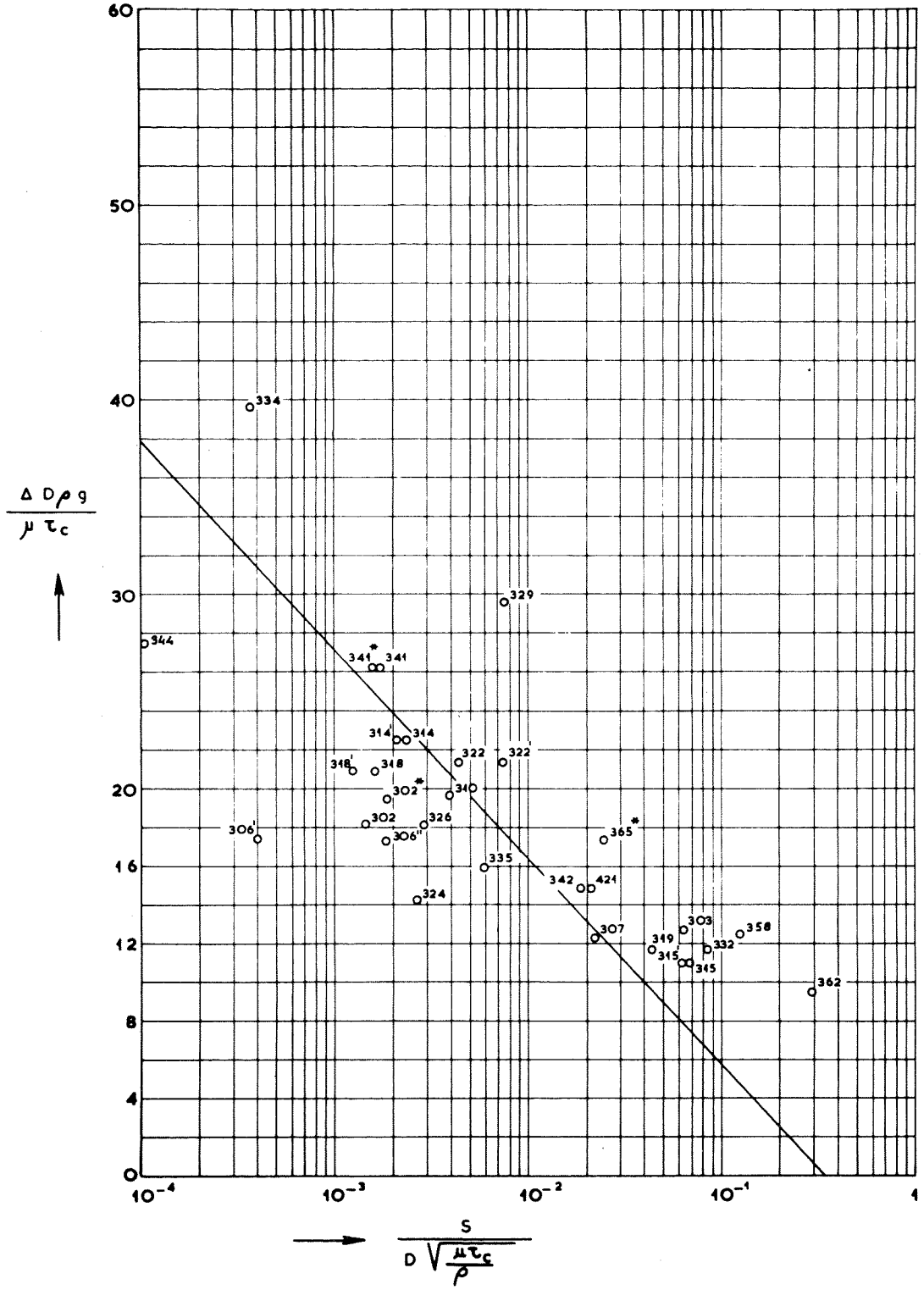

CURRENT ONLY. Series A E

FIGURE IV.2_1

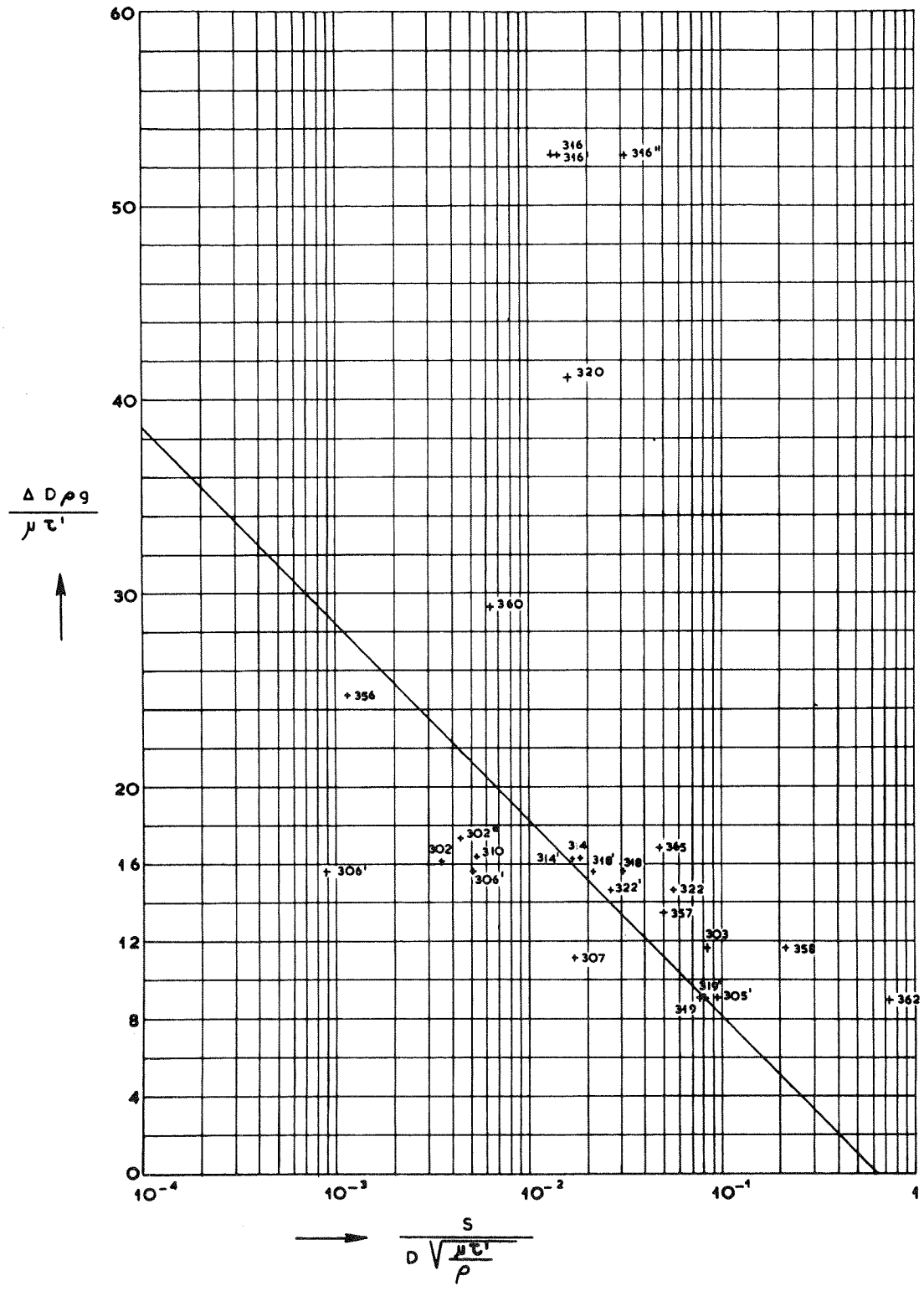

WAVE_APPROACH AT RIGHT ANGLES AND CURRENT Series B

FIGURE IV. 2_2

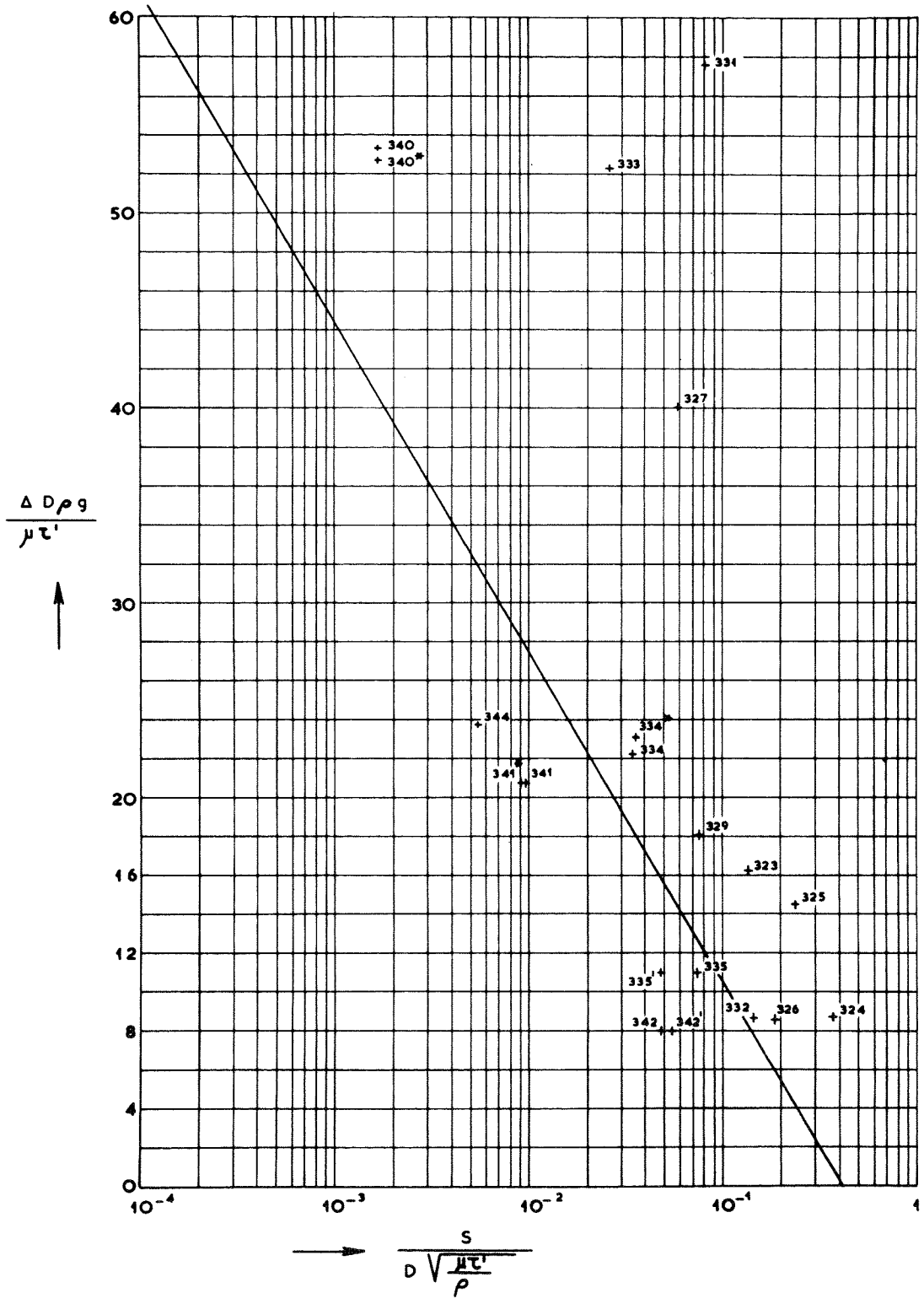

OBLIQUE WAVE_APPROACH AND CURRENT. Series F

FIGURE IV. 2_3

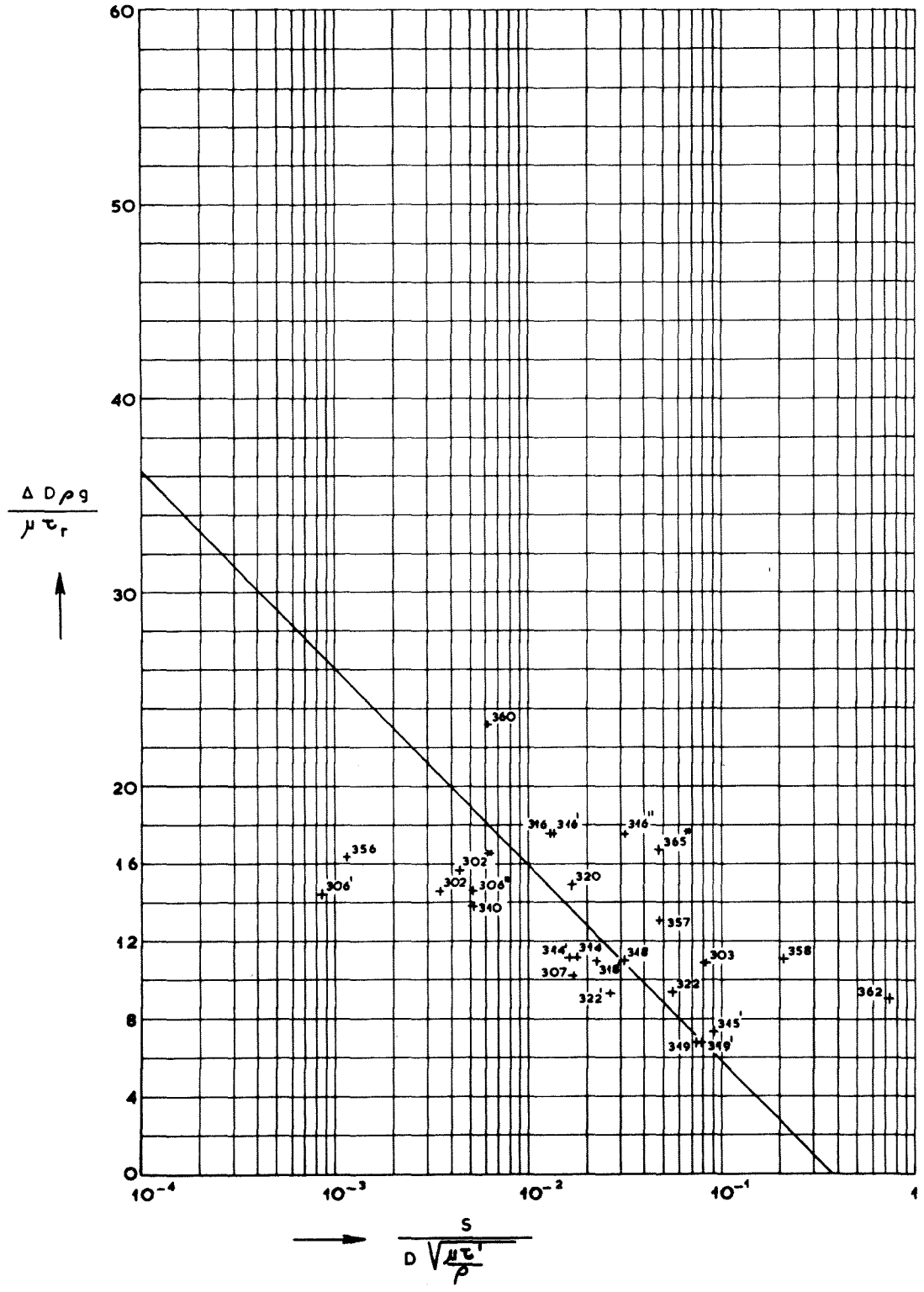

WAVE_APPROACH AT RIGHT ANGLES AND CURRENT. Series C

FIGURE IV. 2_4

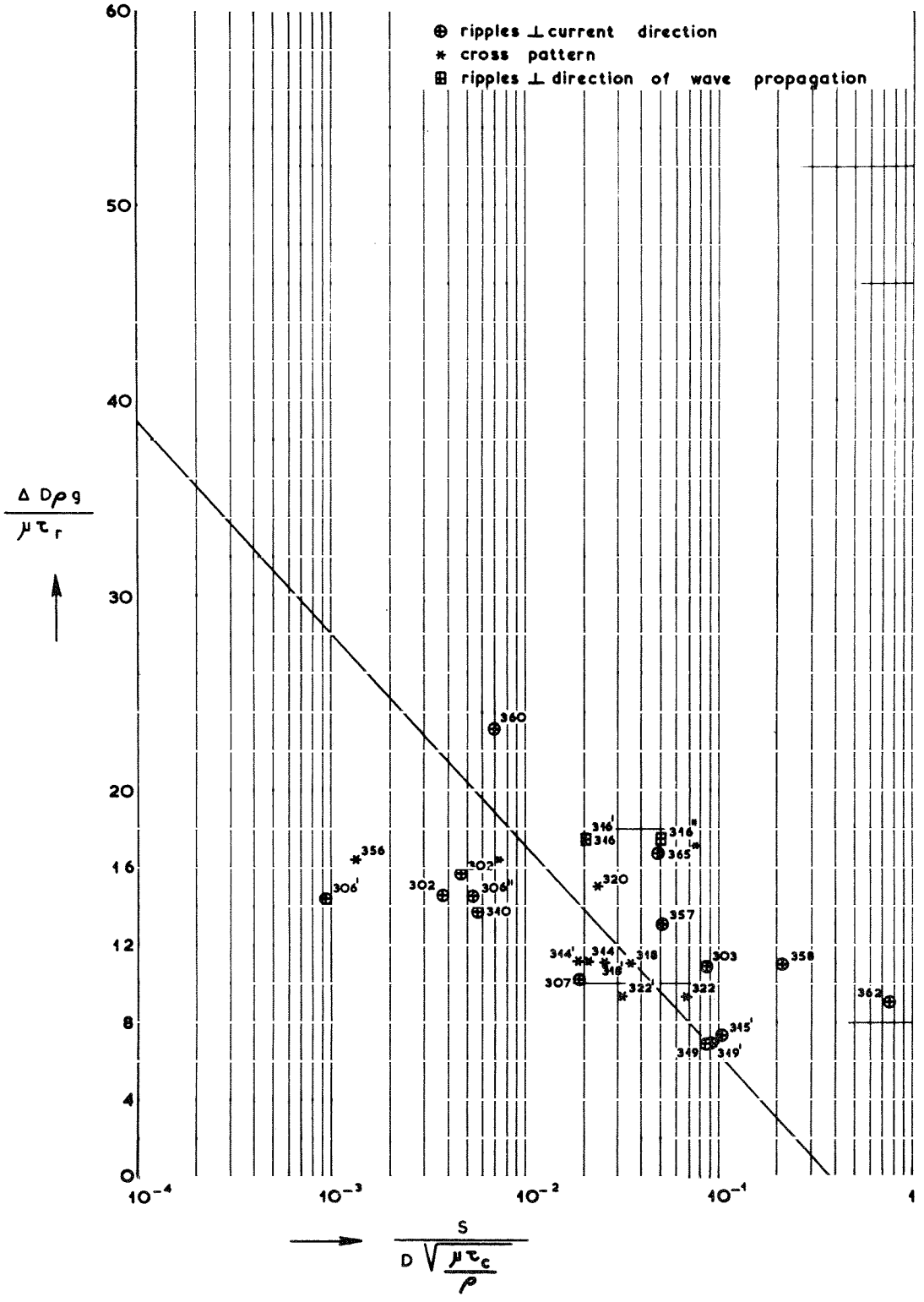

WAVE_APPROACH AT RIGHT ANGLES AND CURRENT. Series D

FIGURE IV. 2_5

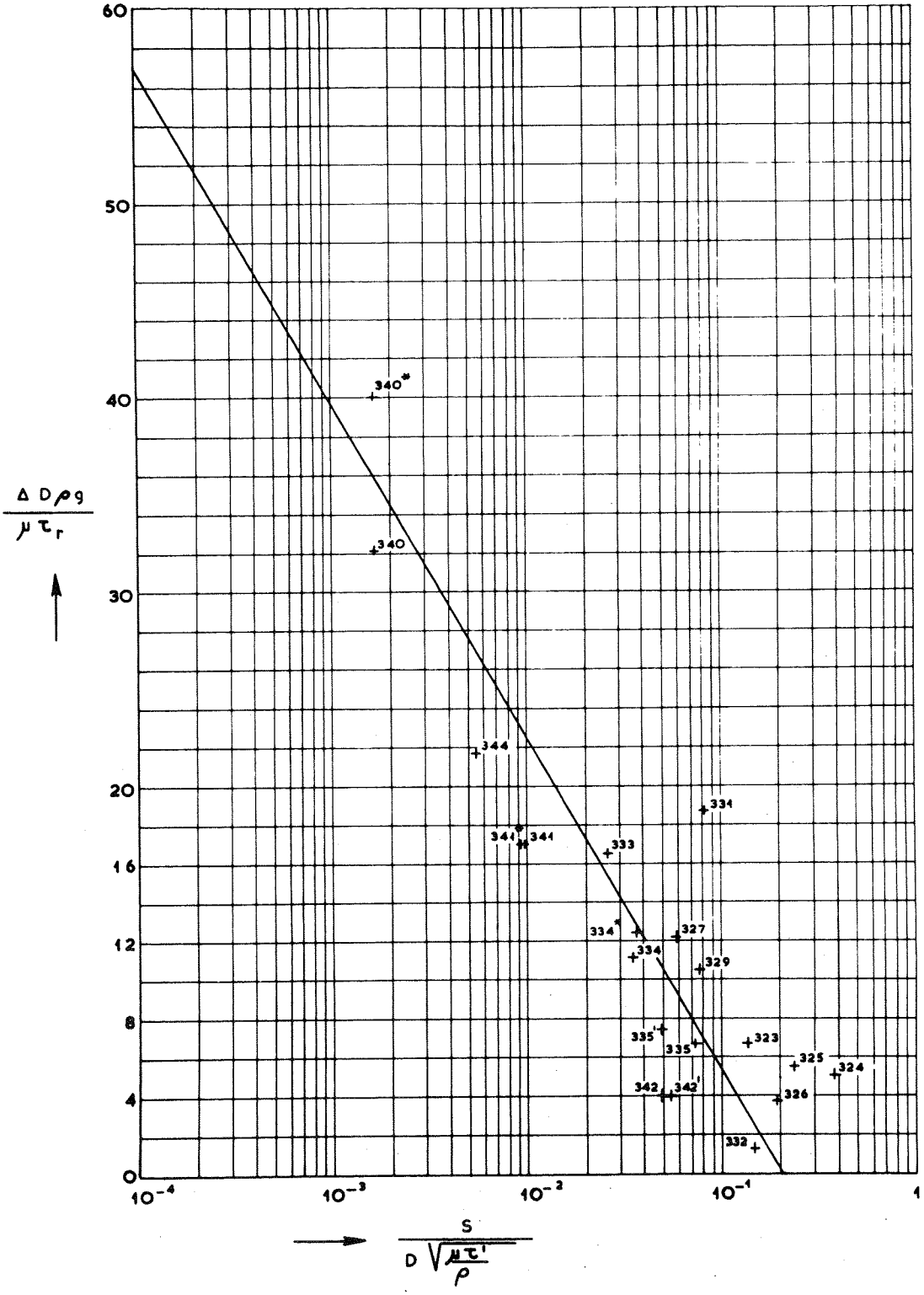

OBLIQUE WAVE_APPROACH AND CURRENT. Series G

FIGURE IV 2_6

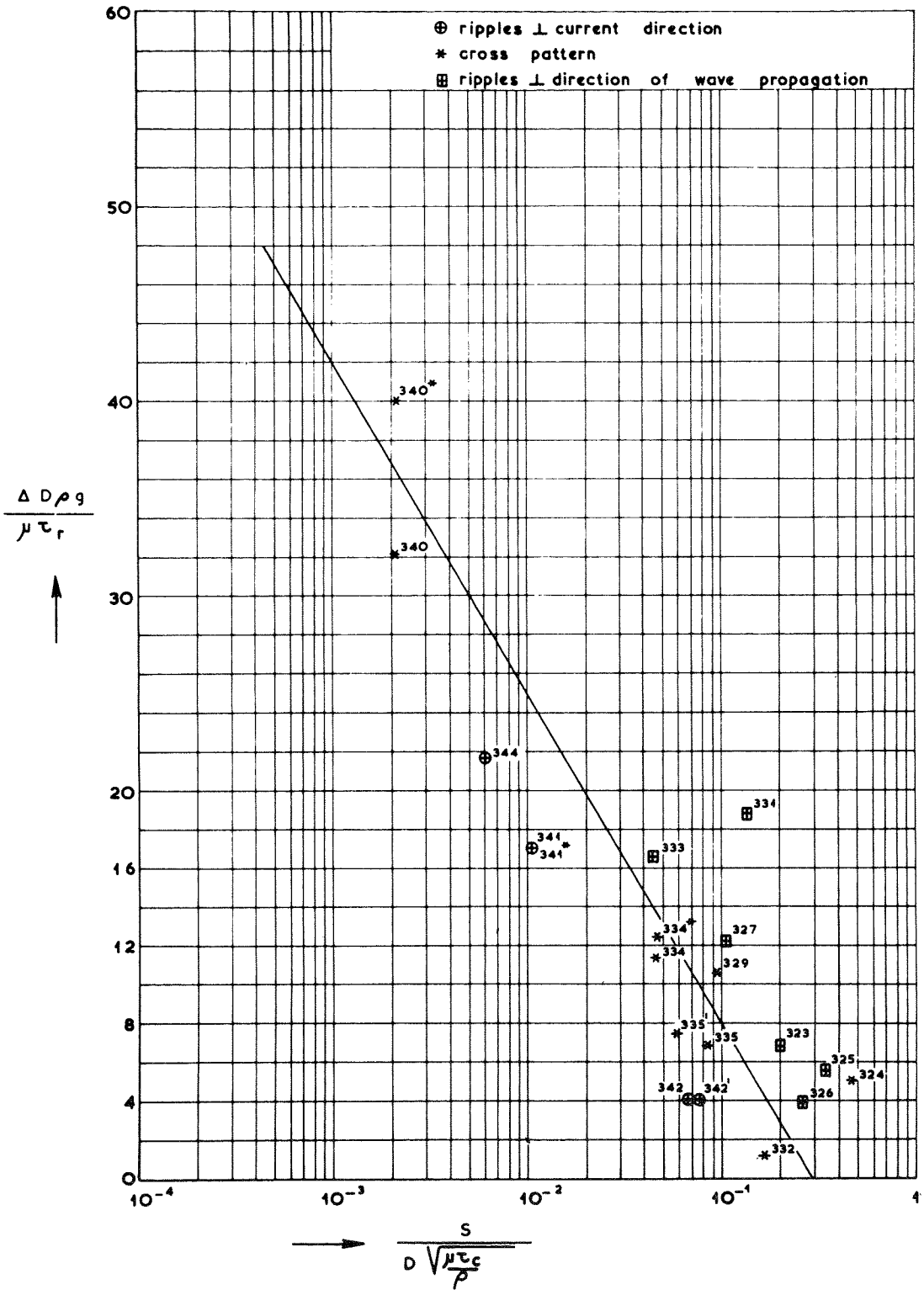

WAVE_APPROACH AT RIGHT ANGLES AND CURRENT. Series H

FIGURE IV.2_7

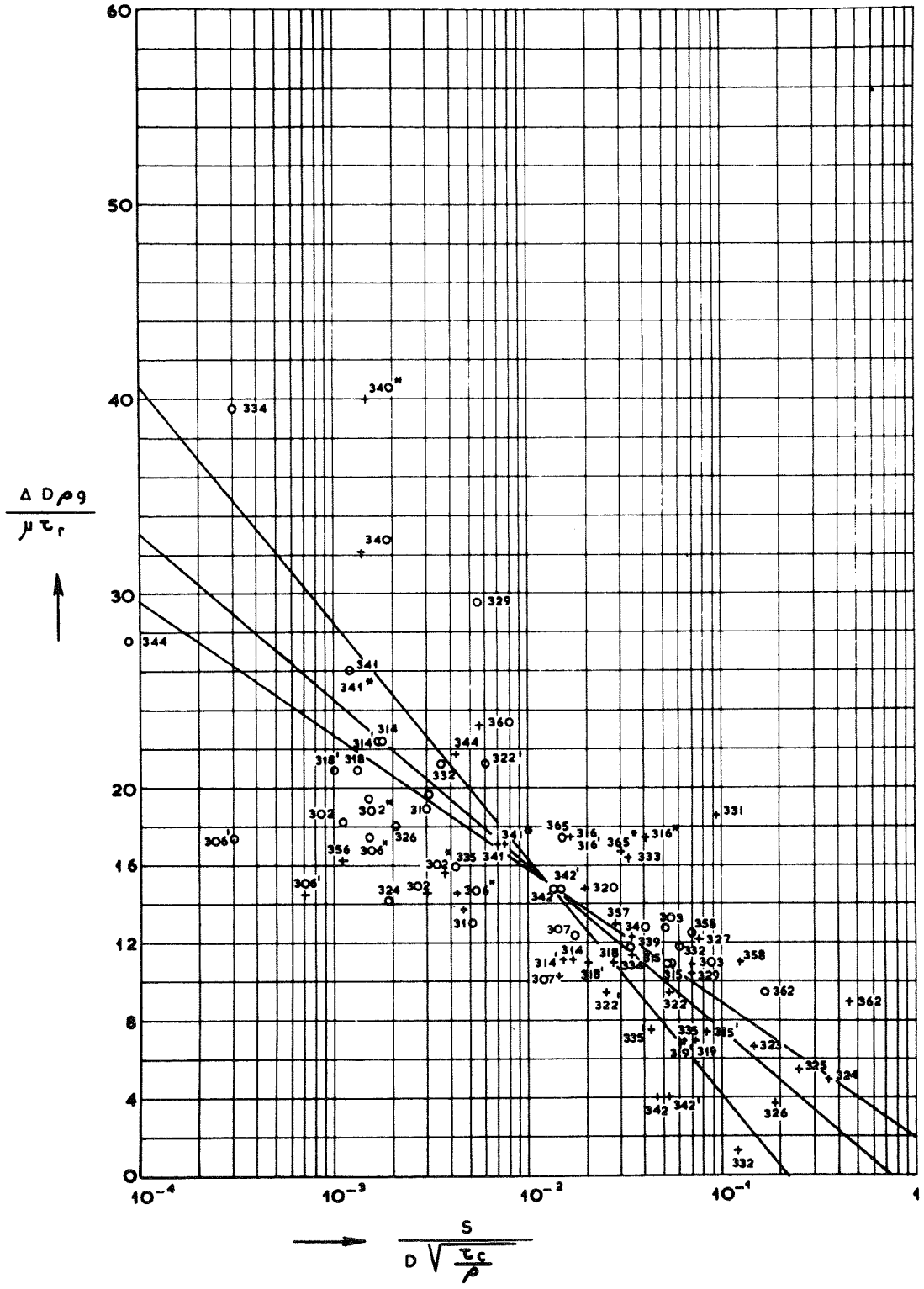

WAVES AND CURRENT. ALL DATA. Series A* E* D* H*

FIGURE IV. 2_8

current, may call for two different roughness coefficients related respectively to each of the above mentioned two different mechanisms. In figures IV.2-5 and 7 for series D and H respectively, the different ripple formations have been indicated. In series D no significant influence of the ripple pattern can be concluded to. In series H, the ripple pattern, with ripples normal to the wave direction, seems to give slightly higher transports. This gives some support for the conclusion that the waves cause an extra transport in the wave direction, due to asymmetry of the waves. The accuracy of the tests does not allow, however, to draw a quantitative conclusion with regard to this point.

In order to determine by which curve the data are best be reproduced, the values of a and b have been calculated according to the following scheme.

Parameters	$\varphi = 0$	$\varphi = 15^{o}$
$a\ \frac{\Delta D \varrho g}{\mu \tau_c}$ and $-\frac{S}{D(\mu\tau_c/\varrho)^{1/2}}$	Series AE table 12 figure IV.2-1	
$a\ \frac{\Delta D \varrho g}{\mu \tau'}$ and $\frac{S}{D(\mu\tau'/\varrho)^{1/2}}$	Series B table 13 figure IV.2-2	Series F table 16 figure IV.2-3
$a\ \frac{\Delta D \varrho g}{\mu \tau_r}$ and $\frac{S}{D(\mu\tau'/\varrho)^{1/2}}$	Series C table 14 figure IV.2-4	Series G table 17 figure IV.2-6
$a\ \frac{\Delta D \varrho g}{\mu \tau_r}$ and $\frac{S}{D(\mu\tau_c/\varrho)^{1/2}}$	Series D table 15 figure IV.2-5	Series H table 18 figure IV.2-7

For series B and F, the value of the bed shear which has been introduced, both in the transport parameter and in the stirring parameter, has been the component of the mean resultant bed shear in the direction of the current, τ'.(paragraph III.3).

For C and G, in the stirring parameter the total bed shear τ_r has been introduced. In the transport parameter the mean resultant bed shear in the current direction is again used. This is based on the assumption that the shear-stress velocity, that is the bed shear, is responsible for the transport in the direction of that shear, just as is done in the normal bed load formula of Kalinske-Frijlink.

For D and H again the total bed shear τ_r has been introduced in the stirring parameter, but in the transport parameter the bed shear τ_c, due to the current without wave influence, has been applied. The reason for this is that, when material is stirred up, the transport of this material will be determined almost entirely by the current immediately above the bottom, that is the shear-stress velocity $v_* = (\tau_c/\varrho)^{1/2} = vg^{1/2}/C$.

The data for the computation are represented in tables 12 through 18. The calculation of a and b is executed with equation (IV.1-5). In order to make it possible to use a standard procedure, it has been assumed that both $\log S/D(\mu\tau/\varrho)^{1/2}$ and $\Delta D\varrho g/\mu\tau$ are stochastic variables. By means of these data, which are, as already has been mentioned, the ordinates of the points in the graphs on which the data are plotted, the regression lines have been calculated. Moreover, the correlation coefficient was determined. Although the accuracy of the transport and the bed shear will not differ very much, the quantity $S/D(\mu\tau/\varrho)^{1/2}$ will be less accurate than the quantity $\Delta D\varrho g/\mu\tau$. The reason for this is that in the transport parameter some accumulation of inaccuracies occurs. Although these inaccuracies are reduced because the logarithme of the transport parameter is used, the values of a and b have been computed with the regression of $\log S/D(\mu\tau/\varrho)^{1/2}$ on $\Delta D\varrho g/\mu\tau$.

For the calculation of series B, the tests 316, 316', 316" and 320 were rejected and for the calculation of series F, the tests 340, 340*, 327, 331 and 333 were rejected, for the reasons given at the beginning of this paragraph.

The results of this computation are given in table 19.

Table 12

Test	$\frac{\Delta Dog}{\mu\tau_c}$	$\frac{S}{D(\mu\tau_c/\varrho)^{1/2}}$ 10^{-4}	$\frac{S}{D(\tau_c/\varrho)^{1/2}}$ 10^{-4}	
Series A				Series A*
302	18.2	14	11	
302*	19.4	19	15	
303	12.8	638	510	
306'	17.4	4	3	
306"	17.4	18	15	
307	12.4	218	174	
310	19.6	39	32	
314	22.4	22	18	
314'	22.4	21	17	
315'	11.0	624	506	
315	11.0	660	536	
318	20.9	16	13	
318'	20.9	12	10	
319	11.8	423	339	
322	21.2	43	35	
322'	21.2	74	60	
358	12.5	1210	695	
362	9.5	2850	1685	
365*	17.4	241	149	
Series E				Series E*
341	26.0	17	12	
342	14.8	188	133	
342'	14.8	206	146	
344	27.5	1.1	0.75	
341*	26.0	16	12	
324	14.2	26	19	
326	18.0	30	21	
329	29.5	76	54	
332	11.8	843	596	
334	39.4	3.8	3	
335	15.9	60	43	

Table 13 Waves and current $\varphi = 0^{o}$

	Test	$\frac{\Delta D \varrho g}{\mu \tau'}$	$\frac{S}{D(\mu\tau'/\varrho)^{1/2}}$ 10^{-4}
Series B			
	302	16.1	35
	302*	17.2	44
	303	11.6	829
	306'	15.6	9
	306"	15.6	51
	307	11.1	170
	310	16.4	52
	314	16.3	178
	314'	16.3	162
	315'	9.0	901
	316	52.4	131
	316'	52.4	132
	316"	52.4	319
	318	15.6	301
	318'	15.6	222
	319	9.2	756
	319'	9.2	772
	320	41.1	160
	322	14.7	548
	322'	14.7	261
	356	24.8	12
	360	29.3	63
	357	13.6	488
	358	11.6	2090
	362	9.1	7370
	365*	16.8	476

Table 14 Waves and current $\varphi = 0^{o}$

	Test	$\frac{\Delta D \varrho g}{\mu \tau_r}$	$\frac{S}{D(\mu\tau'/\varrho)^{1/2}\ 10^{-4}}$
Series C			
	302	14.6	35
	302*	15.6	44
	303	10.9	829
	306'	14.5	9
	306"	14.5	51
	307	10.3	170
	310	13.8	52
	314	11.2	178
	314'	11.2	162
	315'	7.4	901
	316	17.5	131
	316'	17.5	132
	316"	17.5	319
	318	11.0	301
	318'	11.0	222
	319	6.9	756
	319'	6.9	772
	320	14.9	160
	322	9.4	548
	322'	9.4	261
	356	16.3	12
	360	23.2	63
	357	13.0	488
	358	11.1	2090
	362	9.0	7370
	365*	16.7	476

Table 15 Waves and current $\varphi = 0^{o}$

Test	$\frac{\Delta D \varrho g}{\mu \tau_r}$	$\frac{S}{D(\mu\tau_c/\varrho)^{1/2}}$ 10^{-4}	$\frac{S}{D(\tau_c/\varrho)^{1/2}}$ 10^{-4}	
Series D				Series D*
302	14.6	37	30	
302*	15.6	47	37	
303	10.9	870	696	
306'	14.5	9	7	
306"	14.5	54	43	
307	10.3	179	143	
310	13.8	57	46	
314	11.2	208	169	
314'	11.2	189	153	
315'	7.4	1009	820	
316	17.5	206	164	
316'	17.5	206	164	
316"	17.5	500	400	
318	11.0	348	274	
318'	11.0	256	205	
319	6.9	860	689	
319'	6.9	877	701	
320	14.9	237	192	
322	9.4	658	535	
322'	9.4	313	254	
356	16.3	14	11	
360	23.2	70	56	
357	13.0	512	289	
358	11.1	2160	1240	
362	9.0	7550	4460	
365*	16.7	484	304	

Table 16 Waves and current $\varphi = 15^{o}$

Test	$\frac{\Delta D \varrho g}{\mu \tau'}$	$\frac{S}{D(\mu\tau'/\varrho)^{1/2}}$ 10^{-4}
Series F		
340	53.1	17
341	20.8	96
342	8.0	489
342'	8.0	540
344	23.9	56
340*	52.6	17
341*	20.8	95
323	16.2	1364
324	8.8	3730
325	14.5	2305
326	8.6	1850
327	40.0	588
329	18.1	766
331	57.8	820
333	52.1	260
332	8.7	1460
334	22.1	353
335	11.0	720
335'	11.0	487
334*	23.0	360

Table 17 Waves and current $\varphi = 15^{o}$

	Test	$\frac{\Delta D \varrho g}{\mu \tau_r}$	$\frac{S}{D(\mu\tau'/\varrho)^{1/2}}$ 10^{-4}
Series G			
	340	32.1	17
	341	17.0	96
	342	4.0	489
	342'	4.0	540
	344	21.7	56
	340*	40.0	17
	341*	17.0	95
	323	6.7	1364
	324	5.1	3730
	325	5.5	2305
	326	3.8	1850
	327	12.2	588
	329	10.5	766
	331	18.7	820
	333	16.5	260
	332	1.3	1460
	334	11.4	353
	335	6.8	720
	335'	7.5	487
	334*	12.4	360

Table 18 Waves and current $\varphi = 15^{o}$

Test	$\frac{\Delta Dog}{\mu\tau_r}$	$\frac{S}{D(\mu\tau_c/\varrho)^{1/2}}$ 10^{-4}	$\frac{S}{D(\tau_c/\varrho)^{1/2}}$ 10^{-4}	
Series H				Series H*
340	32.1	21	14	
341	17.0	107	72	
342	4.0	666	471	
342'	4.0	735	520	
344	21.7	60	43	
340*	40.0	21	15	
341*	17.0	107	74	
323	6.7	2030	1450	
324	5.1	4750	3420	
325	5.5	3490	2465	
326	3.8	2680	1890	
327	12.2	1040	750	
329	10.5	978	698	
331	18.7	1390	982	
333	16.5	445	321	
332	1.3	1700	1200	
334	11.4	471	340	
335	6.8	865	623	
335'	7.5	586	422	
334*	12.4	471	340	

Table 19

	b	a	correlation	required correlation
AE	0.34	-0.22	0.74	0.37
B	0.64	-0.23	0.67	0.43
F	0.42	-0.14	0.68	0.53
C	0.37	-0.22	0.57	0.40
G	0.21	-0.14	0.88	0.45
D	0.37	-0.21	0.55	0.40
H	0.29	-0.14	0.86	0.45
AEB	0.52	-0.23	0.74	0.28
AEF	0.59	-0.22	0.73	0.30
AEC	0.34	-0.22	0.73	0.27
AEG	0.26	-0.18	0.80	0.28
AED	0.38	-0.22	0.73	0.27
AEH	0.32	-0.19	0.79	0.28
AEBF	0.60	-0.22	0.72	0.24
AECG	0.25	-0.18	0.75	0.24
AEDH	0.24	-0.19	0.75	0.24

As it is not certain that the parameters $\log S/D(\mu\tau/\varrho)^{1/2}$ and $\Delta D\varrho g/\mu\tau$ are indeed stochastic variables, it is not appropriate to use the standard procedures in order to determine whether the values of b and a differ significantly or not for the different series. It is evident, however, that for wave-approach at right angles series C and D and for oblique wave-approach series G and H have to be preferred above series B and F respectively. The correlation of series C, D, G and H for linear regression is certainly sufficient and in these series all data are reproduced, whereas in series B and F the data with very low current velocity had to be rejected. For the series with wave-approach at right angles the coefficients b and a are closer to that for current only in the case that τ_r is used in the stirring factor.

From these tests it is not evident, which value for the bed shear has to be introduced in the transport parameter: τ' or τ_c. From a physical point of view, however, it is more likely that τ_c should be introduced instead of τ' in the transport parameter, since the material, stirred up by the waves, is just moved with the current velocity. This is also

supported by the tests with the wide sand trap which will be discussed in the next paragraph.

There is a marked difference between the lines representing the data with oblique wave-approach and those representing wave-approach at right angles and only current. This is also very clearly demonstrated by the figures IV.2-1, 5 and 7. One of the main reasons will be that, due to the orbital motion, material will be moved from both sides in the sand trap, in the case that the uniform current is small compared to the orbital motion. When corrections would be applied, the line representing the data for oblique wave-approach would come closer to those for mere current and wave-approach at right angles. However, not sufficient accurate data are available to apply these corrections. From the tests with the wide sand trap, described in the next paragraph, an equal function will be found, however, for oblique wave-approach, and for mere current.

Since one of the main objectives was to establish whether the results for current only and those for current and waves from various directions could be represented by one formula, special attention should be paid to the correlation coefficients of all data together, viz. AEBF, AECG and AEDH. In these three cases, it is certainly permissible to represent all data by one formula, but the correlation for AECG and AEDH is slightly better than for AEBF. This is even more striking, since for AEBF some values had to be rejected, as discussed earlier. These values have been taken in account for AECG and AEDH where the value τ_r was used in the stirring factor,

The magnitude of the value a is not too far off from the value of 0.27, used by Frijlink in his formula (14), but the magnitude of the value b is much smaller, viz.: 0.24 versus 5. This difference is probably caused by the small size of the sand trap in the direction of the current as has earlier been mentioned.

It has earlier in this paragraph been concluded that τ_c, instead of τ', has to be introduced in the transport parameter. In this case, however, it is also better to omit the ripple factor μ from the transport parameter. The transport parameter will then be written as: $S/D(\tau_c/\varrho)^{1/2}$ and is listed on tables 12, 15 and 18 as series A^*, E^*, D^* and H^*. The data are represented in diagram IV.2-8.

The correlation coefficients for the single groups, A^* E^*, D^* and H^* are 0.75, 0.56 and 0.89 respectively, which is equal or even slightly

better than for AE, D and H. The correlation factor for all data together is 0.75. The factor a for the two regression lines is listed in table 20. Only for series H^* the two values for a remain below 0.27. For the series A^*E^*, D^* and $A^*E^*D^*H^*$, the two regression coefficients are above and below 0.27.

Table 20

	regression of $\log S/D(\tau_c/\varrho)^{1/2}$ on $\Delta D\varrho g/\mu\tau_r$	regression of $\Delta D\varrho g/\mu\tau_r$ on $\log S/D(\tau_c/\varrho)^{1/2}$
A^*E^*	-0.21	-0.37
D^*	-0.21	-0.66
H^*	-0.14	-0.19
$A^*E^*D^*H^*$	-0.19	-0.33

Since a , as given in table 19, is the lowest of the two regression coefficients, the factor b will be determined also for the value 0.27 for a . With the factor 0.27, the formula representing all data together becomes:

$$S = 0.74\ D\ (\tau_c/\varrho)^{1/2}\ e^{-0.27\ \frac{\Delta D\varrho g}{\mu\tau_r}} \qquad \text{(IV.2-2)}$$

The regression line for all data with regression of $\log S/D(\tau_c/\varrho)^{1/2}$ on $\Delta D\varrho g/\mu\tau_r$ is:

$$S = 0.22\ D\ (\tau_c/\varrho)^{1/2}\ e^{-0.19\ \frac{\Delta D\varrho g}{\mu\tau_r}} \qquad \text{(IV.2-3)}$$

and the regression line for all data with regression of $\Delta D\varrho g/\mu\tau_r$ on $\log S/D(\tau_c/\varrho)^{1/2}$ is:

$$S = 1.95\ D\ (\tau_c/\varrho)^{1/2}\ e^{-0.33\ \frac{\Delta D\varrho g}{\mu\tau_r}} \qquad \text{(IV.2-4)}$$

IV.3. Tests with the wide sand trap

In order to study the influence of the size of the sand trap, tests have been carried out with a sand trap of 0.93 x 0.93 m^2, which was

devided in 9 x 9 small squares. The sandttrap was covered by a screen of small wooden bars, as may be seen in figure IV.3-3. The aim of this screen was twofold: firstly to present roughness which would be almost equal to that of the surrounding bottom which was covered by sand ripples, and secondly to prevent that waves and current would move sand out of the sand trap again. The sand caught in the various small traps was determined separately. In this series tests have, moreover, been executed with waves moving obliquely with and against the current. The bottom material in this test consisted of fine sand with a mean diameter D_m of 0.22 mm and a D_{90} of 0.28 mm.

Two representative samples are given in figures IV.3-1 and IV.3-2, showing the trapped quantities in cm^3 after a test duration of one hour. It is clear, indeed, that in the test with the combination of waves and current the quantities caught in the two side rows are higher than normal. This is, however, also the case in test T11 with only current, although to a smaller extent. In this case, it must be due to side effects of the sand trap which generate secondary currents.

From the results of T12, presented in figure IV.3-2, it is clear that there is also a net drift of sand in the current direction, since the side row at the side from which the waves approach shows a higher catch than the other side row. One of the aims of this test series was to establish whether this undeniable mass-transport effect of the waves would have a marked influence on the transport of the combination of waves and current. To this end, 2 test series with oblique waves against the current and with the current have been executed.

For the elaboration of the data, formula(IV.2-1)in the form of formula (IV.2-2) has been used and the values of the factor b, which is equal to 0.74 in formula (IV.2-2), have been computed.

Figures IV.3-3 through 5 give an impression about the bed roughness. From comparison with figures IV.1-3 and 4, a roughness between 1 and 3 cm may be estimated. From general experience, a roughness of about 3 cm could be expected. However, all computations have been carried out with a roughness of 1 and of 3 cm. The depth during the tests was 0.30 m. The resistance coefficient C and the ripple factor μ have, for the values of 1 and 3 cm for the bed roughness, the values: $C = 46\ m^{1/2}/s$, $\mu = 0.42$ and $C = 37\ m^{1/2}/s$, $\mu = 0.35$ respectively.

The angle φ between wave crests and current direction in still water (in which case the current velocity is zero) was 25°. For a wave direction with a component in the current direction and with a component against the

CURRENT

28	26	15	14	11	9	9	8	27
12	9	10	9	7	6	6	6	10
11	12	9	7	6	6	6	5	9
9	10	8	7	6	6	6	6	7
13	8	7	8	6	5	4	5	7
12	8	7	6	5	5	5	5	7
12	7	6	6	5	5	4	5	6
12	6	6	4	5	4	4	5	6
12	7	6	6	5	11	8	4	5

0.93m

0.93m

CAPTURED QUANTITIES IN cm^3 AFTER 1 HOUR CURRENT WITH $v = 0.31\ m/s$ T11 FIGURE IV. 3_1

WAVES

28°

70	60	55	45	43	40	48	42	50
52	37	31	33	29	27	25	29	37
40	29	28	22	25	24	23	22	29
41	26	24	23	21	21	21	22	27
38	24	21	25	23	20	18	22	28
34	22	19	19	18	19	18	18	23
36	23	21	18	19	22	17	22	22
42	22	22	16	15	15	16	17	19
19	36	26	20	17	17	16	16	20

CAPTURED QUANTITIES IN cm^3 AFTER 1 HOUR CURRENT WITH $v = 0.32\ m/s$, AND A WAVE FROM INDICATED DIRECTION WITH $H = 0.03$ m AND $T = 1.83$ s T 12 FIGURE IV. 3_2

Figure IV.3-3
Test with wide sand trap
T4. waves and current

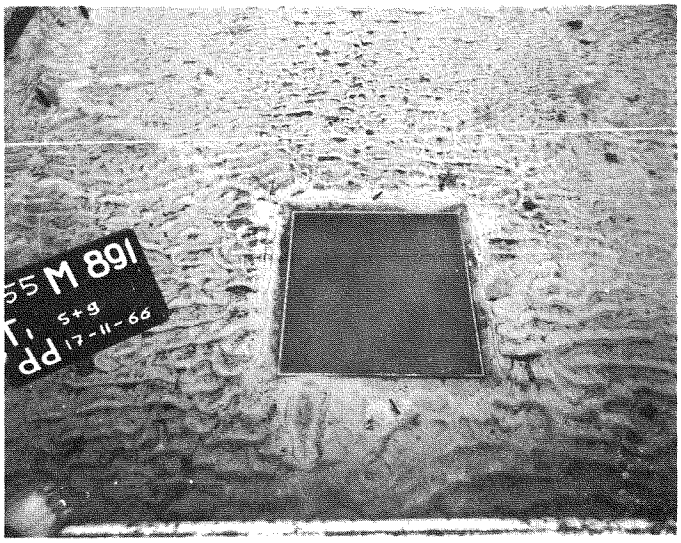

Figure IV.3-4
Tests with wide sand trap
T1. waves and current

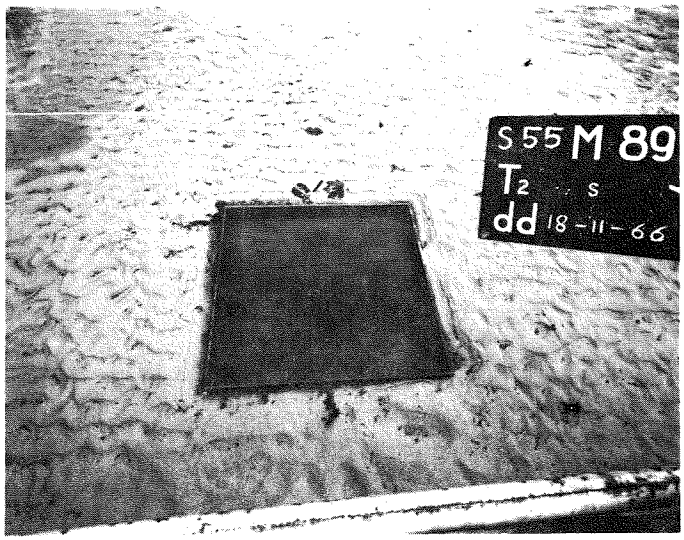

Figure IV.3-5
Test with wide sand trap
T2. only current

Table 21

Test	v	u_o	S_{mes} narrow trap 10^{-9} m^2/s	S_{mes} wide trap 10^{-9} m^2/s	S_{cal} C = 46 $m^{1/2}/s$ 10^{-9} m^2/s	S_{cal} C = 37 $m^{1/2}/s$ 10^{-9} m^2/s
2	0.31	0	34	70	77	141
3	0.32	0	37	50	57	107
11	0.31	0	45	175	57	107
11'	0.30	0	58	210	41	79
1	0.33	0.06	106	177	163	244
4	0.31	0.09	30	67	166	212
12	0.32	0.08	168	600	161	224
12'	0.32	0.07	86	370	139	203
13	0.32	0.15	178	450	463	489
13'	0.30	0.15	140	408	365	368
22	0.36	0.14	263	955	637	740
14'	0.25	0	3	17	4	10
14"	0.26	0	3	27	7	17
14"'	0.29	0	8	28	28	57
17	0.34	0	24	100	131	230
19	0.37	0	183	540	252	419
19'	0.37	0	85	215	252	419
15	0.30	0.06	13	41	73	112
15'	0.27	0.08	16	49	48	62
16	0.28	0.14	15	127	235	229
16'	0.28	0.15	31	93	283	269
16"	0.31	0.13	49	135	304	332
16"'	0.28	0.14	43	125	235	229
18	0.35	0.13	77	246	510	600
20	0.40	0.12	356	1050	801	1017

Table 21

$\frac{u_o}{v}$	narrow trap		wide trap	
	b ($C = 46\ m^{1/2}/s$)	b ($C = 37\ m^{1/2}/s$)	b ($C = 46\ m^{1/2}/s$)	b ($C = 37\ m^{1/2}/s$)
	0.4	0.2	0.9	0.5
	0.6	0.4	0.9	0.5
	0.8	0.4	0.3	1.6
	1.4	0.7	5.1	2.6
	$\bar{b} = 0.8$	$\bar{b} = 0.4$	$\bar{b} = 1.8$	$\bar{b} = 1.3$
	$\sigma_b = 0.4$	$\sigma_b = 0.21$	$\sigma_b = 2.2$	$\sigma_b = 1.01$
0.18	0.6	0.4	1.1	0.7
0.29	0.2	0.1	0.4	0.3
0.25	1.0	0.8	3.7	2.7
0.22	0.6	0.4	2.7	1.8
0.47	0.4	0.4	1.0	0.9
0.50	0.4	0.4	1.1	1.1
0.39	0.4	0.4	1.5	1.3
	$\bar{b} = 0.5$	$\bar{b} = 0.4$	$\bar{b} = 1.3$	$\bar{b} = 1.1$
	$\sigma_b = 0.3$	$\sigma_b = 0.2$	$\sigma_b = 1.2$	$\sigma_b = 0.81$
	0.8	0.3	4.2	1.7
	0.4	0.2	3.9	1.6
	0.3	0.1	1.0	0.5
	0.2	0.1	0.8	0.4
	0.1	0.4	2.1	1.3
	0.3	0.2	0.8	0.5
	$\bar{b} = 0.4$	$\bar{b} = 0.2$	$\bar{b} = 2.1$	$\bar{b} = 1.0$
	$\sigma_b = 0.2$	$\sigma_b = 0.12$	$\sigma_b = 1.5$	$\sigma_b = 0.6$
0.20	0.2	0.1	0.6	0.4
0.30	0.3	0.3	1.0	0.8
0.50	0.1	0.1	0.5	0.6
0.54	0.1	0.1	0.3	0.4
0.42	0.2	0.2	0.4	0.4
0.50	0.2	0.2	0.5	0.5
0.37	0.2	0.1	0.5	0.4
0.30	0.4	0.4	1.3	1.0
	$\bar{b} = 0.3$	$\bar{b} = 0.2$	$\bar{b} = 0.6$	$\bar{b} = 0.6$
	$\sigma_b = 0.1$	$\sigma_b = 0.1$	$\sigma_b = 0.3$	$\sigma_b = 0.23$

current direction, the new value of φ has been calculated. For waves, going with the current, the value of φ varies between 27^o and 28^o and for waves, going against the current, the value of φ varies between 22^o and 23^o. With these angles, also the corrected values of the orbital velocity at the bottom have been computed.

The transports were calculated on a computer by means of the following formula:

$$S = b.\ D\ \frac{v}{C}\ g^{1/2}\ e^{-0.27\ \frac{\Delta DC^2}{\mu v^2 (1 + \frac{1}{2}(\xi \frac{u_o}{v})^2)}} \qquad \text{(IV.3-1)}$$

This formula is equal to formula(IV.2-2),where $D\ \frac{v}{C}\ g^{1/2}$ stands for $D(\tau_c/\varrho)^{1/2}$ and

$\frac{\Delta DC^2}{\mu v^2 (1 + \frac{1}{2}(\xi \frac{u_o}{v})^2)}$ stands for $\frac{\Delta D \varrho g}{\mu \tau_r}$.

All results are represented in table 21. In this table the quantities trapped in the whole sand trap,excluding both side rows,are given as "S_{mes} wide trap". For comparing these results with those of the tests with a narrow sand trap, the quantities trapped in the first upstream row, and half the quantities of the second row are given in the table as "S_{mes} narrow trap". This trap corresponds with the narrow trap of 0.15 m width used in the previous tests.

Since the roughness of 3 cm is the most likely, the results of the computations with this roughness will be discussed in more detail. Finally, it will be argued that results obtained with a bed roughness of 1 cm will not lead to other conclusions.

In table 22 all results are summarized.

The following conclusions from the tests with a roughness of 3 cm may be drawn.

(i) The scatter in the results with the wide trap is very great. The reason is most probably that in the lower layers of the flow part of the material is moved in suspension (saltation). It is quite to be expected that in the quantities of this part, caught in the trap, a great variation will occur. This is supported by the fact that the values for b, which are computed with the quantities measured in the wide trap for waves and current, are smaller than for current only. This may be explained by the fact that the turbulence for the combination of waves and current is higher than for current only,

Table 22 Values of b

		current ←	current ← and waves ↙ $\varphi = 28^{o}$	current →	current → and waves ↙ $\varphi = 22^{o}$
roughness r = 3 cm	narrow trap	0.4 ± 0.21	0.4 ± 0.20	0.2 ± 0.12	0.2 ± 0.10
	wide trap	1.3 ± 1.01	1.1 ± 0.81	1.0 ± 0.60	0.6 ± 0.23
roughness r = 1 cm	narrow trap	0.8 ± 0.40	0.5 ± 0.3	0.4 ± 0.2	0.3 ± 0.1
	wide trap	1.8 ± 2.2	1.3 ± 1.2	2.1 ± 1.5	0.6 ± 0.3
number of observations		4	7	6	8
Tests		2,3,11,11'	1,4,12,12' 13,13',22	14',14",14"' 17,19,19'	15,15',16, 16',16",16"' 18,20.

so that a smaller part of the total quantity of transported material will be trapped.

(ii) The transports in the two different directions, for current only, differ significantly, when it is assumed that the values of b, as calculated by this procedure, are distributed around their mean values like stochastic variables. The reason may be found in the fact that although sand with the same diameter was applied, the packing of the sand at both sides of the sand trap was different. Another explanation may be that, although the mean velocity was equal, the upstream conditions for the two current directions were not equal. This results in a different vertical velocity distribution and from that in a different bed shear. Although from visual judgement, the ripple patterns and heights for both situations were equal, a slight change in ripple coefficient might also cause this difference in the values of b . Since it was not possible to predict the difference in the ripple coefficient beforehand, it has not been introduced in the calculations.

(iii) For wide and narrow sand traps the values of b for current only and for the combination of current and waves, are not significantly different. Hence the conclusion may be drawn, that the transport of material is increased by the waves, independent of the fact whether the waves are propagating obliquely with the current, or against the current.

Although the agreement in the results with a roughness value of 1 cm - which value is less likely - is not so good, the major conclusion, viz. that transport by the current is increased by the waves by an equal factor, irrespective of the fact that the waves propagate obliquely with or against the current, holds equally good.

IV.4. Conclusions

The main conclusions from the tests described in the foregoing paragraph are the following.

(i) The transport of a combination of waves and current can be written as:

$$S = b \cdot D \frac{v}{C} g^{1/2} e^{-0.27 \frac{\Delta D C^2}{\mu v^2 (1 + \frac{1}{2} (\xi \frac{u_o}{v})^2)}} \qquad \text{(IV.4-1)}$$

in which $\xi = p \varkappa C / g^{1/2}$, or:

$$S = b \cdot D \, (\tau_c/\varrho)^{1/2} \, e^{-0.27 \frac{\Delta D \varrho g}{\mu \tau_r}} \qquad \text{(IV.4-2)}$$

(ii) The principal difference of this equation with the original one of Kalinske-Frijlink is, that the ripple factor is operative only in the stirring parameter, and not in the transport parameter. Keeping in mind the definition of the ripple factor, as defining that part of the bed shear which is not used to overcome bed resistance, it is physically more justified to introduce this factor only in the stirring parameter. Once the material is stirred up, it is moved with the current velocity. Hence, a ripple factor seems here to have less sense.

(iii) A rather important variation may occur in the factor b. For the determination of the scales of the velocity and the wave height this is not so important. It will, however, always be necessary to carry out some calibration tests for the determination of the transport and time scale.

(iv) The values for the resistance coefficient C, which are introduced for prototype and model in the equations, may have a rather important influence on the results. Since it is not always possible to predict these values with sufficient accuracy, computations of the scale factor will have to be performed with different values of C. From these computations the possible variation in the scale factors resulting from a wrong evaluation of the resistance, can then be predicted.

CHAPTER V

SCALE LAWS FOR MODELS WITH MOVABLE BED

V.1. Scales with respect to the reproduction of the current pattern

As stated already in par. II.3, the main requirement for a coastal model with a movable bed is, that the transport scale is invariable all over the model. From the results obtained by the author and presented in chapter IV, it follows that the transport by a combination of waves and current may be described by the formula:

$$S = b\, D\, \frac{v}{C}\, g^{1/2}\, e^{-0.27\, \frac{\Delta DC^2}{\mu v^2 (1 + \frac{1}{2}(\xi \frac{u_o}{v})^2)}} \qquad (V.1\text{-}1)$$

According to this formula, and also according to the experience of the Delft Hydraulics Laboratory, the transport of material offshore the breaker region is determined almost exclusively by the current. In order to obtain the correct development of the bottom configuration the current pattern should, therefore, be reproduced with similarity to the prototype.

The requirement for the reproduction of the bed resistance with respect to reproduction of the current pattern is discussed by Bijker, Stapel and de Vries (7). If, otherwise than in the aforementioned publication, where the ratio between convective and resistance terms in the model is taken as reference, the ratio between these terms in the prototype is taken, the following derivation can be given for the determination of the scale n_R of the radius of curvature R.

The two equations which determine the current pattern are:

$$\frac{\partial \frac{1}{2} v^2}{\partial s} + g \frac{\partial z}{\partial s} + g \frac{v^2}{C^2 d} = 0 \qquad (V.1\text{-}2)$$

and:

$$\frac{v^2}{R} + g \frac{\partial z}{\partial n} = 0 \qquad (V.1\text{-}3)$$

where z is the ordinate of the water level and s and n are the ordinates in the direction of the current and at right angles thereto. Since the scales of n and s should be the same and equal to n_l the two equations may be combined to :

$$n\left(\frac{\partial \frac{1}{2} v^2}{\partial l} + g \frac{v^2}{C^2 d}\right) = n\left(\frac{v^2}{R}\right) \qquad (V.1\text{-}4)$$

The ratio $$K = \frac{\Delta\left(\frac{v^2}{2g}\right)}{\frac{v^2}{C^2 d} \cdot \Delta(l)} \qquad (V.1\text{-}5)$$

indicates the ratio between the convective and resistance terms in the prototype, and the scale for K is:

$$n_K = \frac{n_C^2 \, n_d}{n_l} \qquad (V.1\text{-}6)$$

The equation (V.1-4) may now be written as:

$$n\left((K + 1)\,\frac{gv^2}{C^2 d}\right) = n\left(\frac{v^2}{R}\right) \qquad (V.1\text{-}7)$$

From the latter equation the following scale relationship can be derived.

$$\frac{(K + 1)_{pr}}{(K + 1)_m} \cdot \frac{n_v^2}{n_C^2 \, n_d} = \frac{n_v^2}{n_R} \qquad (V.1\text{-}8)$$

Hence: $$n_R = \frac{(K + 1)_m \, n_C^2 \, n_d}{(K + 1)_{pr}} \qquad (V.1\text{-}9)$$

and: $$\frac{n_R}{n_l} = \frac{K + \frac{n_C^2 \, n_d}{n_l}}{K + 1} \qquad (V.1\text{-}10)$$

The variation of n_R/n_l with variating value of K as function of $n_C^2 \, n_d/n_l$ is shown in figure V.1-1.

However, the wave motion may also cause a change in the current pattern, due to the bed shear component at right angles to the main current, τ''. For a current which is determined by differences in water level, the current direction will coincide with the direction of the slope of the water surface. Deviation will occur only due to inertia effects and due to secondary currents. When wave motion is superimposed on such a current, the current pattern will change due to the fact that the resultant bed shear will be directed in the direction of the original slope. The current will , therefore, tend to deviate from its original direction. If the wave motion has a component in the direction of the current, the bed shear component normal to the original current will be directed in the direction

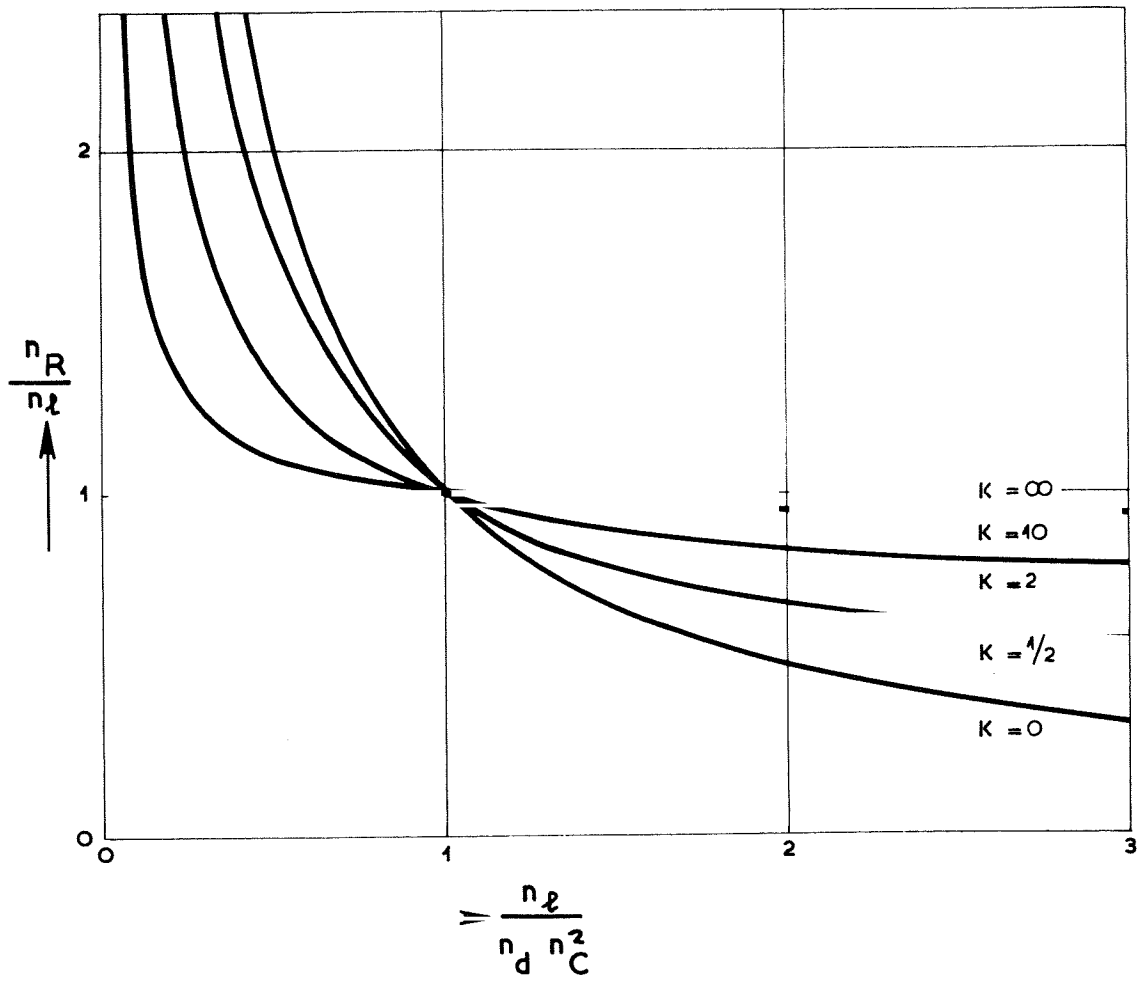

$$\frac{n_R}{n_\ell} = f\left(K, \frac{n_\ell}{n_d\, n_C^2}\right)$$

FIGURE V.1_1

of the component of the wave motion normal to the current (see figure III.3-2). The resultant bed shear would be deflected in the direction of wave propagation. Since, however, the main cause of the current is an energy gradient, this resultant bed shear will be directed in the original current direction and the current will be deflected in the opposite direction, viz. against the direction of wave propagation. The opposite effect will occur if the wave motion opposes the current, that is when the wave motion has a component against the direction of the current. In this case, the resultant bed shear will have the tendency to be deflected against the direction of wave propagation. According to the same reasoning as given above, this will result in a deflection of the current in the direction of wave propagation.

This phenomenon is demonstrated in the figures V.1-2 through V.1-5. In these figures the current is made visible by dye. Figure V.1-2 shows the current pattern around an obstruction along the coast, and figure V.1-3 shows the same situation but with waves with a component in the direction of the current. It is clear that in the vicinity of the construction,where the correcting influence of the continuity conditions has not yet exerted its influence,the current is deflected against the direction of wave propagation. In figure V.1-4 a current in the opposite direction around the obstruction is shown, without waves and in figure V.1-5 with waves with a component against the direction of the current. In this case the current deflects in the direction of wave propagation. A qualitative computation of this deflection will be given later on in this paragraph.

If this effect is superimposed on a current parallel to a long straight beach, the current would have the tendency to be deflected off the coast in case the direction of wave propagation is directed slightly with the current. If, however, the component of wave propagation parallel to the coast has a direction opposite to that of the current, the current will be directed towards the coast. For reasons of continuity, both situations are impossible over long distances, and for this reason secondary currents will be generated, together with a transverse slope at right angles to the shoreline.

Taking into consideration the inevitable divergences between prototype and model, it would not be sensible to study these secondary currents in detail. However, both with respect to the reproduction of current patterns around structures and with respect to the reproduction of similar conditions along a straight beach, it will be important to have, as much as possible, the same ratio τ''/τ' in the prototype and in the model.

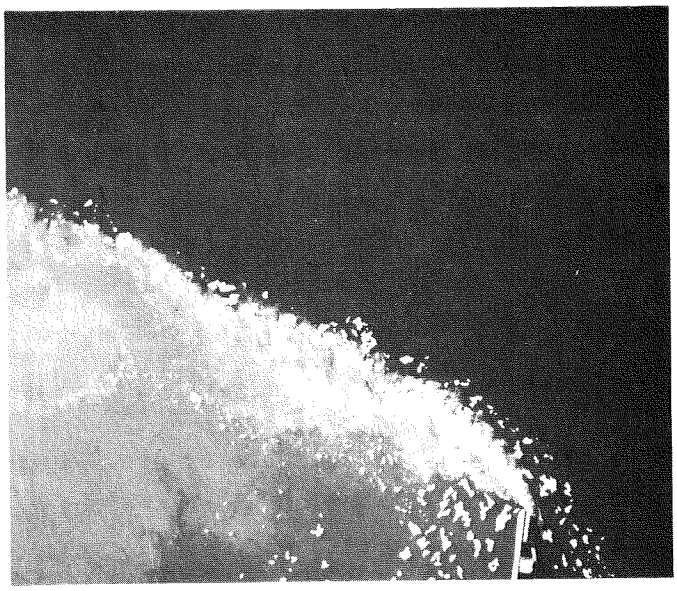

Figure V.1-2

Current pattern without waves

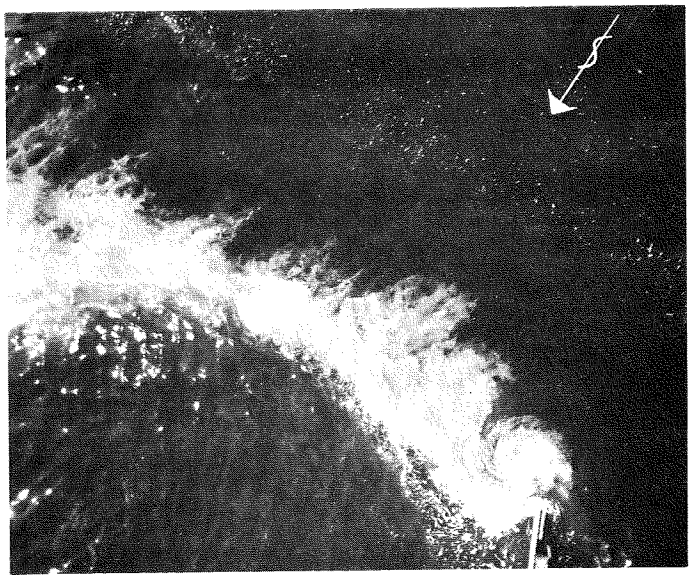

Figure V.1-3

Current pattern with waves

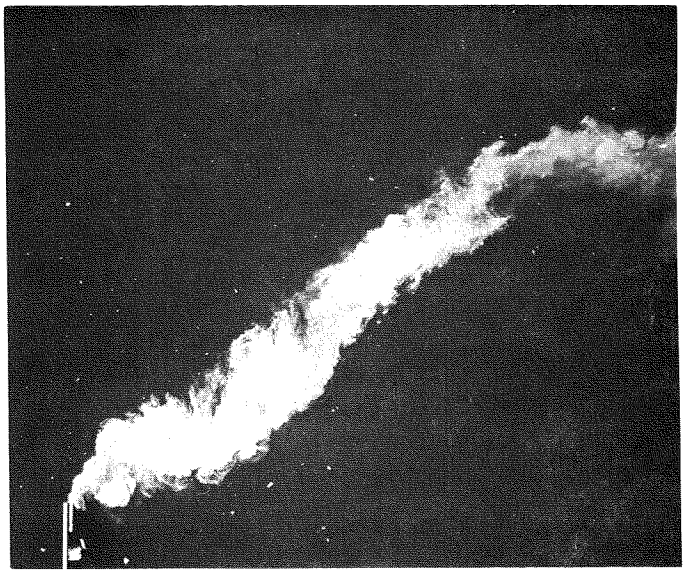

Figure V.1-4
Current pattern without waves

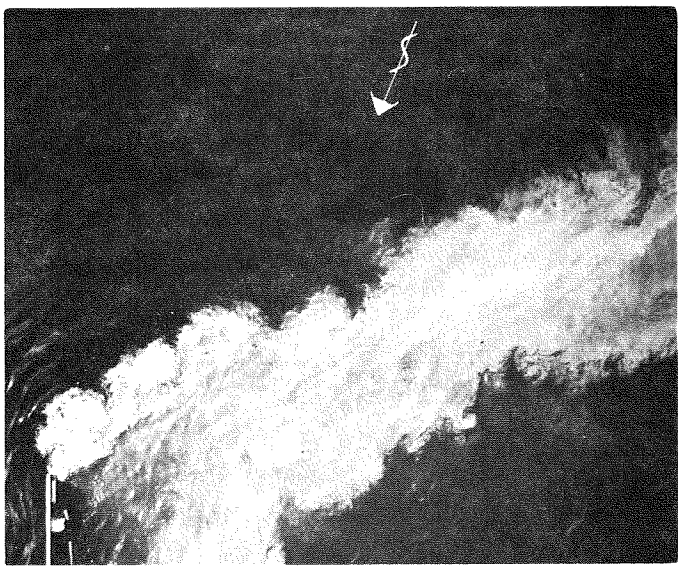

Figure V.1-5
Current pattern with waves

According to par. III.3, equations (III.3-18) and (III.3-24) for values of φ less than 20^{o}:

$$\tau' = \tau_c \left[0.75 + 0.45 \left(\xi \frac{u_o}{v}\right)^{1.13}\right] \qquad (V.1\text{-}11)$$

and:

$$\tau'' = \tau_c \varphi \left[-0.3 + 0.7 \left(\xi \frac{u_o}{v}\right)^{0.98}\right] \qquad (V.1\text{-}12)$$

According to the approximation given in paragraph III.3,(equations (III.3-19), (III.3-20) and (III.3-25), (III.3-26)),which is more general and which gives, moreover, better results for values of $\xi\, u_o/v$ smaller than 1:

$$\tau' = \tau_c \left[1 + (0.36 - 0.14 \cos 2\varphi)\left(\xi \frac{u_o}{v}\right)^{1.5}\right] \qquad (V.1\text{-}13)$$

and:

$$\tau'' = \tau_c \; 0.205 \sin 2\varphi \left(\xi \frac{u_o}{v}\right)^{1.25} \qquad (V.1\text{-}14)$$

From these formulae it is evident that the necessary and sufficient requirement for true reproduction of τ''/τ' is that $\xi\, u_o/v$ is equal for prototype and model.
Hence:

$$n_\xi \frac{n_{u_o}}{n_v} = n_C \frac{n_{u_o}}{n_v} = 1 \qquad (V.1\text{-}15)$$

Normally n_C will be in the order of magnitude of 2, so that $n_{u_o} \simeq n_v/2$. Hence, when the main current velocity is exaggerated due to transport reproduction requirements, the orbital velocity should be exaggerated even more. In most cases this will not be possible, however. For this reason discrepances in the ratio $\tau''/\tau' = \Theta$ due to deviations from this scale requirement, will be inevitable. In order to relate these discrepancies to the actually occurring phenomena the deviation $\Delta(\theta)$ from θ, as should occur theoretically in the model, will be computed. When the value of $\Delta(\theta)$ remains small, no serious discrepancies will occur.

From equations (V.1-11) and (V.1-12) follows:

$$\frac{\Delta(\theta)}{\varphi} = \frac{-0.3 + 0.7 \left(\xi \frac{u_o}{v}\right)^{0.98} \cdot \left(\frac{n_v}{n_C\, n_{u_o}}\right)^{0.98}}{0.75 + 0.45 \left(\xi \frac{u_o}{v}\right)^{1.13} \cdot \left(\frac{n_v}{n_C\, n_{u_o}}\right)^{1.13}} - \frac{-0.3 + 0.7 \left(\xi \frac{u_o}{v}\right)^{0.98}}{0.75 + 0.45 \left(\xi \frac{u_o}{v}\right)^{1.13}} \qquad (V.1\text{-}16)$$

The factors $\xi\, u_o/v$ without subscript denote in this and the following expression the values for the prototype.
From (V.1-13) and (V.1-14) follows:

$$\Delta(\theta) = \frac{0.205 \sin 2\varphi \left(\xi \frac{u_o}{v}\right)^{1.25} \cdot \left(\frac{n_v}{n_c\, n_{u_o}}\right)^{1.25}}{1 + (0.36 - 0.14 \cos 2\varphi)\left(\xi \frac{u_o}{v}\right)^{1.5} \cdot \left(\frac{n_v}{n_c\, n_{u_o}}\right)^{1.5}} - \frac{0.205 \sin 2\varphi \left(\xi \frac{u_o}{v}\right)^{1.25}}{1 + (0.36 - 0.14 \cos 2\varphi)\left(\xi \frac{u_o}{v}\right)^{1.5}} \qquad \text{(V.1-17)}$$

A positive value of $\Delta(\theta)$ indicates an increase of the deflection θ, whereas a negative value of $\Delta(\theta)$ indicates a decrease of θ.

From the results of the computations, represented in the figures V.1-6 through V.1-11, the following conclusions may be drawn.

For rather high values of $\xi\, u_o/v$, say > 7, important discrepancies have only to be expected when $n_v/n_c\, n_{u_o} < 0.4$. This will occur rather seldom.

For more normal values of $\xi\, u_o/v$, say between 1 and 4, more important discrepancies may occur. These discrepancies will be smaller for values of $n_v/n_c\, n_{u_o} > 1$, than for values of $n_v/n_c\, n_{u_o} < 1$. The deflection of the resultant bed shear from the original current direction, or the deflection of this current will increase in the model as compared to the prototype when $n_v/n_c\, n_{u_o} > 1$, and decrease when $n_v/\, n_c\, n_{u_o} < 1$.

In general, the discrepancies will be so small that no great influence on the model results has to be feared. This is also confirmed by the results of various investigations where this requirement was not met. Of more importance is probably the situation where bottom material may be shifted by the wave motion from the main current into an area of bar formation.

V.2. Scales with respect to the reproduction of bed load

The requirements for invariability of the transport scale all over the model can be obtained by dividing the sediment transport in the prototype by that in the model and by establishing the conditions that should be met to obtain a constant value of this transport scale. This method is also used by Bijker, Stapel and de Vries (6, 7) for movable bed models with current only.

Using the formula (V.1-1), the following expression is obtained:

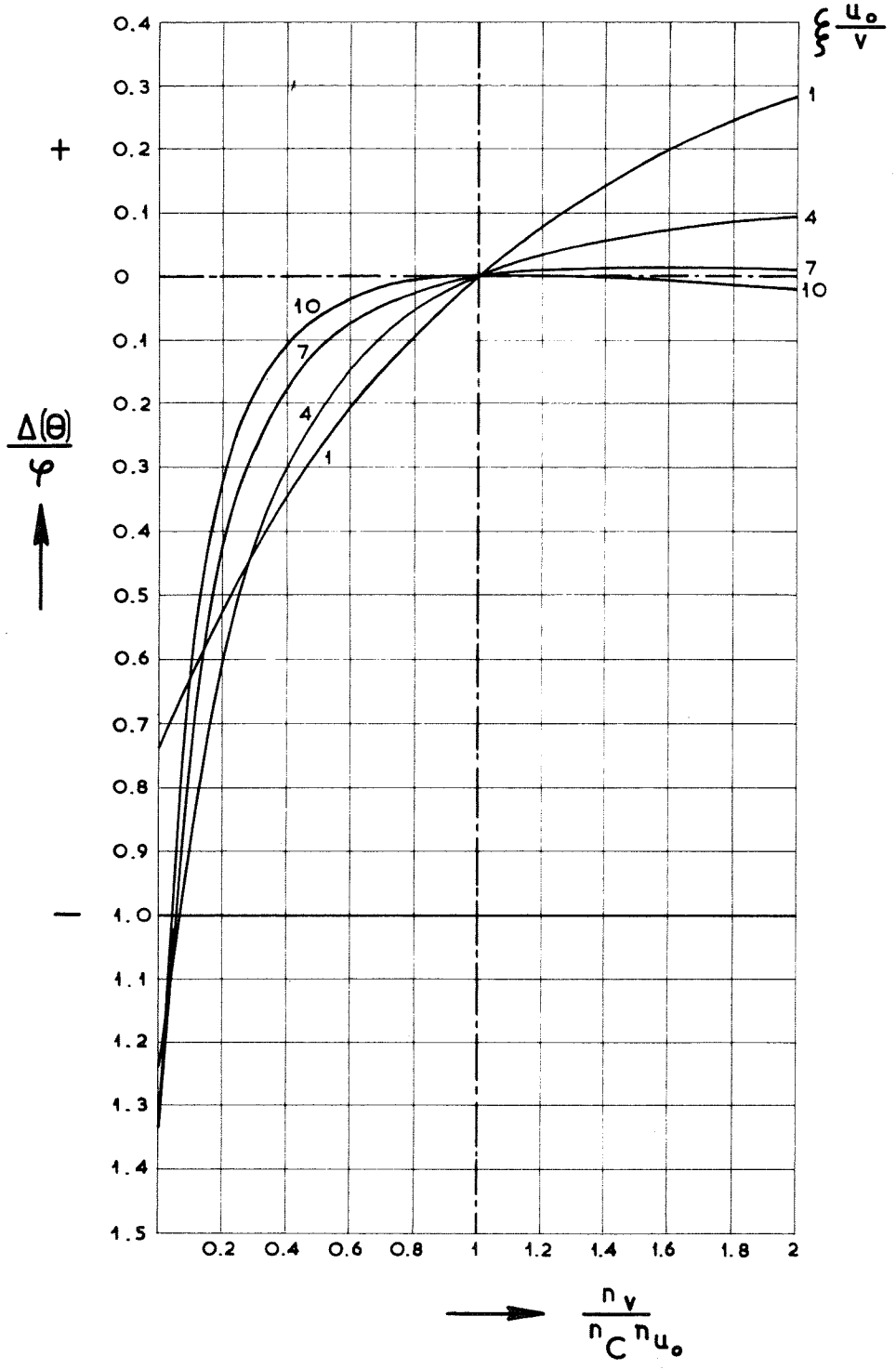

$$\frac{\Delta(\theta)}{\varphi} = f\left(\frac{n_v}{n_C n_{u_o}}, \xi \frac{u_o}{v}\right)$$

FIGURE V.1_6

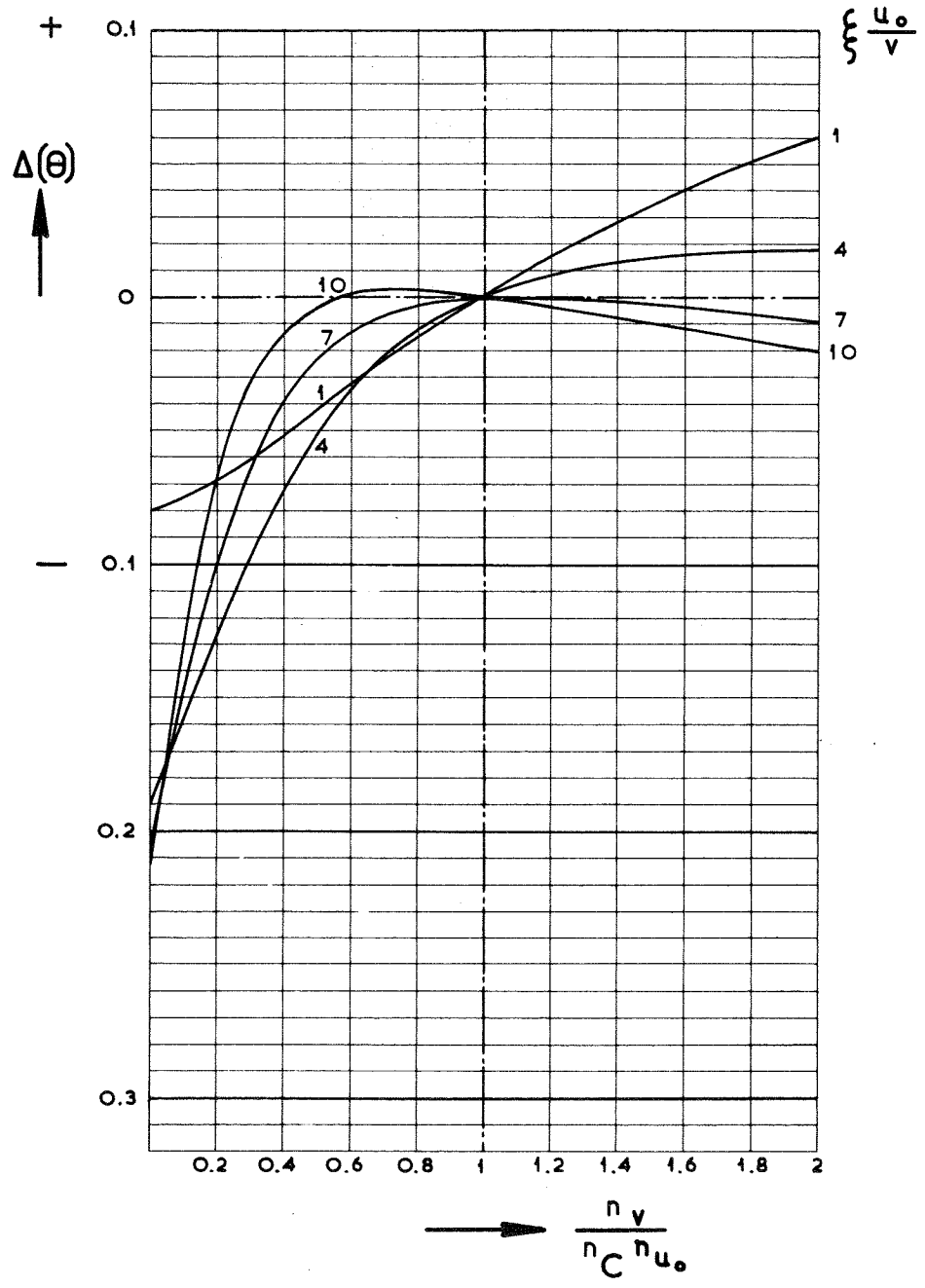

$$\Delta(\theta) = f\left(\frac{n_v}{n_C n_{u_o}},\ \xi\frac{u_o}{v}\right) \text{ FOR } \varphi = 15^\circ$$

FIGURE V.1_7

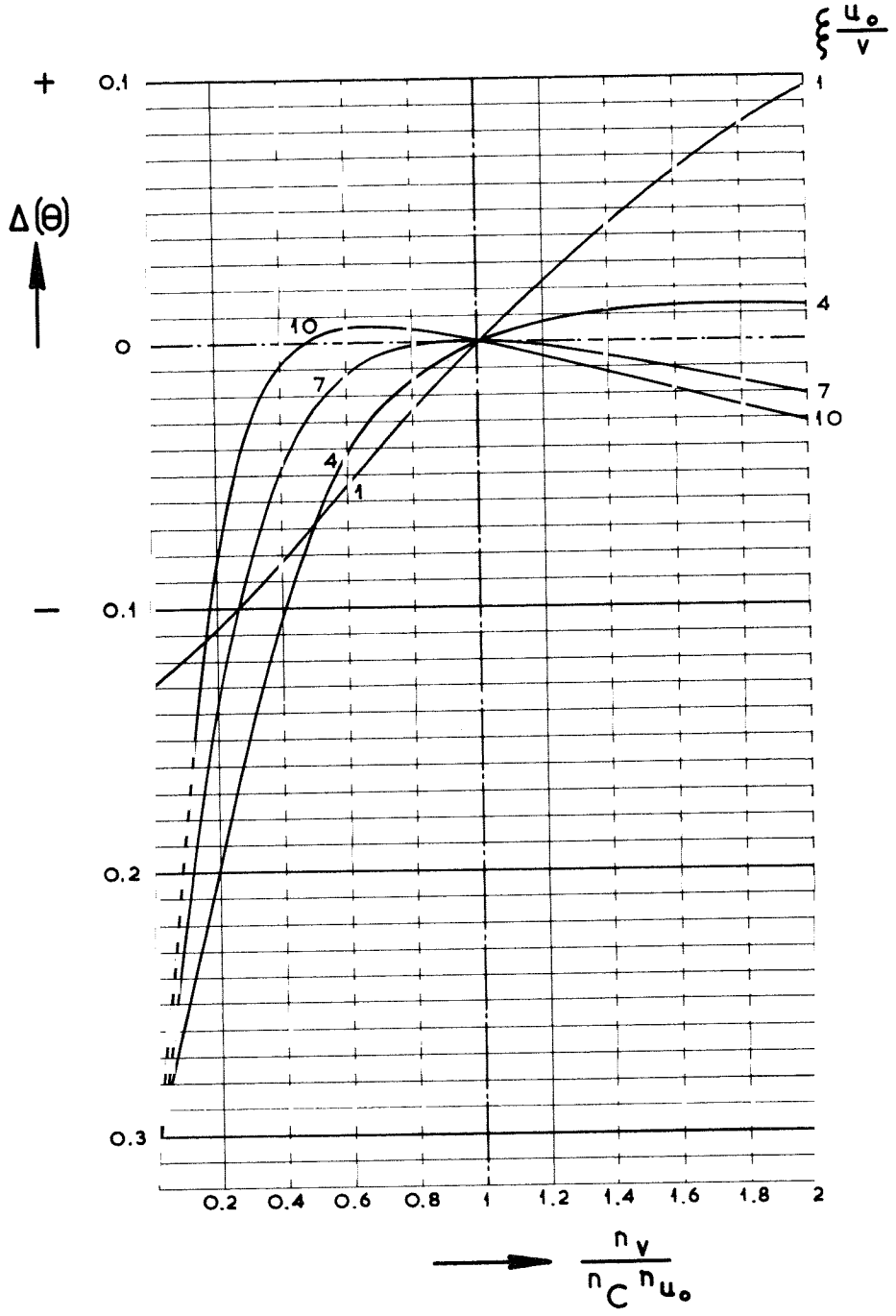

$$\Delta(\theta) = f\left(\frac{n_v}{n_C n_{u_o}}, \xi \frac{u_o}{v}\right) \text{ FOR } \varphi = 30^\circ$$

FIGURE V.1_8

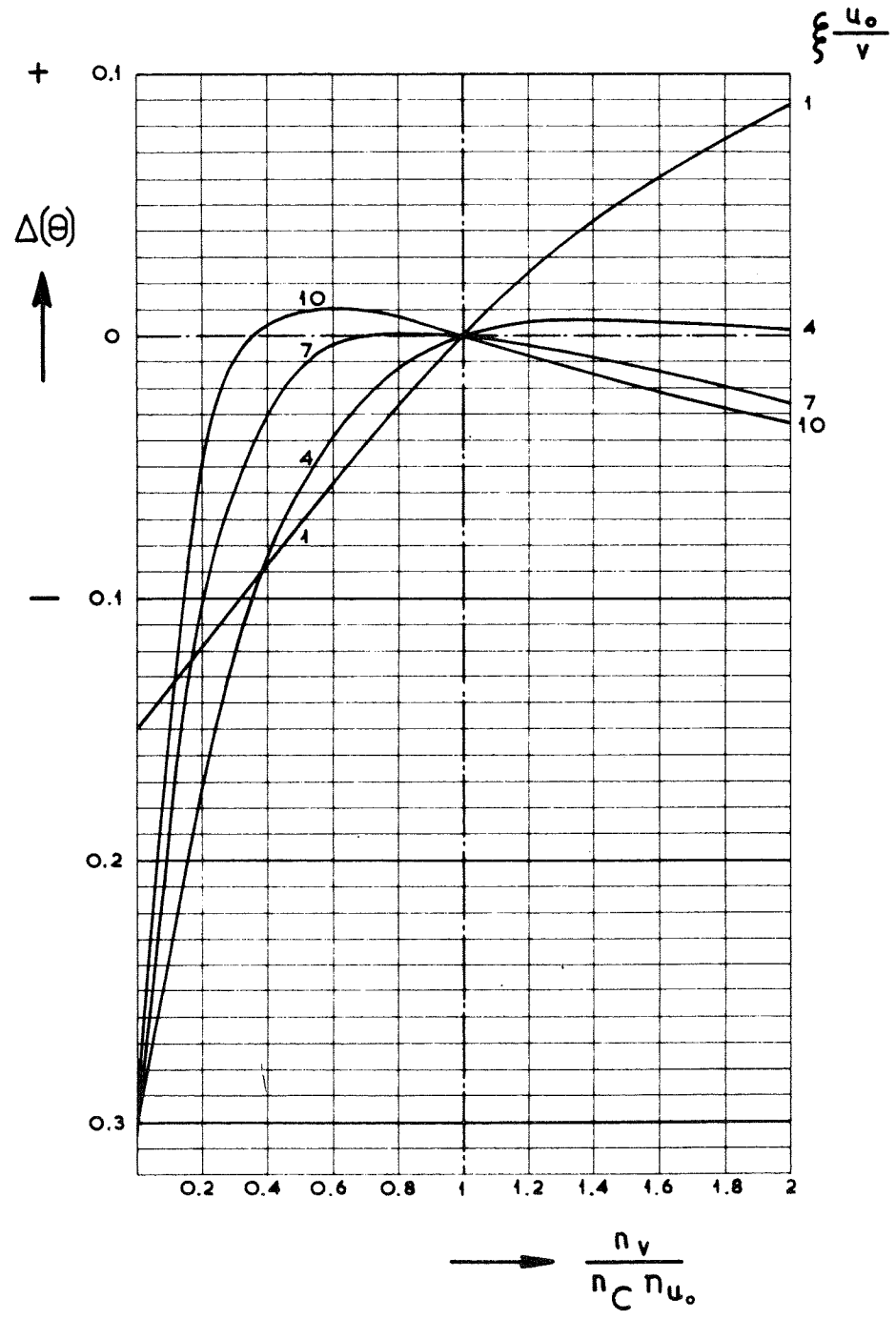

$$\Delta(\theta) = f\left(\frac{n_v}{n_C n_{u_o}}, \xi \frac{u_o}{v}\right) \text{ FOR } \varphi = 45^\circ$$

FIGURE V.1_9

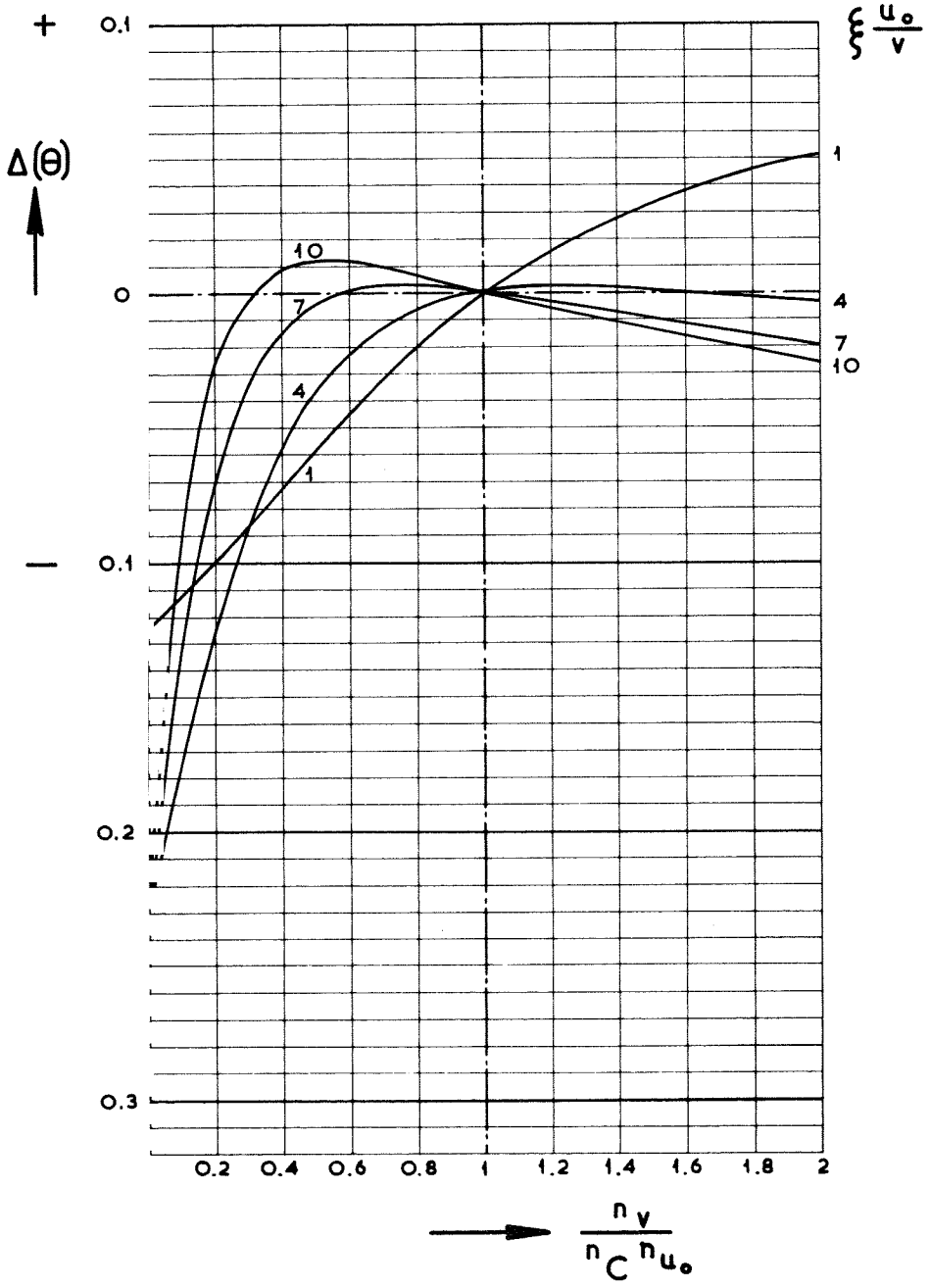

$$\Delta(\theta) = f\left(\frac{n_v}{n_C n_{u_o}}, \xi \frac{u_o}{v}\right) \text{ FOR } \varphi = 60^\circ$$

FIGURE V.1_10

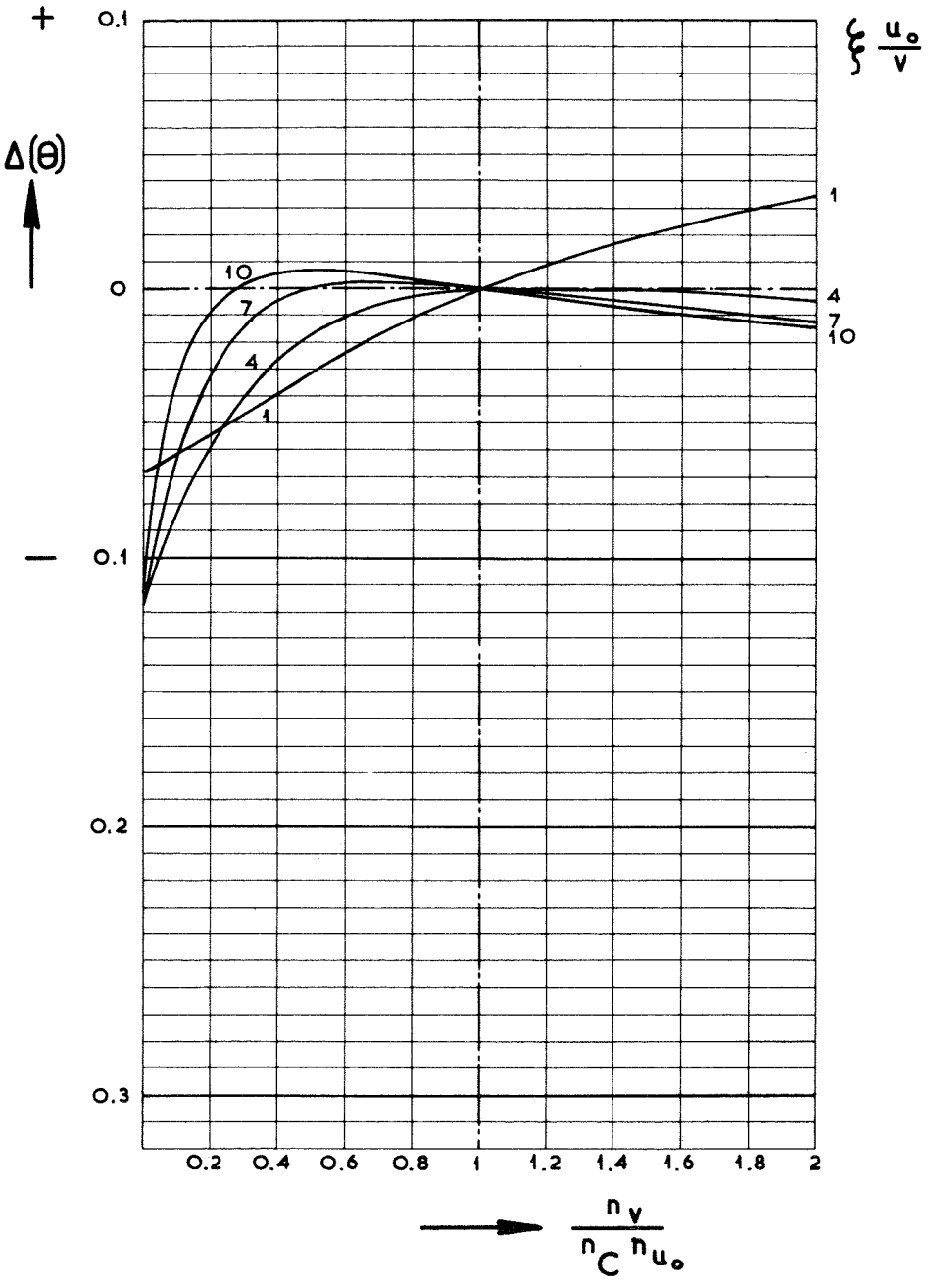

$$\Delta(\theta) = f\left(\frac{n_v}{n_C n_{u_o}}, \xi\frac{u_o}{v}\right) \text{ FOR } \varphi = 75^\circ$$

FIGURE V.1_11

$$n_S = n_D \frac{n_v}{n_C} e^{-0.27\left[\left\{\frac{\Delta DC^2}{\mu v^2(1+\frac{1}{2}\xi^2\frac{u_o^2}{v^2})}\right\}_{pr} - \left\{\frac{\Delta DC^2}{\mu v^2(1+\frac{1}{2}\xi^2\frac{u_o^2}{v^2})}\right\}_{m}\right]} \qquad (V.2\text{-}1)$$

When the various values, ξ, u_o, v and C of the prototype are written without subscripts and the values for the model are obtained by dividing these values by the scales, this formula may be written as:

$$n_S = \frac{n_D n_v}{n_C} e^{-0.27 \frac{\Delta DC^2}{\mu v^2} \cdot \frac{\frac{n_\Delta n_D}{n_\mu} n_C^2 - n_v^2\left[1+\frac{1}{2}\xi^2\frac{u_o^2}{v^2} - \frac{1}{2}\xi^2\frac{u_o^2}{v^2}\frac{n_\Delta n_D}{n_\mu n_{u_o}^2}\right]}{\frac{n_\Delta n_D}{n_\mu} n_C^2\left[1+\frac{1}{2}\xi^2\frac{u_o^2}{v^2}\right]\left[1+\frac{1}{2}\xi^2\frac{u_o^2}{v^2}\frac{n_v^2}{n_C^2 n_{u_o}^2}\right]}} \qquad (V.2\text{-}2)$$

In order to achieve that n_S is invariable over the model, n_S should be independent of the values of v, C and u_o which vary over the model. This can be only obtained when the power of e is zero. So

$$\frac{n_\Delta n_D}{n_\mu} n_C^2 - n_v^2\left[1+\frac{1}{2}\xi^2\frac{u_o^2}{v^2} - \frac{1}{2}\xi^2\frac{u_o^2}{v^2}\frac{n_\Delta n_D}{n_\mu n_{u_o}^2}\right] = 0 \qquad (V.2\text{-}3)$$

From this follows for the velocity scale,

$$n_v = \sqrt{\frac{\frac{n_\Delta n_D}{n_\mu} n_C^2}{1+\frac{1}{2}\xi^2\frac{u_o^2}{v^2} - \frac{1}{2}\xi^2\frac{u_o^2}{v^2}\frac{n_\Delta n_D}{n_\mu n_{u_o}^2}}} \qquad (V.2\text{-}4)$$

Since, for practical reasons, it is impossible to vary n_v over the model, the following final requirement is obtained:

$$\frac{1}{2}\xi^2\frac{u_o^2}{v^2} = \frac{1}{2}\xi^2\frac{u_o^2}{v^2}\frac{n_\Delta n_D}{n_\mu n_{u_o}^2}, \qquad (V.2\text{-}5)$$

assuming that n_C and n_μ are constant over the model.
In that case the following scales for current and orbital velocity are obtained:

$$n_v = (n_\Delta n_D / n_\mu)^{1/2} \cdot n_C \qquad (V.2\text{-}6)$$

and: $$n_{u_o} = (n_\Delta n_D / n_\mu)^{1/2} \qquad (V.2\text{-}7)$$

The first relationship is the same as that obtained for the ideal velocity scale (6, 7) with current only.
From the combination of (V.2-6) and (V.2-7) follows a relationship between v and u_o, viz.:

$$\frac{n_{u_o}}{n_v} n_C = 1 \qquad (V.2\text{-}8)$$

which is the same relationship as required for correct reproduction of a current pattern under influence of wave motion.

Since it will not always be possible to reach the ideal velocity scale, the deviations of the transport scale, with variation of velocity and depth have to be calculated. In order to determine what variation of n_S may be expected for varying ratio of $\xi\, u_o/v$ and for different values of u_o and v, a computation has been made for the following data:

$\Delta DC^2/\mu v^2 = 2.75$; $n_\Delta n_D/n_\mu = 1$; $n_C = 2$; $n_D = 1$;

$\xi\, u_o/v = 150$, 300, 450 and 600; n_v and $n_{u_o} = 1.5$, 3, 4.5 and 6.

The results of this computation are represented in figures V.2-1 through 4. From equation (V.2-6) follows for the velocity scale, giving a transport scale which is invariable over the model: $n_v = n_C\,(n_\Delta n_D/n_\mu)^{1/2} = 2$ and from equation (V.2-7): $n_{u_o} = (n_\Delta n_D/n_\mu)^{1/2} = 1$. Comparing figures V.2-1 and 2, it is evident, indeed, that the value of the ideal velocity scale for the current should lay between 1.5 and 3.

Although the curves give an indication of the variation of n_S with $\xi\, u_o/v$ for different values of n_v and n_{u_o}, this indication is not sufficient to determine the variation with only v, as in formula (V.2-2) also $\Delta DC^2/\mu v^2$ should be varied. To obtain an impression about this variation, which could be seen as a variation with the location for some combinations of n_v and n_{u_o}, also values of n_S have been computed with $\Delta DC^2/\mu v^2$ varying with v, in the same way as $\xi\, u_o/v$ varies with v. These results are given with dotted lines on figures V.2-2 through 4.

From these curves, the following conclusions about variation of n_S, when the ideal scales cannot be achieved, may be drawn. The deviation of n_S is greater when $\xi\, u_o/v$ is smaller. Not only the deviation from the ideal value, but also the variation with a certain variation of u_o and v becomes greater. It is not possible to influence this phenomenon on one

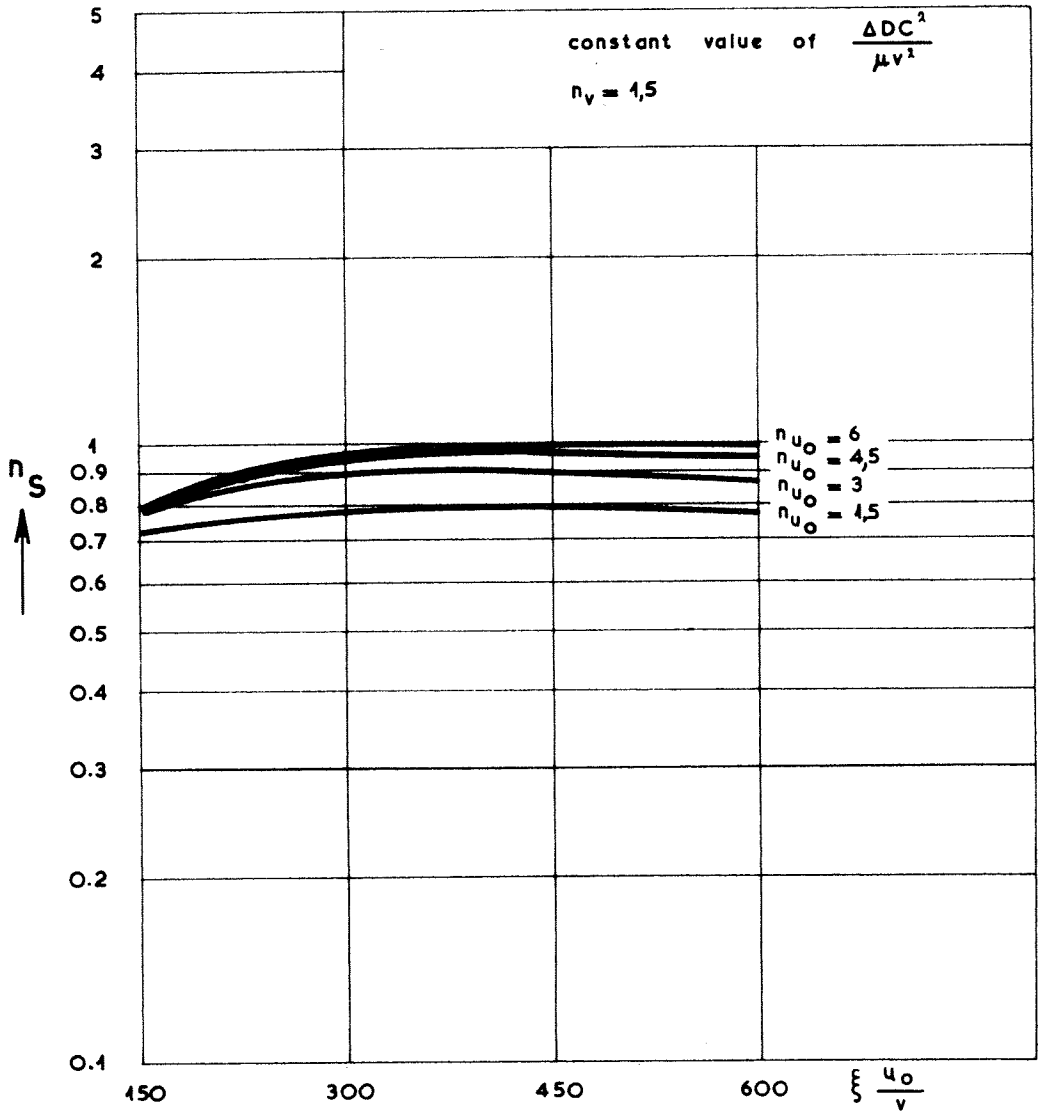

$$n_s = f\left(n_{u_o}, \xi \frac{u_o}{v}\right) \text{ FOR } n_v = 1,5$$

FIGURE V.2_1

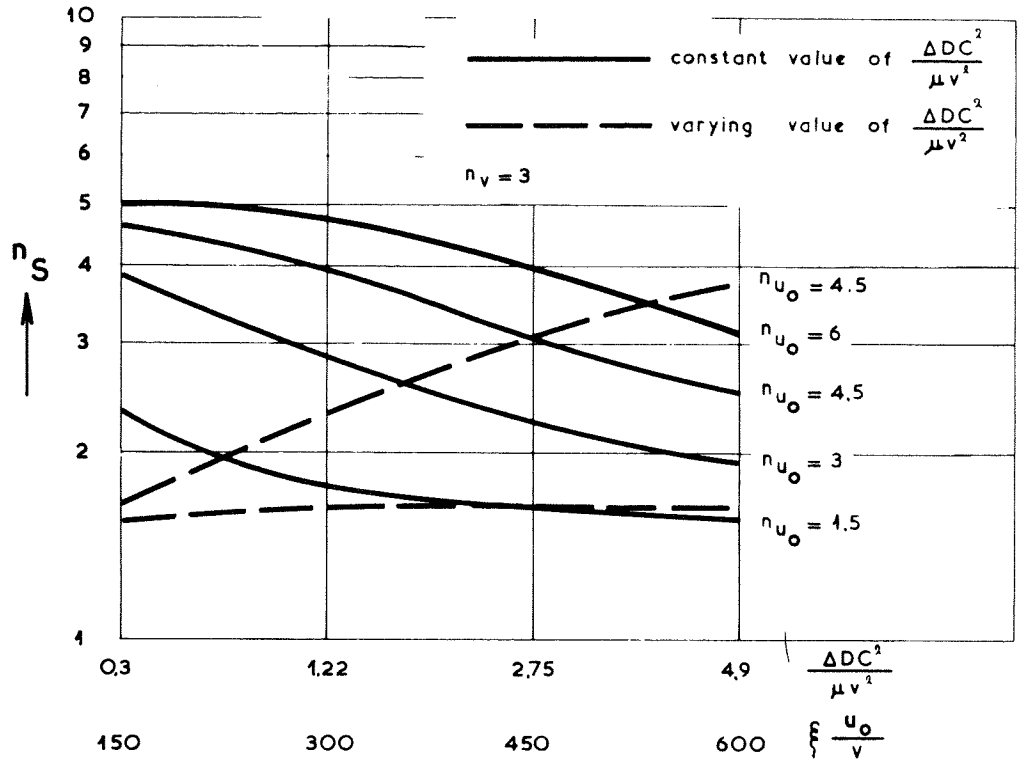

$$n_S = f\left(n_{u_o}, \xi \frac{u_o}{v} \text{ and } \frac{\Delta DC^2}{\mu v^2}\right) \text{FOR } n_v = 3$$

FIGURE V.2_2

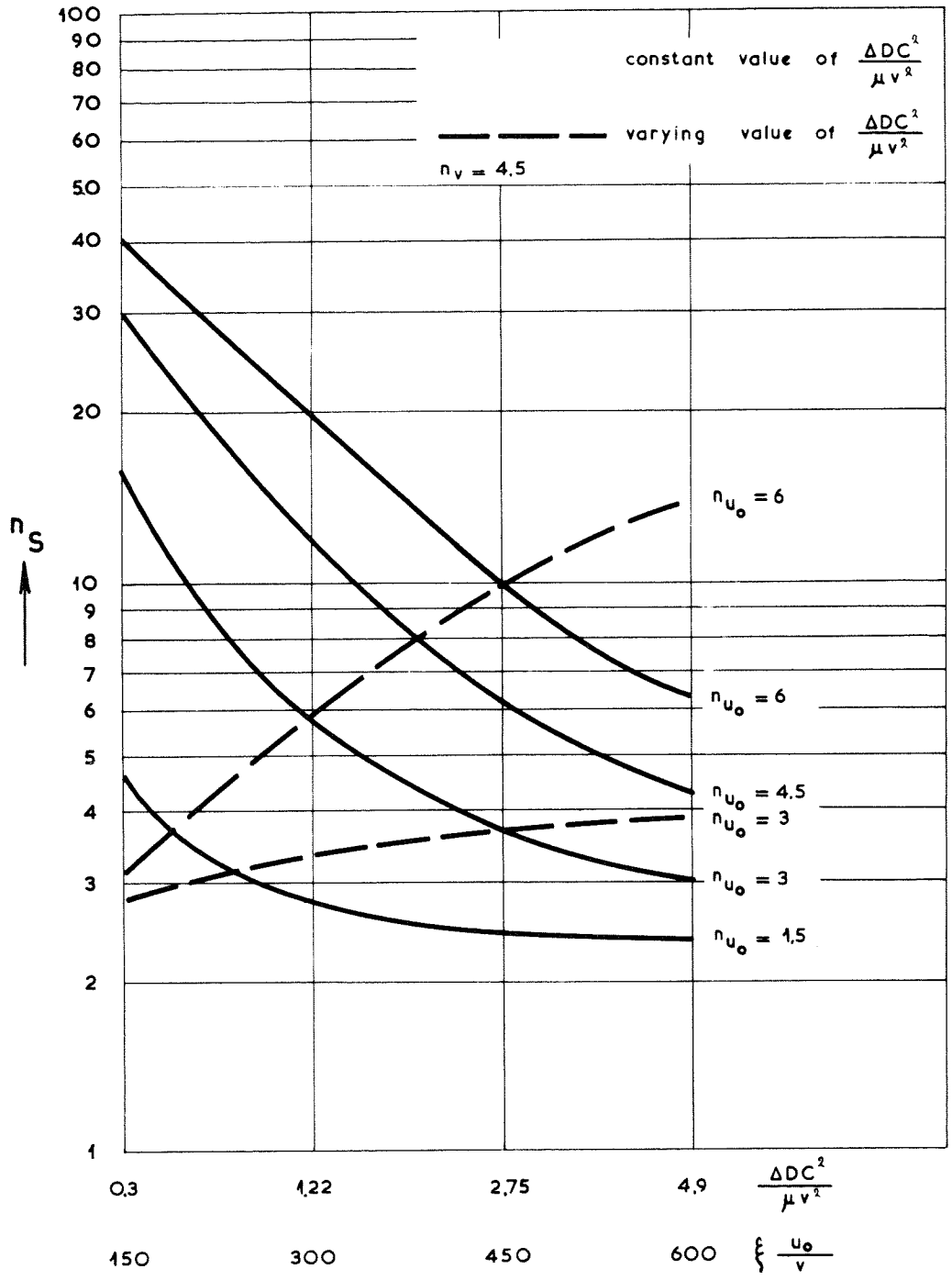

$$n_s = f\left(n_{u_o}, \xi \frac{u_o}{v} \text{ and } \frac{\Delta DC^2}{\mu v^2}\right) \text{FOR } n_v = 4,5$$

FIGURE V.2_3

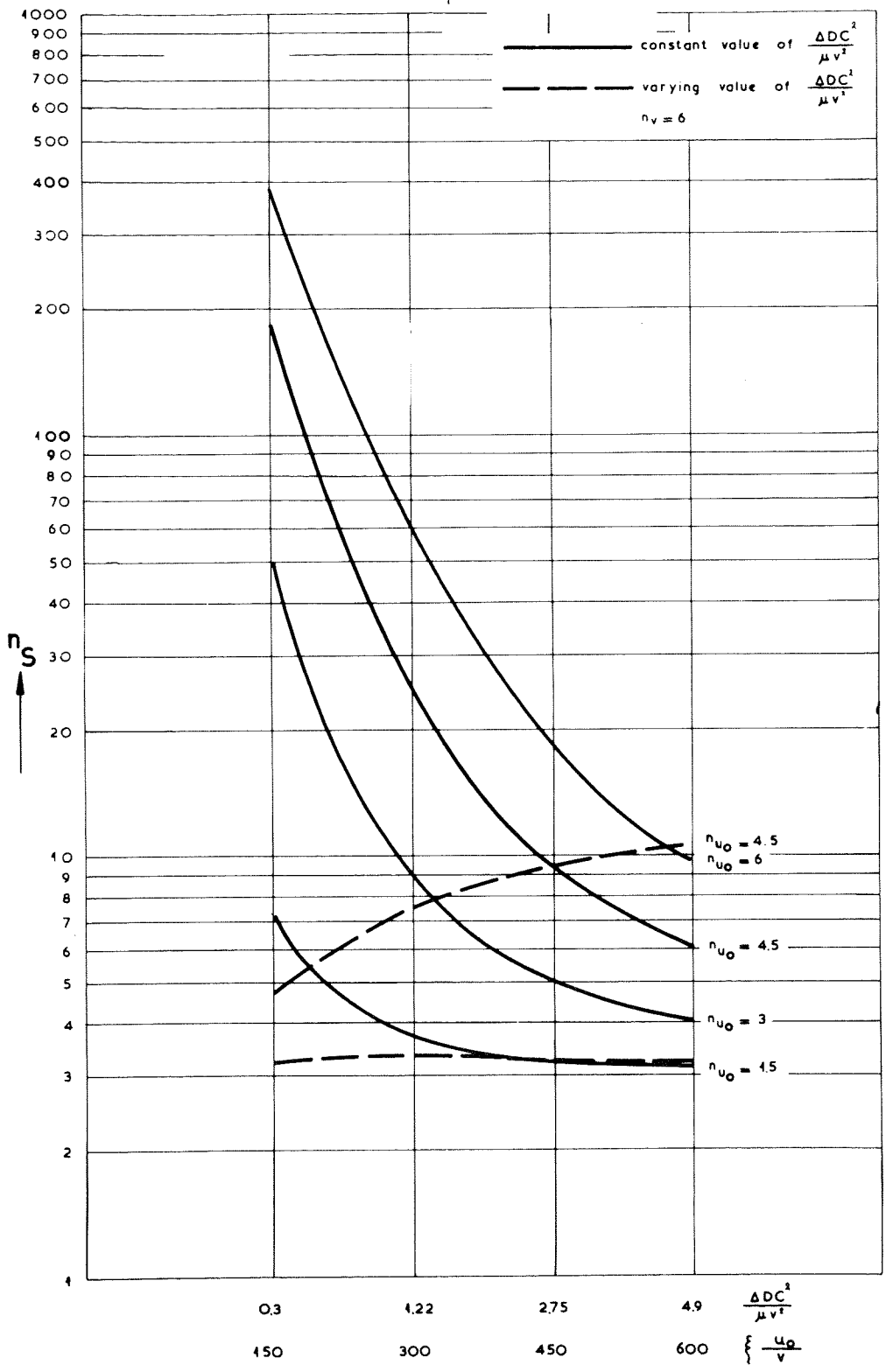

$$n_s = f\left(n_{u_o}, \frac{u_o}{v} \text{ and } \frac{\Delta DC^2}{\mu v^2}\right) \text{FOR } n_v = 6$$

FIGURE V . 2 _ 4

way or another, since $\xi\, u_o/v$ is exclusively governed by the prototype conditions. It is quite understandable, however, that variations in n_S become smaller for high values of $\xi\, u_o/v$, since the wave motion stirres up the material. This effect has the tendency to decrease the limit of the critical shear-stress velocity at which movement is possible. Reproduction of bed load movement is in most cases easier when the conditions are not too close to the limit of this critical velocity. This effect is also demonstrated by the fact that variations in n_S are smaller for low values of n_{u_o}, that is for relative high orbital velocities in the model.

The tendency, known in normal movable bed models with current only, of relatively too deep scour holes, is found also in coastal models. From the dotted curves it becomes clear that, for velocity scales which are above the ideal velocity scale, n_S increases with $\xi\, u_o/v$, hence decreases with increasing current velocity. A decreasing transport scale means a transport in the model which increases more, compared to the surroundings, than in the prototype. Hence, since scouring normally occurs at places with higher velocities, this leads to higher transports in the model at these locations and, therefore, to deeper scour holes. A similar reasoning leads to the conclusion that shoals in the model are too high in comparison with the prototype. These effects are even strengthened by the fact that in deep areas u_o will decrease, whilst in shallow areas u_o will increase. This has an equal effect on $\xi\, u_o/v$ as increase, respectively decrease, of the velocity.

No attempt has been made to develop graphs on which variations of n_S can be read. With modern computer techniques it will be much easier to compute these variations. An example is given in the next paragraph.

V.3. Conclusions

From the results, presented in the first two paragraphs of this chapter, and from the general conditions discussed in paragraph I.2 the following outline for the most appropriate procedure for establishing the scales for a coastal model can be given.

For a correct and invariable reproduction of the transport phenomena in the model, the following relationships should be satisfied:

$$\frac{n_C^2\, n_d}{n_l} = 1 \qquad (V.3\text{-}1)$$

$$\frac{n_v}{n_{u_o} n_C} = 1 \qquad (V.3\text{-}2)$$

$$\left(\frac{n_\Delta n_D}{n_\mu}\right)^{1/2} \cdot \frac{n_C}{n_v} = 1 \qquad (V.3\text{-}3)$$

$$\left(\frac{n_\Delta n_D}{n_\mu}\right)^{1/2} \cdot \frac{1}{n_{u_o}} = 1 \qquad (V.3\text{-}4)$$

Relationship (V.3-1) gives the requirement for true reproduction of the current pattern as far as this reproduction is influenced by the bed roughness. This requirement is equal for models with current only and for models with a combination of current and waves. Particularly in coastal models where n_l/n_d has a rather high value (between 5 and 10) determined by the ratio of the equilibrium slopes of the beach in model and prototype, n_C will have a value which is higher than will be attained without further measures. The first, and in many cases best, solution will be the application of artificial roughness as discussed by Bijker, Stapel and de Vries (6, 7) and Reinalda (31). Since this artificial roughness will not only influence the resistance coefficient but also the ripple coefficient, the influence on the transportation of material will not be very great. This is also demonstrated by the tests executed by Aspden et al as groupwork of the International Course in Hydraulic Engineering Delft (18).

Equation (V.3-3) indicates the velocity scale which gives an invariable transport scale over the entire model. The parameter $n_\Delta n_D/n_\mu$ will have, depending on the material in prototype and model, values which are somewhat higher than 1, say between 1 and 3. This leads to values of n_v which are normally lower than the square root of the depth scale, which is the velocity scale for which the energy slope is reproduced according to the distortion of the model, assuming that requirement (V.3-1) is fulfilled. Application of this velocity scale and of artificial roughness leads, therefore, to energy slopes in the model which may be too steep. This may lead to unacceptable deviations of the water depth at both sides of the model. In order to deminish this disadvantageous effect, the artificial roughness is normally only applied in that part of the model where the flow lines are strongly curved and where true reproduction of the current pattern is essential (6, 7, 31).

However, if this would not give sufficient release, a too low value of n_C, giving a too high value of C in the model, will have to be accepted. The scale for the radius of curvature of the flow lines is

represented in figure V.1-1. Since in this case, $n_l/n_d n_c^2 > 1$, n_R will be too low, which results in values of R in the model which are to high. In this case, the flow lines in the model will not be sufficiently curved. From equation (V.1-10) and also from figure V.1-1, it can be judged whether these deviations will be acceptable or not.

Relationship (V.3-2) gives the requirement for correct reproduction of the current pattern, in case this would be influenced by the wave motion. Especially when n_c is reproduced according to relationship (V.3-1), so that it has a rather high value, this leads to rather low values of n_{u_o}. Since this is often not possible because of the fact that the wave height cannot be exaggerated too much, $n_v/n_{u_o} n_c$ will be smaller than 1. From figures V.1-6 and V.1-7 through 11, it is evident that this should be avoided as much as possible, since for values of $n_v/n_c n_{u_o} < 1$ the discrepancies in the reproduction of the current pattern increase more rapidly than for values of $n_v/n_c n_{u_o} > 1$. Figures V.1-7 through 11 indicate, however, that when $n_v/n_c n_{u_o}$ is not too small, the deflection of the flow lines, $\Delta(\theta)$, is not more than some degrees.

More important than the discrepancies in the current pattern are, however, the discrepancies in the sediment transport scale n_s. These discrepancies will be discussed with the aid of a model of a fishing harbour, as shown on figure V.3-1.
For this case the following data are available:

		Prototype	Model
Wave period,	T	6 s	1.8 s
Wave height,	H	1.00 m	0.052 m
Current,	v	0.17 - 0.75 m/s	0.20 - 0.45 m/s
Depth,	d	6.8 m	0.23 m
Bottom material,	D_m	$0.4\ 10^{-3}$ m	$0.20\ 10^{-3}$ m
	D_{90}	$0.5\ 10^{-3}$ m	$0.29\ 10^{-3}$ m
	Δ	1.65	1.65

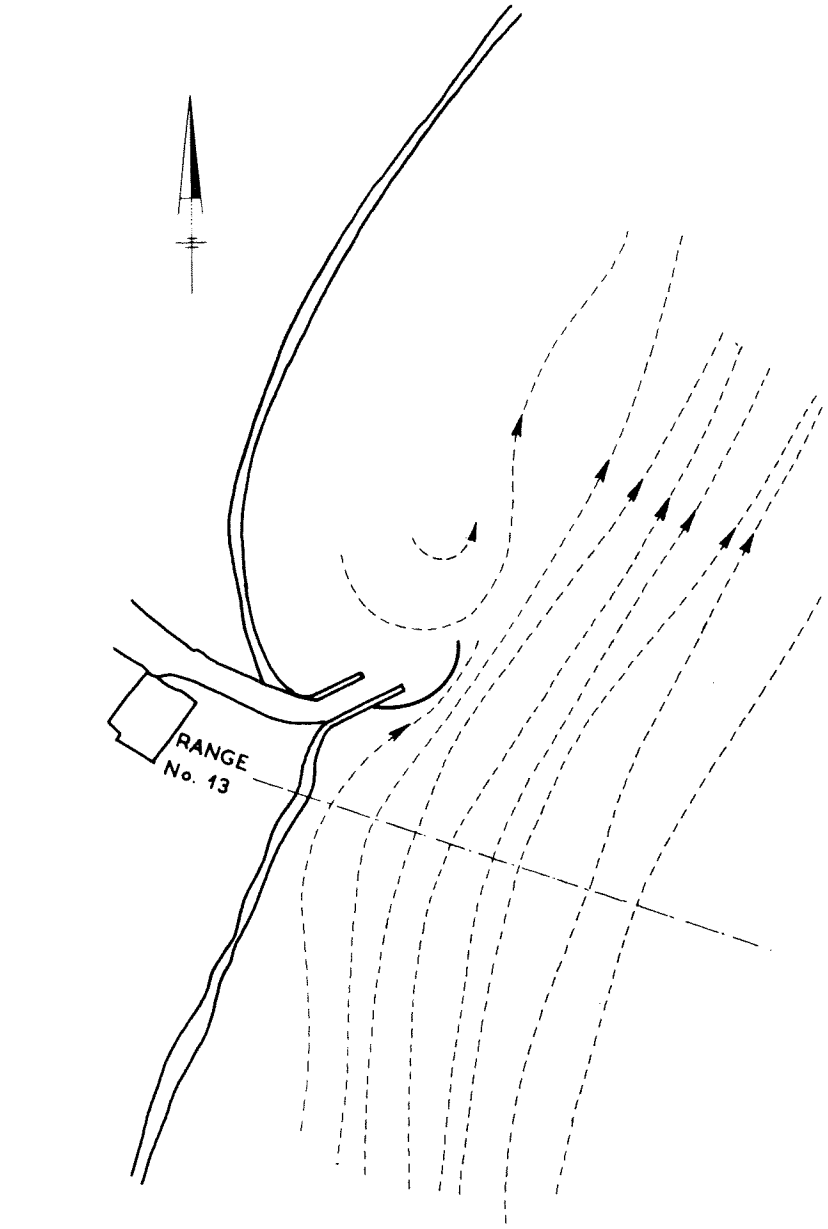

FISHING HARBOUR

FIGURE V.3-1

Possible bottom conditions are:

		Prototype		Model
r	i	0.025 m	(i)	0.005 m
C		64 $m^{1/2}/s$		49 $m^{1/2}/s$
μ		0.58		0.56
r	ii	0.05 m	(ii)	0.01 m
C		58 $m^{1/2}/s$		44 $m^{1/2}/s$
μ		0.48		0.48
r	iii	0.10 m	(iii)	0.02 m
C		52 $m^{1/2}/s$		39 $m^{1/2}/s$
μ		0.42		0.40

Due to the required reproduction of the slope of the beach, the distortion of the model should be about 5. Since the dimensions of the harbour entrance to be studied are not very large, a rather small length scale will be required. Hence, for the length scale should be chosen, for instance, a value of 150 and for the depth scale a value of 30. The most likely combination of bottom conditions for model and prototype will be (ii), i and (ii), ii. For these combinations the velocity scales, determined by means of formula (V.3-3), are 1.86 and 1.84. These values are too small for application since the energy gradient required to attain this velocity in the model is far to steep. The slope of the water surface is reproduced according to the normal resistance law as:

$$n_I = \frac{n_v^2}{n_C^2 \, n_d} \qquad (V.3\text{-}5)$$

This leads in this case to a scale for I of about 0.06, whereas this value should be $n_d/n_l = 30/150 = 0.2$. For this reason, a value different from the "ideal velocity scale" has to be chosen. With this velocity scale the variation of the transport scale has to be calculated.

From equation (V.3-5) follows for the velocity scale, when $C_{pr} = 58\ m^{1/2}/s$ and $C_m = 44\ m^{1/2}/s$ (conditions ii and (ii)), $n_v = 3.2$. Since, however, in order to meet the requirement (V.3-2) for reproduction of the influence of the wave motion on the current, the velocity scale should not be too low, $n_v = 3.8$ has been chosen. The fact that the energy slope in the model is relatively somewhat too small has no serious effects.

Near the entrance of the harbour the velocity will increase from 0.35

to 0.45 m/sec or 0.45 to 0.55 m/sec over a distance of 500 m. The convective term $\Delta (v^2/2g) = 4.10^{-3}$ to 5.10^{-3} and the resistance term $(v^2/C^2d)\Delta l = 3.5\ 10^{-3}$ to $5.5\ 10^{-3}$. Hence, $K \simeq 1.0$, and as $n_l/n_d n_C^2 = 2.9$, the deviation in $n_R/n_l \simeq 0.7$, so that the deviation of n_R will be as much as 30%. Since, however, in this case no strongly curved flow lines are present in the region of main interest, this deviation is accepted.

In this case a possible bar formation will occur in an region with a strong velocity gradient immediately in front of the harbour entrance. The true reproduction of τ'/τ'', which indicates the angle which the resultant bed shear makes with the current, is very important as this may determine the quantity of material which is moved out of the influence of the main current. According to requirement (V.3-2), the scale for the orbital motion should, therefore, be $n_u = n_v/n_C = 3.8/1.3 = 2.9$. For a depth of 6.8 m in the prototype, the orbital velocities at the bottom in prototype and model are 0.45 and 0.15 m/s, respectively. This leads to $n_{u_o} = 3$ which is sufficiently close to 2.9, to avoid any serious discrepancies.

With equation (V.2-2), the variation of n_S can now be calculated. The results are represented in figure V.3-2. From this figure follows a variation of n_S of about 25% in the region of interest. This causes a depth in front of the harbour which is slightly too great. On the other hand, due to the slightly exaggerated transport in this region, as well as due to the increasing value of the transport scale in areas with lower velocities, the shoal in the entrance will be reproduced somewhat too high.

Since the wave height in the model is too great, due to the fact that $n_H = 20$ instead of 30, one may expect that the breaker phenomena are not reproduced exactly to scale. However, special tests have been carried out in order to ascertain that the beach slope is reproduced to scale.

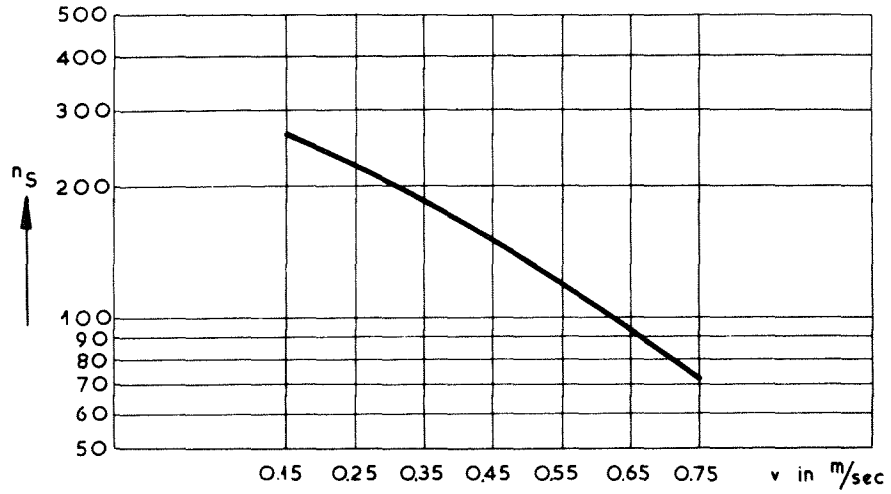

VARIATION OF TRANSPORT SCALE n_s WITH VELOCITY v

FIGURE V. 3_2

SAMENVATTING

Bij kustmodellen is de weergave van de gezamenlijke werking van golven en stroom van uitermate groot belang. In deze studie is daarom een poging gedaan een basis te vinden voor de schaalbepaling die tot nu toe op voornamelijk empirische wijze gebeurde.

Hiertoe is in de eerste plaats onderzocht op welke wijze de schuifspanning van de stroom, zoals deze op de bodem wordt uitgeoefend, door de golfbeweging wordt beinvloed.

Met de op deze wijze verkregen resultaten blijkt het mogelijk een verklaring te geven van de empirisch reeds bekende verandering van de stroomrichting door de aanwezigheid van golven.

Uitgaande van de bekende bodemtransport formules en de berekende toename van de bodemschuifspanning van de stroom door de golven, is een formule voor bodemtransport onder invloed van golven en stroom afgeleid.

Met behulp van de formule voor toename en richtingverandering van de bodemschuifspanning en die voor het bodemtransport is vervolgens afgeleid aan welke eisen de schalen moeten voldoen om een goede weergave van het stroombeeld en het materiaaltransport te verkrijgen.

Tot slot is aangegeven welke afwijkingen kunnen optreden als niet volledig aan deze schaalwetten kan worden voldaan.

MAIN SYMBOLS

a	various coefficients	
A	various coefficients	
b	various coefficients	
B	various coefficients	
c	various coefficients	
c_*	celerity of wave propagation	LT^{-1}
c(..)	concentration of suspended material at a certain level	
C	resistance coefficient	$L^{1/2}T^{-1}$
d	depth	L
D	grain diameter	L
e	base of natural logarithme	
E	energy flux per unit of width	MLT^{-3}
F	parameter	
g	acceleration of gravity	LT^{-2}
G	parameter	
H	wave height	L
I	energy gradient and slope of water surface	
k	wave number	L^{-1}
K	parameter	
l	length and mixing length	L
L	wave length	L
M	parameter	
n	ordinate normal to flow direction	L
n	scale	
N_{**}	parameter	
p	coefficient	
r	bed roughness	L
R	radius of curvature	L
s	ordinate in flow direction	L
s	standard deviation	
S_{**}	transport of material per unit of time	L^2T^{-1} or L^3T^{-1}
t	time	T
T	wave period	T
u	orbital velocity	LT^{-1}
U	mass-transport velocity	LT^{-1}
v	current velocity	LT^{-1}
v_*	shear-stress velocity	LT^{-1}
V	resultant velocity of main current and orbital motion	LT^{-1}

w	falling velocity of grain	LT^{-1}
x	horizontal ordinate	L
X	parameter	
y	vertical ordinate	L
Y	various parameters	
α	amplitude of orbital excursion at the bed	L
β	coefficient	L^{-1}
γ	angle	
δ	thickness of boundary layer	L
Δ	relative apparent density	
$\Delta(..)$	small increment	
ε	eddy viscosity coefficient	L^2T^{-1}
ζ	coefficient	
θ	angle of deviation of flow	
$\varkappa$	constant of von Karman	
μ	ripple coefficient	
ν	viscosity coefficient	L^2T^{-1}
ξ	parameter	
ϱ	density	ML^{-3}
τ	shear stress	$ML^{-1}T^{-2}$
φ	angle between wave crest and flow direction	
ψ	phase angle of waves	
ω	wave frequency	T^{-1}

LITERATURE

1 ABOU SEIDA, M.M.
Bed load function due to wave action.
University of California, Berkeley 1965.

2 BAJORUNAS, L.
Rate of littoral sand transport in the Great Lakes.
Proc. of the 7th Conf. on Coastal Engg., The Hague, 1960, pp. 326-431.

3 BIJKER, E.W.
Increase of bottom shear stress of a current due to wave action.
Seminar on sediment transport and diffusion problems in coastal hydraulics.
Proc. of the 11th Congr. of the I.A.H.R., Leningrad, vol.V, 1965, paper 3.14.

4 BIJKER, E.W.
The increase of bed shear in a current due to wave motion.
Proc. of the 10th Conf. on Coastal Engg., Tokyo, 1966, pp. 746-765.

5 BIJKER, E.W.
The increase of bed shear in a current due to wave motion.
Publication no. 46 of the Delft Hydraulics Laboratory, 1967.

6 BIJKER, E.W.
Determination of scales of movable bed models.
Symposia Golden Jubilee of the Central Water and Power Res. Station Poona, Vol. 2, 1966, pp. 1-4.

7 BIJKER, E.W., STAPEL, D.R.A. and DE VRIES, M.
Some scale effects in models with bed load transportation.
Proc. of the 7th Congr. of the I.A.H.R., Lisbon, 1957, paper A1.

8 BIRKHOFF, G.
Hydrodynamics, a study in logic, fact and similitude.
Princeton Univ. Press, 1960.

9 BRUUN, P.
Longshore currents and longshore troughs.
Journ. of Geoph. Res. Vol. 68, nr. 4, 1963, pp. 1065-1078.

10 EAGLESON, P.
Theoretical study of longshore currents on a plane beach.
M.I.T., Dep. of Civ. Engg. Hydr. Lab., Report nr. 82, 1965.

11 EGUIAZAROFF, I.
l'Equation Générale du Transport des alluvions non cohesives par un courant fluide.
Proc. of the 7th Congr. of the I.A.H.R., Lisbon 1957, paper D43.

12 EINSTEIN, H.A.
Movement of beach sands by water waves.
Tr. Am. Geoph. Union, Vol. 29, no. 5, 1948, pp. 653-655.

13 EINSTEIN, H.A.
The bed load function for sediment transportation in open channel flow.
U.S. Dep. of Agr. Techn., Bull. nr. 1026, 1950.

14 FRIJLINK, H.C.
Discussion des formules de débit solide de Kalinske, Einstein et Meyer-Peter et Mueller compte tenue des mesures récentes de transport dans les rivières Néerlandaises.
2me Journ. Hydraulique. Soc. Hydr. de France, Grenoble 1952, pp. 98-103.

15 GODDET, J.
Etude du débit d'entraînement des matériaux mobiles sous l'action de la houle.
La Houille Blanche nr. 2, 1960, pp. 122-135.

16 GODDET, J. and JAFFRY, P.
La similitude des transports de sédiments sous l'action simultanée de la houle et des courants.
La Houille Blanche nr. 2, 1960, pp. 136-147.

17 HUON LI
Stability of oscillatory laminar flow along a wall.
Beach Erosion Board, Techn. Mem. 47, 1954.

18 International Course in Hydraulic Engineering Delft,
The use of artificial roughness in movable bed models, 1962.

19 JOHNSON, J.W.
Engineering aspects of diffraction and refraction.
Trans. A.S.C.E., vol. 118, pp. 617-652.

20 JONSSON, I.G.
Measurements in the turbulent wave boundary layer.
Proc. of the 10th Congress of the I.A.H.R., London, vol. I, 1963, paper I.12.

21 JONSSON, I.G. and LUNDGREN, H.
Bed shear stresses induced by a wave motion.
Coastal Engg. Lab. of Techn. Univ. of Denmark. Basic research progress report 1, 1961.

22 KALINSKE, A.A.
Movement of sediment as bed load in rivers.
Tr. Am. Geoph. Union, Vol. 28, 1947, pp. 615-620.

23 KALKANIS, G.
Transportation of bed material due to wave motion.
Coastal Engg. Res. Center, Techn. Mem. 2, 1964.

24 KAMPHUIS, J.W.
A mathematical model to advance the understanding of the factors involved in the movement of bottom sediment by wave action.
Civ. Engg. Dept. Queens Univ. Kingston, Ontario, Rep. nr. 53, 1966.

25 KEMP, P.H.
The relationship between wave action and beach profile characteristics.
Proc. of the 7th Conf. on Coastal Engg., The Hague, 1960, pp. 262-277.

26 KRUMBEIN, W.C.
Shore currents and sand movement on a model beach.
Beach Erosion Board, Techn. Mem. 7, 1944.

27 LAMB Sir, H.
Hydrodynamics.
Cambridge, Univ. Press, 1963.

28 LONGUET-HIGGINS, M.S.
Mass transport in water waves.
Phil. Tr. Royal Soc. London, Vol, 245, Series A, 1952, pp. 535-581.

29 MANOHAR, M.
Mechanics of bottom sediment movement due to wave action.
Beach Erosion Board, Techn. Mem. 75, 1955.

30 MEYER-PETER, E. and MUELLER, R.
Formulas for bed load transport.
Proc. of the 2nd Congr. of the I.A.H.R. Stockholm, Vol. 2, 1948, paper 2.

31 REINALDA, R.
Scale effects in models with littoral sand drift.
Proc. of the 7th Conf. on Coastal Engg. The Hague, 1960, pp. 318-325.

32 SCHONFELD, J.C.
Wrijvings- en weerstandsformules voor leidingen en waterlopen.
De Ingenieur, 1953, pp. B219-226 and B244-249.

33 SELIM YALIN, M.
Method for selecting scales for models with movable bed involving wave motion and tidal currents.
Proc. of the 10th Congr. of the I.A.H.R. London, vol. I. 1963, paper I.30.

34 Shore Protection Planning and Design.
Coastal Engg. Res. Center, Techn. rep. 4. Part I, 1966.

35 STRICKLER, A.
Beitrage zur Frage der Geschwindigkeitsformel und der Rauhigkeitszahlen für Ströme, Kanäle und geschlossene Leitungen.
Mitt. des Amtes für Wasserwirtschaft, Bern, 1923.

36 THIJSSE, J.Th.
Formulae for the friction head loss along conduit walls under turbulent flow.
Proc. of the 3rd Congr. of the I.A.H.R. Grenoble 1949, paper III.4.

37 VALEMBOIS, J.
Etude sur modèle du transport littoral. Conditions de similitude.
Proc. of the 7th Conf. on Coastal Engg., The Hague, 1960, pp. 307-317.

38 VINCENT, G.E.
Contribution to the study of sediment transport on a horizontal bed due to wave action.
Proc. of the 6th Conf. on Coastal Engg. Florida, 1957, pp. 326-335.